The Physics and Engineering of Laser Ablation of Hard Tissue for Osteotomy Purposes

Inauguraldissertation

zur Erlangung der Würde eines

Dr. sc. med.

vorgelegt der Medizinischen Fakultät der Universität Basel

von

Waldemar Deibel
aus Bookholzberg, DE

Basel, February 2021

Genehmigt von der Medizinischen Fakultät auf Antrag von

Prof. Dr. Philippe C. Cattin
Dissertationsbetreuer, Fakultätsverantwortlicher

Prof. Dr. med. Dr. med. dent. Philipp Jürgens
Koreferent

Prof. Dr. Martin Frenz
Externer Gutachter

Basel, den 01. Februar 2021

Prof. Dr. Primo Schär
Dekan

For everyone who takes the time to read this work.

Acknowledgements

When I first came to Switzerland in October 2011 as an intern for a small, not yet even seed funded start-up, I never imagined to end up doing my PhD in one of the most exciting and innovative scientific fields. This chance was presented to me when I finished my diploma in Photonics six months later. One of the founders of this start-up, the AOT AG, is Prof. Dr. Philippe C. Cattin who suggested and encouraged me to start my PhD application in biomedical engineering. One of the other founders is Dr. Alfredo E. Bruno, a laser physics scientist and the CEO, who always believed in me and made it possible to pursue my PhD while working for AOT AG as a hardware developer. One year later, I was accepted by the Medical Faculty of the University of Basel. The journey I started that day was difficult and challenging on many levels. Now seeing this time from a little distance, I realize how much scientific knowledge and incredible work experience I gained. It is thanks to the constant support and guidance of these two founders that I was able to finish it. Thank you sincerely for the trust you have placed in me.

I am also deeply thankful to my colleagues who were always there to help me and joke with me, even in the hardest of times. Our software developers Mathias Griessen, Jonas Walti and Adrian Schneider were always patient to explain me their work and let me feel as part of the team. Further, I am very grateful to Michael Peyer for his camaraderie and support during our shared time in the hardware development lab.

Our team grew and changed over the time and each and every one influenced me in one way or another. Mireille Segesser joined the team as the project manager rather late during my time but is nevertheless

a person I would like to thank. She showed me that even in rough times you can be kind, enthusiastic and determined. David Morgenthaler did his master thesis in AOT AG. Despite his short time in the company, he became a dear friend and I hope to keep him and his lovely woman Katharina in my life.

Last but not least, I thank all my friends and family who supported me in more ways that I can express here.

Summary

Till today bone surgeries (osteotomies) are performed with conventional mechanical tools like drills and saws. Because of massive contact pressure, vibration and friction these conventional methods carry great risks of damaging the surrounding tissue as well as the bone itself in form of mechanical trauma and thermal damage even if performed with great care. Moreover, a broadening of cuts and a subsequent deposition of metal shavings and bacterial contamination are negative side effects. The more complicated the anatomical location and the closer the surgery is to nerves and vascular structures the higher the risk of collateral damage. A beneficial alternative presents contact-free laser osteotomy which offers blood-loss-reduction, vibration-reduction, a free choice of the cutting geometry, a small operation field and the prevention of massive bone flour and metal abrasion. The successful development of a laser osteotome was so far limited by technological and engineering drawbacks. Now, this next step for osteotomies is feasible with the introduction of computers in surgical navigation, pre-operative planning, medical imaging, medical robotics, software development and suitable laser sources. This thesis describes the engineering of a suitable optical system, i.e. a cutting laser head, and examines the resulting laser light and hard tissue. First and foremost, the laser head must ensure a most effective tissue ablation without inducing any mechanical or thermal damage to the treated or surrounding tissue. This is achieved by beam shaping and guiding elements and the development of a tissue cooling system, i.e. a nozzle array, Furthermore, it must have a large working distance to the operating field, be light enough not to overload the medical robot it is attached to. Both are achieved through a compact and light

weight laser head design. Since the work for this thesis was part of the development of a commercial computer assisted laser osteotome, aspects like safety and ergonomics were taken into account, e.g. visual cameras for intervention observation and recording. During the development of the laser head, the interaction of laser light and hard tissue was investigated. After developing the laser head to a state that it was used successfully for three animal studies, in depth analyses for the resulting minimized heat induction during the laser osteotomies were investigated.

Zusammenfassung

Bis heute werden Knochenoperationen (Osteotomies) mit mechanischen Werkzeugen wie Bohrern oder Sägen durchgeführt. Aufgrund des massiven Anpressdrucks, der Vibration und der Reibung bergen diese konventionellen Methoden große Risiken, das umliegende Gewebe und den Knochen selbst thermisch oder mechanisch zu schädigen, auch wenn die Interventionen mit großer Sorgfalt durchgeführt werden. Darüber hinaus sind eine Verbreiterung der Schnitte und eine anschließende Ablagerung von Metallspänen sowie eine bakterielle Kontamination negative Nebenwirkungen. Je komplizierter die anatomische Lage und je näher die Operation an Nerven und Gefäßen ist, desto höher ist das Risiko einer Schädigung. Eine vorteilhafte Alternative ist die berührungslose Laserosteotomie, die eine Verringerung des Blutverlusts und der Vibrationen, eine freie Wahl der Schneidegeometrie und ein kleineres Operationsfeld bietet. Weiterhin wird massiver Knochenmehl und Metallabrieb verhindert. Die erfolgreiche Entwicklung eines Laserosteotoms war bisher durch technologische und konstruktive Nachteile begrenzt. Jetzt sind Laser-Osteotomien mit der Einführung von Computern in der chirurgischen Navigation, der präoperativen Planung, der medizinischen Bildgebung, der medizinischen Robotik, der Softwareentwicklung und geeigneten Laserquellen möglich. Diese Arbeit beschreibt die Konstruktion eines geeigneten optischen Systems, d. H. Eines Schneidlaserkopfes, und untersucht die Interaktion zwischen dem resultierende Laserlicht und dem behandelten Hartgewebe. In erster Linie muss der Laserkopf eine möglichst effektive Gewebeablation gewährleisten, ohne dass das behandelte oder umgliegende Gewebe mechanisch oder thermisch geschädigt wird. Dies

wird durch Strahlformungs- und -führungselemente und die Entwicklung eines Gewebekühlsystems, d. H. eines Düsensystems, erreicht. Außerdem muss es einen großen Arbeitsabstand zum Operationsfeld haben und leicht genug sein, um den medizinischen Roboter, an dem es befestigt ist, nicht zu überlasten. Beides wird durch ein kompaktes und leichtes Laserkopfdesign erreicht. Da diese Arbeit Teil der Entwicklung eines kommerziellen computergestützten Laserosteotoms war, wurden Aspekte wie Sicherheit und Ergonomie berücksichtigt, z. B. visuelle Kameras zur Interventionsbeobachtung und -aufzeichnung. Während der Entwicklung des Laserkopfes wurde die Wechselwirkung von Laserlicht und Hartgewebe intensiv untersucht. Nachdem der Laserkopf so weit entwickelt worden war, dass er erfolgreich für drei Tierversuche eingesetzt werden konnte, wurden eingehende Analysen zur Minimierung der Wärmeinduktion während der Laserosteotomien durchgeführt.

Contents

Chapter 1

Introduction

1.1 Lasers in Medicine

The last century was the most productive in terms of technological advancements for humanity. There are countless innovations that made life easier, longer, safer and more fun. For instance, medical care benefited greatly from the combination of technological advancements such as robotics and imaging systems with newly found pharmaceutical products, becoming a very diverse and interdisciplinary field. One of the most exciting and fascinating innovations was the laser in 1960 [1], which also became a significant tool in the medical field. The first reported experiment for the use of lasers in medicine was performed by Zaret et al. [2] with a pulsed ruby laser at a wavelength of 694 µm, who produced ocular lesions in rabbits. These experiments were accompanied by heavy thermal injuries. Nevertheless, the progress for lasers in Ophthalmology was fast, and first treatments on patients were performed by Campbell et al. in 1963 [3] and Zweng et al. in 1964 [4]. About the same time, again a ruby laser was used to demonstrate its value as a surgical tool in dentistry [5]. Applications for medical care grew as improvements of existing lasers and inventions of new ones advanced in the 1970s. For example in Gynecology, Stafl et al. [6] used a CO_2 laser (carbon dioxide laser) at a wavelength of 10.6 µm for the treatment of cervical and vaginal neoplasia in 1977. The development of a fiber optic endoscope by Nath et al. in 1973 [7] enabled Staehler et al. [8] three years later to perform basic

studies in urology with an argon ion laser. Further major medical fields that were explored for laser applications at that time include neurology [9], angioplasty and cardiology [10], dermatology [11], otorhinolaryngology and pomology [12], gastroenterology [13] and orthopedics [14]. Since then, the laser became a frequent and standard medical tool in various medical fields, showing unique benefits in terms of antibacterial activity, induction of wound healing, reduction in bleeding, improved surgical access and ease of use [15]. Today, probably the most advanced laser devices and techniques within the medical field are found in ophthalmology. Confocal laser tomography can be applied as a diagnostic tool to detect retinal alterations in their early stages, which increases the success rate of the according treatment [16]. Optical coherence tomography (OCT) is another diagnostic tool that sees a variety of applications in ophthalmology such as the detection of progressive glaucomatous damage [17] or the determination of peripapillary retinal nerve fiber layer thickness (RNFL) abnormalities [18]. Other ophthalmic applications are mostly therapeutic such as retinal coagulation [19], cataract surgery of the lens [20] and LASIK [21].

While laser applications in most of the above mentioned medical fields are fairly advanced, their use for hard tissue ablation is not yet at a stage where it can be considered as a standard tool for osteotomy purposes, which is the focus of this thesis. Hard tissue ablation has its origin in dental applications as early as 1964 [5]. In this these first experiments, the treatment induced severe thermal damage to nerve fibers and caused cracking of the hard tissue. Only in 1972 Stern et al. resumed the investigation of lasers for tooth treatment, this time with the CO_2 laser [22]. But since the results did not improve much compared to Goldman et al. [5], Stern et al. [23] concluded two years later that the laser is not an applicable tool for dentistry as long as thermal damage is not eliminated completely. In 1973 Moore [14] used a CO_2 laser for orthopedic experiments, i.e. laser osteotomies, which was further investigated by Claymen et al. in 1978 [24]. Gertzbein et al. [25] and Pao-Chang et al. [26] continued with studies on bone healing after laser treatments in 1981. All authors found that the osteotomies could not be performed without the induction of thermal damage to the surrounding tissue, which resulted in impaired healing processes as compared to conventional tools. During the next years, several other laser

systems were tested, like the Ho:YAG laser with a wavelength of 2.12 µm by Nuss et al. [27], without significant improvements though. In 1989 Hibst and Keller introduced the Er:YAG laser (erbium-doped yttrium aluminum garnet laser) for hard tissue ablation [28]. Its wavelength of 2.94 µm has an absorption peak in water which enhances the efficiency of the hard tissue ablation process. Frentzen et al. [29] discovered in 1994 that this thermomechanical interaction resulted in small fissures or cracks within the hard tissue. They proposed an external cooling of the treated tissue during the interventions to reduce these negative effects. Still, CO_2 and Er:YAG laser systems continued to produce thermal damage to the surrounding tissue [30, 31] until Kang et al. [32] investigated laser hard tissue ablation under various environments in 2008. They reported that the ablation was particularly clean and without any thermal damage during water spray cooling and suggested such systems as a viable technology for laser osteotomies. A breakthrough for cutting and treatment of normal and diabetic bone without any histological detectable damage was achieved and investigated by Akyol et al. with the use of an Er:YAG laser in 2009 [33]. An animal study in sheep was performed by Stübinger et al. in 2010 [34] to compare osteotomies with an Er:YAG laser system as compared to a state-of-the-art piezoelectric device. They used an Er:YAG laser with an external water spray cooling system to prevent thermal damage to the surrounding tissue. The resulting osteotomy cuts in the sheep's tibia were histologically evaluated after a two and three months healing period, respectively. The authors stated that the "*laser osteotomies were well-defined leaving no carbonization effects or any other negative surface alterations*".

This PhD thesis was started in 2013. Until then, no more significant developments were made compared to Stübinger et al.'s results from 2010 in the field of laser osteotomies. It was part of the development of a computer assisted and robot-guided laser osteotome (CARLO) at the private company Advanced Osteotomy Tools AG (AOT AG) in collaboration with the University of Basel and the University Hospital of Basel, all located in Basel, Switzerland.

A lot of medical interventions require cutting or drilling of hard tissue, i.e. different bone and teeth. The development of novel cutting tools for osteotomies focuses on more precise, more efficient and less traumatic performances, resulting in an overall better outcome for patients. But the most frequently used tools are

conventional drills [35] or surgical saws. These tools carry great risks of damaging the surrounding tissue as well as the bone itself through massive contact pressure, the increase of local temperatures due to frictional heat generation, the broadening of cuts, the deposition of metal shavings and bacterial decontamination [36, 37, 38]. Progress was made with the development of piezo electric tools which reduce but not avoid the above mentioned side effects, resulting in a better biological outcome [39]. Still, its cutting or drilling tip provides the typical limitations associated with mechanical tools; cutting geometries are limited by the size and shape of the tip which can create only straight or gently curved lines and rotation symmetric holes [40]. A beneficial alternative would be contact free laser osteotomes, which eliminate all the mentioned drawbacks of mechanical tools and can be used in a small operation field, offering functional cutting geometries as well as hemostatic and aseptic effects [36, 41, 42].

The first laser cleared by the US Food and Drug Administration found its application in the dental field for cutting teeth in 1997 [43]. However, the limiting factors for a routine application of lasers for osteotomies are mainly technical drawbacks as listed below [38, 44]:

- Depth control along the beam path.
- Optical system design and the engineering of an according cutting tool, i.e. laser head.
- Safe and precise guidance of the laser head and cutting laser beam.
- Investigation and definition of laser light and hard tissue interaction.
- Conditioning of the treated and surrounding tissue to prevent any thermal or mechanical damage.
- Healing support for the achieved laser osteotomy cuts.
- Preoperative planning.

The CARLO device includes besides the medical applications pre-operative planning, medical imaging, robotics, software development and laser physics. To

be successful in such a multi-disciplinary project, a very close collaboration with experts in their respective fields was necessary. The main contributions of this thesis to develop a commercial medical laser osteotome are described in the following paragraphs. Preliminary experiments were mostly performed in in-vitro studies on animal and human cadaver bone. Afterwards, the results were applied successfully in three animal studies.

1.2 Contribution of this Thesis

Laser light and hard tissue interaction Investigation of light and hard tissue interaction using a variety of lasers with different beam characteristics such as wavelength, beam profile and operating modes (pulsed, quasi-continuous wave), were performed before the start of this thesis. The application and investigation of the found laser system, i.e. a pulsed, flash lamp pumped Er:YAG laser, and the resulting thermo-mechanical interaction was a big part of this thesis. Methods and results were evaluated and compared to find the best suited laser conditions, e.g. pulse width and repetition rate, to perform functional and precise cuts for laser osteotomies in the most efficient way, without inducing thermal or mechanical damage.

Optical system design and laser head engineering The beam coming out of the laser system was conditioned in shape, focal point (size and energy density) and working distance to the targeted tissue. The optical arrangement to achieve the desired cutting performance includes several optics amongst others a beam expander, a focusing lens and a scanner which guides the beam in cooperation with the robotic arm according to the preoperative planning to achieve the desired functional cuts. Here also parameters like optical losses, scanning mode, lens materials and long-term stability were taken into account. Furthermore, a visual system in form of a CCD-Camera was integrated to monitor the whole surgery. The monitoring in real-time acts primarily to observe and record the osteotomy, secondarily as another safety feature and thirdly as an additional navigation and calibration support device. All these parts were aligned and integrated in a very compact laser head to be able to mount it on a robotic arm without exceeding its

payload. Such a compact design was necessary to ensure the accessibility of the operating field for the medical instruments, e.g. suction tubes or surgical staples. Furthermore, a small laser head can reach more areas along the patients body than a larger one. This part was focused on opto-mechanics, light conditioning and the interaction between the individual parts. Other elements, like an optical feedback system for depth control and several safety features, were integrated into the laser head, but not developed within the scope of this thesis.

Treated and surrounding tissue conditioning During laser osteotomy, issues like heat control, i.e. prevention of carbonization of the targeted and surrounding tissue are crucial for the healing process. A well establish method applied in many cutting techniques of all kinds is to cool the tissue with a water spray produced by a nozzle during the procedure. Such a nozzle was developed and after successful applications in animal studies patented. Main parameters for such tissue cooling methods are the amount of liquid flow, the pressure applied to vaporize the liquid and the resulting droplet size of the vapor. Furthermore, engineering and application conditions like a very short design to maximize the working distance between the laser head and targeted area were overcome. At the same time, the vapor is used to clean the cuts from blood, other liquids and bone debris. The cleaning is necessary to avoid that these liquids fill up the cuts and avert the ablation of hard tissue by absorbing the light.

Chapter 2

Background

2.1 Laser Light Fundamentals

This section describes basic physical interactions for lasers, beam propagation and beam parameters. All given information is based on two books. The first is *Optik für Ingenieure* [45] Chapter 21 and Chapter 22. The second book is *Laser: Bauformen, Strahlführung, Anwendungen* [46] Chapter 1, 2 and chapter 12. Both books are published by the Axel Springer publishing house.

2.1.1 Elementary Light and Matter Relations

The nature of light is closely related to the elemental structure of matter. According to the Bohr atom model, all matter is made from atoms. A positively charged nucleus (consisting of neutrons and protons) is encircled by negatively charged electrons. The electrons move on concentric orbits around the atomic nucleus. The balance (in the rotating system) between the centrifugal force acting on the electrons, and the electrostatic attraction by the oppositely charged core keeps them in orbit. The Bohr atom model does not show the complete interdependency, but is sufficient enough to explain the basics without the need to dive into the quantum mechanical model. An atom can absorb energy from the environment and store it for a certain amount of time before releasing it, during which the atom is in a so-called *excited state*. However, an atom is unable to absorb energy of any size but only strictly defined quantities. The energy absorption can

be imagined as the lifting of the electrons into strictly defined wider concentric orbits around the nucleus. The orbit radius does not change continuously, but performs so-called quantum leaps. Thus, when an electron leaps from one orbit to another, a fixed amount of energy is absorbed or released. This interaction of energies create quantized energy states E_0, E_1, E_2, etc. This quantum of energy is exchanged between atoms in the form of electromagnetic radiation (photons).

The physical nature of electromagnetic radiation can not be clearly defined. On the one hand, it has a wave nature, which is evident by phenomena such as interference and diffraction. On the other hand, light shows a particle character, i.e. quantum optics. Such particles are called photons. These two models can not be comprehended at the same time, since an electromagnetic wave is an energy transport process without any mass, and a particle has a mass by definition. In physics, this state is referred to as wave-particle dualism. The relationships between photon energy, wavelength, frequency and propagation velocity are described by the following two equations.

$$c = \lambda\nu \ [\mathrm{m\,s^{-1}}] \tag{2.1}$$

c: propagation velocity (speed of light)
λ [m]: wavelength
ν [Hz]: frequency

$$E = h\nu = h\frac{c}{\lambda} \ [\mathrm{J}] \tag{2.2}$$

E: photon energy
h [J s]: Plancks constant (natural constant)

The photon energy can be calculated directly from the wavelength of the light. Conversely, this determines the wavelength of the light emitted by an excited atom. It is determined by the energy difference between the excited state (E_1 and above) and the ground state (E_0), which is also equal to the energy released

as a photon.

$$E_{excited} - E_{ground} = h\nu \tag{2.3}$$

The leaps of electrons to other energy states originate from absorption, spontaneous emission or stimulated emission of photon energy as shown in Figure 2.1. As mentioned above, absorption occurs when an incident photon has exactly the energy to lift an electron from the ground energy state of the atom to an excited state. Excited states can be differentially stable and have a lifetime. At the end of this lifetime, an atom will release its stored energy without external influence. This process is defined as spontaneous emission. In addition, stimulated emission occurs when an excited atom is hit by a photon whose energy value corresponds exactly to the stored energy. Whereupon, stimulating the atom to transit from its excited to its ground state, by emitting a photon that has the same energy, direction and polarization as the triggering photon. Consequently, this process produced two identical photons and an increase in intensity, which allows the amplification of light in the laser.

2.1.2 Essential Components and Functionality of the Laser

The essential components of a laser are an active laser medium (amplifier), a resonator and a pumping energy source as shown in Figure 2.2. The resonator consists of a highly reflective rear mirror and a partially reflecting out-coupling mirror. The formation of laser radiation is based on the above discussed process of stimulated emission, which induces an amplification of radiation. Hence the name LASER (light amplification by stimulated emission of radiation).

The probability of the absorption of a photon by an unexcited atom is the same as the probability of stimulated emission of an excited atom. Hence, an increase in the number of photons passing through the laser medium is only possible if there are more atoms in the excited state than in the ground state. However, this is not achievable under normal circumstances, since energetic excitation can at most cause an equal occupation of the upper level. In order to achieve a higher

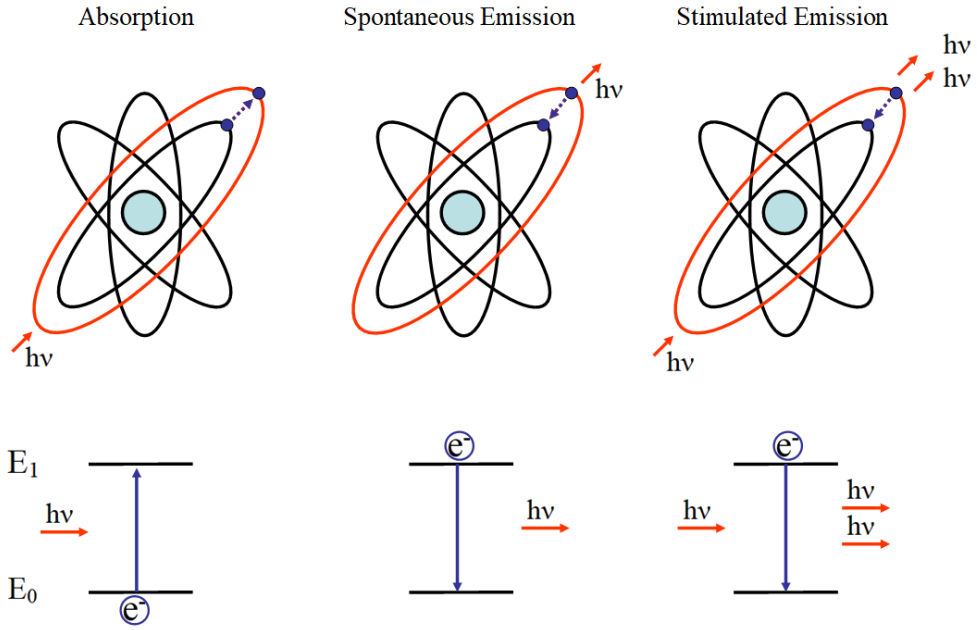

Figure 2.1: Absorption, spontaneous emission and stimulated emission of photon energy by atoms.

occupation in the upper level than in the lower level at least three energy levels of different lifetimes are exploited. Thus, a population inversion can be achieved between the upper and lower laser levels as shown schematically in Figure 2.3 for the example of a 4-level system (Nd:YAG laser). The atoms are initially excited by the pumping energy to a higher level. In principle, all atoms, molecules, etc. strive for their lowest energy state and relax very quickly to the long-lived upper laser level. If now one electron leaps through spontaneous emission to the energetically lower level (lower laser level), the energy difference is emitted in the form of a photon. This one photon stimulates another electron of the active laser medium to the transition to the lower energy level (stimulated emission). However, the occupation of the lower laser level remains low, since it is very short-lived. Thus, a very effective population inversion can be achieved, which causes a chain reaction like amplification of the radiation. The amplified light is reflected back and forth within the resonator exactly in itself to be further amplified. Finally, a part of it exits the resonator through the out coupling mirror as the actual laser beam.

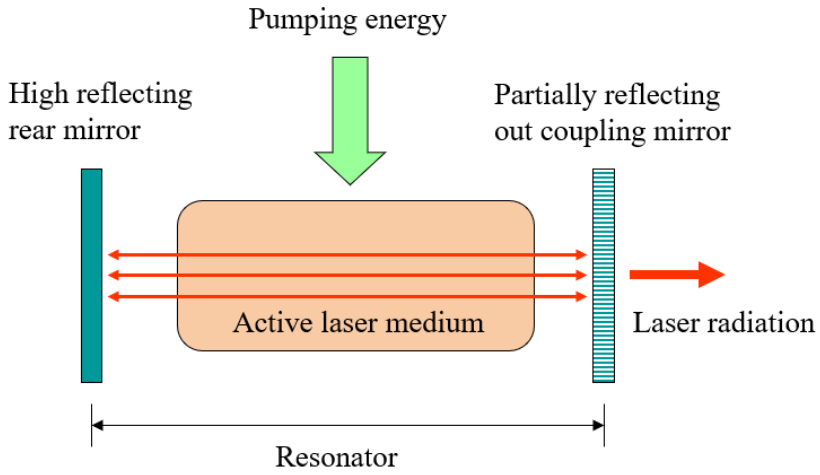

Figure 2.2: Basic structure of a laser, consisting of laser medium (amplifier), resonator and pumping energy source.

In each resonator, the amplification of several vibration frequencies is possible. In addition to the fundamental frequency, even integer multiples of the fundamental frequency are generally amplified. Reason is the forming of standing waves in the resonator. The condition for the formation of standing waves is that the length of the resonator is an integer multiple of half the wavelength. The various standing waves that are possible in the resonator are referred to as resonator modes.

$$L = n\frac{\lambda}{2} \text{ [m]} \tag{2.4}$$

L: resonator length

n: number of wave trains

Since the geometrical dimensions in optical resonators are generally large in relation to the wavelength, the number of wave trains in the resonator is very high. Conversely, the wavelengths of adjacent modes are very close together and are usually not resolved. In addition to these so-called longitudinal modes, transverse modes also occur in the optical resonator. These are of greater importance for the achievable beam quality. They are the result of diffraction and interference phenomena in the resonator and reflect the spatial distribution of the vibrational

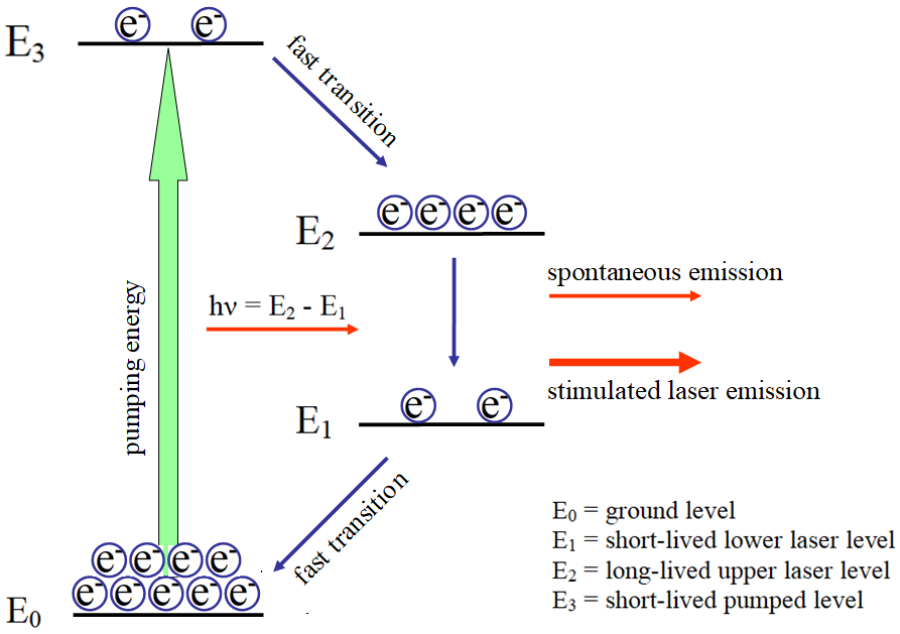

Figure 2.3: Generation of a population inversion using the example of a 4-level system (Nd:YAG laser).

energy in the resonator. According to their order in two dimensions, they are referred to as TEM_{mn} (transverse electromagnetic mode). Maximum focus-ability of a laser beam can only be achieved if the entire laser power comes from only the fundamental mode TEM_{00}, which is called a *Gaussian Beam*.

2.1.3 The Gaussian Beam

The following paragraphs give an overview of the most important parameters for Gaussian and non-Gaussian rotationally symmetric laser beams. Figure 2.4 shows a Gaussian beam propagating along the optical axis z, with all relevant parameters that are explained in the following paragraphs.

Beam Quality In laser applications, there are usually no Gaussian beams (TEM_{00}). Reasons for this are oscillation of higher transverse modes in the resonator, amplitude- or phase shifts, interference of beam parts and inhomogeneous gain and temperature distribution within the laser medium. Therefore, the beam propagation ratio M^2 and the beam quality factor K are introduced. For

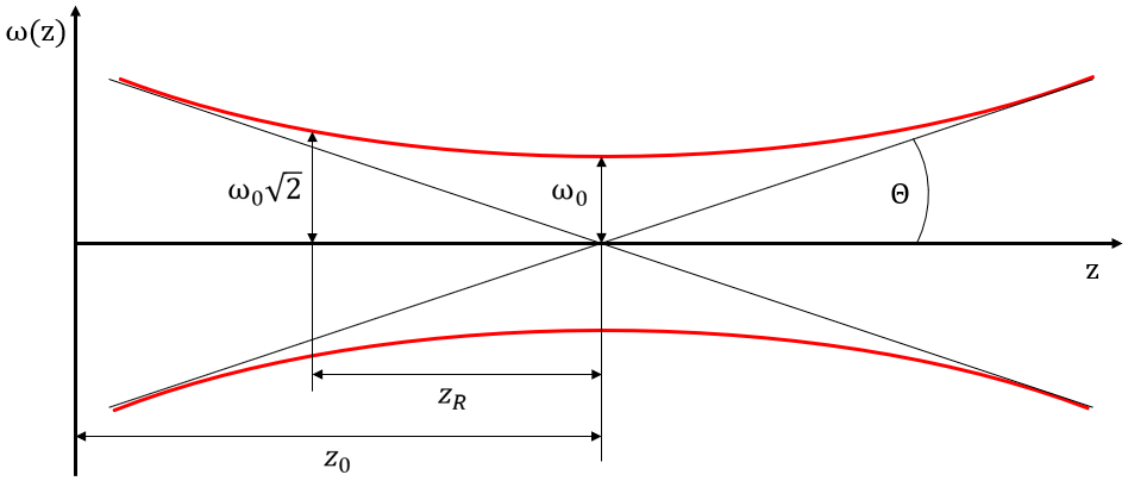

Figure 2.4: Gaussian beam radius ω as a function of the beam propagation along the optical axis z.

Gaussian beams the relationship is $M^2{=}K{=}1$. Both describe how close a non-Gaussian beam is to a Gaussian beam. A good beam quality and beam stability are important parameters for reliable and reproducible results.

$$M^2 = \frac{1}{K} = \frac{\pi\omega_0\Theta}{\lambda} \tag{2.5}$$

ω_0: focal spot radius (half the beam waist)

Θ: half opening angle in the far field for the divergence

$$\Theta = \frac{\lambda}{\pi\omega_0} \tag{2.6}$$

Beam Parameter Product To fully define the beam quality the beam parameter product q is introduced.

$$q = M^2\frac{\lambda}{\pi} \tag{2.7}$$

$$q = \omega_0 \Theta \tag{2.8}$$

The beam parameter product and the focal spot radius can be influenced with beam shaping optics, e.g. expander, but their product stays constant. Also, the higher the beam parameter product, the lower is the beam quality.

Depth of Focus The depth of focus Δz is the region around the beam waist position z_0, in which the beam waist is within defined parameters.

$$\Delta z = \pm \frac{n\pi\omega_f^2}{\lambda} \sqrt{\left(\frac{\omega}{\omega_f}\right)^2 - 1} \tag{2.9}$$

ω/ω_f: tolerable change of the beam width
n: refractive index of the material the light is propagating through

For $\omega >> \omega_f$ follows:

$$\Delta z = \pm \frac{n\pi\omega\omega_f}{\lambda} \tag{2.10}$$

This defines two different sections of the laser beam propagating away from the beam waist along the z-axis. The near field, where $\omega \approx \omega_f$ and the far field, where $\omega > \omega_f$. The near field is also called the Rayleigh-range, with the Rayleigh-length z_R.

$$z_R = \pm \frac{n\pi\omega_0^2}{\lambda M^2} \tag{2.11}$$

Whereas n is usually 1 for air, and M^2 is the beam propagation ratio taken into account only for non-Gaussian beams. The beam radius is $\sqrt{2}$ times larger at z_R then at z_0. The Energy density decreases quadratic along the z-axis and has only half of its value at z_R.

Focusing A Gaussian beam has a width evolution along the direction of the optical axis z, when being focused by a focusing element, e.g. lens or mirror. The focal spot radius ω_0 at z_0 depends on the focal length F of the focusing optic, and the beam parameters ω_D (radius) and Θ_D (divergence) before the optic.

$$\omega_0 = F\Theta_D = \frac{Fq}{\omega_D} = \frac{M^2\lambda F}{\pi\omega_D} \tag{2.12}$$

2.1.4 Important Mathematical Relations for pulsed-Laser

Average Power, P The average power is equivalent to the optical power of a laser system, which is a measure of how much energy is transferred in a unit of time, i.e within the duty cycle of a pulsed laser system. Hence, the average power is literally the average of the power delivered over the course of one on/off cycle of the laser system.

$$P = E_p\nu \text{ [W]} \tag{2.13}$$

ν [Hz]: pulse repetition rate (frequency)

Peak Power, P_p To get the actual maximum power delivered per pulse, the peak power must be calculated.

$$P_p = \frac{E_p}{\tau} \text{ [W]} \tag{2.14}$$

E_p [J]: pulse energy
τ [s]: pulse duration

Average power, peak power, pulse energy, pulse duration and pulse repetition rate are important properties to actually chose and characterize a pulsed laser system. Though for the work with such a laser system are the resulting power densities and energy densities for a given point along the propagation of the laser beam far more important. They determine the interaction between the laser light and targeted matter, e.g. biological tissue [47], with the highest values at the smallest beam waist.

Focus Area

$$A = \frac{\pi d^2}{4} \ [\mathrm{m}^2] \tag{2.15}$$

d [m]: beam waist diameter

Power Density in Focus

$$S = \frac{P_p}{A} \ [\mathrm{W/m}^2] \tag{2.16}$$

Energy Density in Focus

$$W = \frac{E_p}{A} \ [\mathrm{J/m}^2] \tag{2.17}$$

2.2 Actions of Matter on Light

This section describes how matter can influence incident light in three basic ways; reflection, absorption and scattering. Which of these actions occur or how dominant they are depends mostly on the type of material and the wavelength of the incident light. All given information are based on the book *Laser-Tissue Interactions: Fundamentals and Applications* [47] Chapter 2 and Chapter 3, published by the Axel Springer publishing house.

2.2.1 Reflection and Refraction

When light hits the surface of a medium (e.g. tissue) with a different refractive index (n_2) as the medium (n_1) it travels in (e.g. air), parts of it will be sent back into the original medium (n_1) at the same angle as the angle of incidence. This

phenomenon is called specular reflection and assumes a smooth surface of the hit medium, i.e. surface irregularities are small compared to the lights wavelength. Both, the incident beam and the reflected beam lie in the plane of incidence. The refractive index of a medium is defined as following.

$$n = \frac{c}{v} \tag{2.18}$$

c [$\mathrm{m\,s^{-1}}$]: speed of light in a vacuum
v [$\mathrm{m\,s^{-1}}$]: speed of light in a medium

In the case of tissue, the surface irregularities are usually large compared to the lights wavelength. This leads to the so-called diffuse reflection, where several beams are reflected in different angles into different planes.

Unreflected light enters the new medium and travels within, whereas the new refractive index (n_2) changes the speed of light and the propagating direction resulting in the phenomena known as refraction. Figure 2.5 shows the principle of specular reflection and refraction.

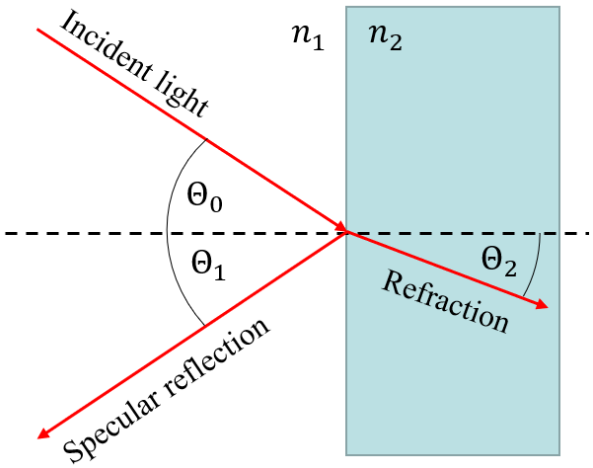

Figure 2.5: Principle of specular reflection and refraction.

The mathematical relationship between incident beam and refracted beam is given by Snell's law.

$$\frac{\sin\Theta_0}{\sin\Theta_2} = \frac{v_0}{v_2} \tag{2.19}$$

Θ_0: angle of incidence
Θ_2: angle of refraction
v_0 [$\mathrm{m\,s^{-1}}$]: speed of light in original medium with n_1
v_2 [$\mathrm{m\,s^{-1}}$]: speed of light in new medium with n_2

Snell's law can be simplified by taking the definition of the refractive index into account.

$$n_1 \sin\Theta_0 = n_2 \sin\Theta_2 \tag{2.20}$$

Whereas, for $\sin\Theta_2 > n_2/n_1$ no refraction occurs and all light is reflected back. This special case is known as total reflection.

2.2.2 Absorption

When light passes through a medium, its intensity can be attenuated through a partial conversion into heat motion or vibrations of the molecules within the medium. This effect is called absorption. The absorbance of a medium is defined as the ratio of absorbed and incident intensities. A medium is called transparent when no absorption occurs, and opaque when all incident light is absorbed. The absoption capabilities of a medium depend mainly on the electronic constitution of its atoms and molecules (quantized energy states E_0, E_1, etc.), the wavelength of radiation (photon energy must be equal to the quantized energy states gaps), thickness of the absorbing layer and internal parameters, e.g. temperature. Absorption of radiation through a medium can be described using the Lambert-Beer law.

$$I_{(z)} = I_0 e^{-\alpha z} \text{ [J]} \tag{2.21}$$

$I_{(z)}$: intensity at a distance z within the medium
I_0 [J]: incident intensity
z [m]: distance within the medium along the optical axis

α [1/m]: absorption coefficient of the medium

2.2.3 Scattering

Scattering is the basic origin of dispersion and occurs when light enters a medium and its photon energy does not correspond to the quantized energy state gaps of the medium, i.e. it does not get absorbed. In other words, the frequency of the incident photons is out of resonance to the natural frequency of the mediums particles. The photons now interact with the particles through forced vibration, which amplitude is much smaller as in the case of resonance (absorption). Forced vibration will have the same frequency and direction as the incident light, but a different phase which causes the photons to slow down when penetrating a denser medium. There are different forms of scattering; elastic and inelastic scattering, which are distinguished by whether parts of the incident photon energy is converted during the scattering or not. In biological tissue, photons are preferably scattered in the forward direction as shown in Figure 2.6. Further explanations of these processes and special scattering cases like the Rayleigh scattering or Mie scattering can be found in the given source [47].

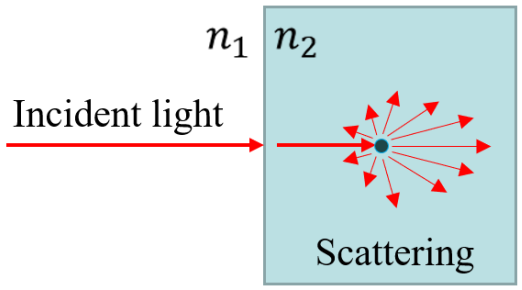

Figure 2.6: Principle of scattering, which occurs preferably in the forward direction within biological tissue.

2.3 Actions of Laser-Light on Matter

The interaction mechanisms for laser light on biological tissue depends mostly on its optical properties like the coefficients of reflection, absorption and scattering

and its thermal properties like heat conduction and heat capacity. The laser light itself influences these interaction mechanisms through its wavelength, exposure time, applied energy, focal spot size, energy density and power density. Together they attribute the five main categories of interaction types; *photochemical interactions, thermal interactions, photoablation, plasma-induced ablation and photodisruption*. The most significant parameter here is the energy density, which ranges from $1\,\mathrm{J/cm^2}$ to $1000\,\mathrm{J/cm^2}$. The energy density is in a rather narrow spectrum when compared to the range of the power density of over 15 orders of magnitude. Figure 2.7 shows the main laser tissue interactions based on their associated laser parameters. Exposure times of Er:YAG lasers, i.e. their pulse length, lie in the time scale of 1 min down to 1 µs, which determines its interaction with biological tissue as a thermal one. Such a laser is used in the CARLO device. Hence, the focus of the following discussion is on thermal interactions and why the Er:YAG laser is a perfect fit for hard tissue treatment.

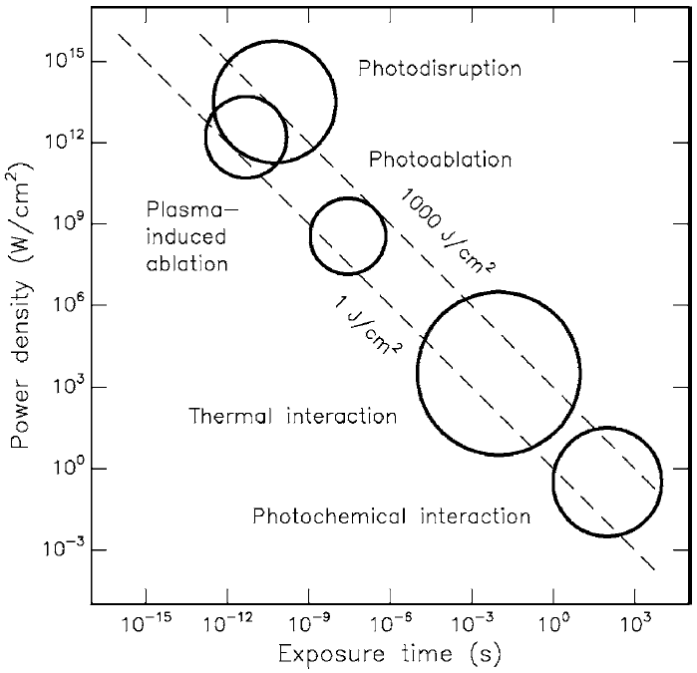

Figure 2.7: Main laser tissue interactions based on their associated laser parameters [47].

Thermal interactions are based on the local temperature increase within the

tissue induced by laser radiation, which can cause different effects based on the duration and peak value of the tissue temperature achieved; *coagulation, vaporization, carbonization and melting*. For all effects, the absorption of a certain wavelength within the different molecules of the tissue determines its nature. The Er:YAG laser radiation with a wavelength of 2.94 µm is strongly absorbed in the water content of tissue, leading to the effect of vaporization. As shown in Figure 2.8, it has the highest absorption coefficient based on its wavelength compared to other laser. Water molecules absorb the laser radiation until they expand as vapor at 100 °C , which is contained by the rest of the tissue. The resulting localized pressure build-up from this phase transition leads to microexplosions which ablate the tissue as a thermomechanical effect called thermal decomposition.

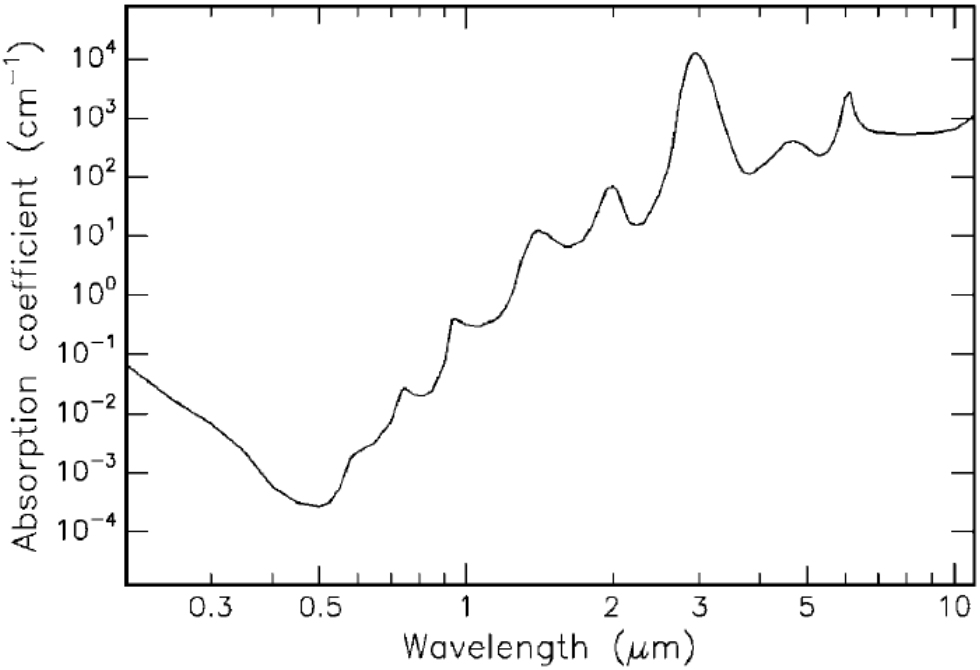

Figure 2.8: Absorption of water based on the absorption coefficient at a given laser radiation wavelength [47].

Chapter 3

A compact, efficient and light weight laser head for CARLO: integration, performance and benefits

This chapter presents the peer-reviewed publication presented at the *SPIE* conference in August 2015, San Diego, California, United States. Afterwards, it was published online as an article for *Novel Optical Systems Design and Optimization XVIII* under the proceedings of *SPIE* 0277-786X, Vol. 9579 957905-1.

The paper introduces the results of the CARLO laser head development after the second animal study. It describes the engineering of a compact and robust laser head as a cutting tool for a laser osteotomies. The central element is a flash lamp pumped Er:YAG laser as the cutting light source. Further, a CCD-camera is installed to calibrate the laser head and to monitor and record the cutting process in real-time. The laser beam is guided and profiled by optical components, before a fast steering mirror scans it along the pre-planned cutting geometry. Lastly, a nozzle array conditions the targeted tissue to cool it and prevent thermal damages, i.e. it rehydrates it, while keeping the operating field clean of liquids and bone debris.

It was shown in in-vitro experiments that such a laser head performs arbitrary,

3D navigated osteotomies with less than 1 mm cutting width and achieves maximum precision compared to conventional tools. Furthermore, a controlled, safe and precise transfer of pre-operatively planned osteotomy patterns to the surgical site is made possible. With the fully automated cut execution and its precise reproducibility, the CARLO opens up new possibilities in osteotomic procedures.

A compact, efficient and light weight laser head for CARLO®: integration, performance and benefits

Waldemar Deibel*[a,b], Adrian Schneider*[a,b], Marcello Augello*[c,d], Alfredo E. Bruno*[a], Philipp Juergens*[c,d], Philippe Cattin*[b]

[a]Advanced Osteotomy Tools AG, Basel 4057, Switzerland; [b]Medical Image Analysis Centre, University of Basel, Switzerland; [c]Hightech Research Centre of Cranio-Maxillofacial Surgery, University of Basel, Switzerland; [d]Department of Cranio-Maxillofacial Surgery, University Hospital Basel, Switzerland

ABSTRACT

Ever since the first functional lasers were built about 50 years ago, researchers and doctors dream of a medical use for such systems. Today's technology is finally advanced enough to realize these ambitions in a variety of medical fields. There are well-established laser based systems in ophthalmology, dental applications, treatment of kidney stones, and many more. Using lasers presents more than just an alternative to conventional methods for osteotomies. It offers less tissue damage, faster healing times, comparable intervention duration and in consequence improves postoperative treatment of patients. However, there are a few factors that limit routine applications. These technical drawbacks include missing depth control and safe guiding of the laser beam. This paper presents the engineering and integration of a miniaturized laser head for a computer assisted and robot-guided laser osteotome (CARLO®), which can overcome the mentioned drawbacks. The CARLO® device ensures a safe and precise guidance of the laser beam. Such guidance also enables new opportunities and methods, e.g. free geometrical functional cuts, which have the potential to revolutionize bone surgery. The laser head is optimized for beam shaping, target conditioning, working distance, compactness and the integration of all other parts needed, e.g. CCD-cameras for monitoring and referencing, a visible laser for cut simulation, etc. The beam coming out of the laser system is conditioned in shape, energy properties and working distance with an optical arrangement to achieve the desired cutting performance. Here also parameters like optical losses, operating mode, optics materials and long-term stability have are taken into account.

Note: Prof. Philippe C. Cattin and Dr. Philipp Juergens contributed equally to this paper.
Keywords: laser osteotomy, robot guided surgery, laser head, functional cuts, bone, navigation

1. INTRODUCTION

Conventional mechanical rotating or oscillating tools like drills or saws are still standard to perform drill-holes and cuts in bone tissue during surgical interventions. The large variety of different tools for drilling and cutting have in common that they only provide very limited freedom in their cutting geometries (straight or gently curved lines and rotation symmetric wholes). Furthermore, because of massive contact pressure, vibration and friction, these conventional methods carry great risks of damaging the surrounding tissue as well as the bone itself [1,2]. Such mechanical trauma and thermal damage occur even if the intervention is performed with great care. Moreover, a broadening of cuts and a subsequent deposition of metal shavings and bacterial contamination are negative side effects [15]. The more complicated the anatomical location, and the closer the surgery is to nerves and vascular structures, the higher the risk of damage. Cranio-maxillofacial surgery is a good example of a high risk and delicate interventions, which are conducted with these conventional cutting tools[3]. Recently, piezoelectric osteotomy was introduced that reduces the above-mentioned side effects. But its cutting tip is still in direct contact with the bone providing the typical limitations associated with mechanical cutting: the cutting geometry is limited by the size and shape of the tip being in contact with the bone, and the condition of bone itself [4].

A beneficial alternative would be contact-free laser osteotomy, which reduces mechanical vibration and prevents massive bone debris and metal abrasion. Furthermore, it can be performed in a small operation field and offers functional cutting geometries [5,6,7]. The ablation of hard tissue with light depends on several parameters of which the wavelength, the energy density and the laser pulse duration are the most influential ones. The wavelength dependence has been attributed

to the spectral absorption properties of the tissue's water and mineral components [8]. A breakthrough for cutting and treatment of normal and diabetic bone without any histological detectable damage was achieved and investigated by Akyol et al. with the use of an Er:YAG lasers because of the high absorption of their wavelength (2,94µm) in the main components of bone, i.e. water and proteins [9,10]. By additional adequate water cooling, tissue necrosis and charring could be dramatically reduced [11].

However, the limiting factors for a routine application of lasers for osteotomy are mainly technical drawbacks like missing depth control and a safe guidance of the laser beam. The latter problem could be solved by a miniaturized laser system in combination with robotic guidance and an optical feedback system. Most of the technologies to realize such a system already exist, whereas the problem of depth control has only been solved for very specific conditions. Besides some research prototypes no functional system has yet been introduced in the clinic.

The work presented here is part of the development of a computer assisted and robot-guided laser osteotome (CARLO®) at the private company Advanced Osteotomy Tools AG in collaboration with the University of Basel and the University Hospital of Basel, all located in Basel, Switzerland. This paper focuses on the integration, performance and benefits of a compact, efficient and light weight laser head, which can be mounted on an articulated robotic arm to ensure safe and precise guidance of the laser beam.

2. MATERIALS AND METHODS

The CARLO® consist of four major parts; the laser head, the robot, the trolley and the navigation system. The laser head is the cutting tool and is mounted on the robotic arm for safe and precise guidance. The base of the system containing all control units, power supplies, a monitor, etc. is the trolley on which the robot arm is mounted. Last but not least the optical navigation system is guiding the movements of the robot in respect to the operating field. This paper focuses on the optimized laser head for functional cuts in hard tissue. Such an optimization includes several compromises among the influencing parameters to integrate CARLO® into an operating room (OR), see Figure 1.

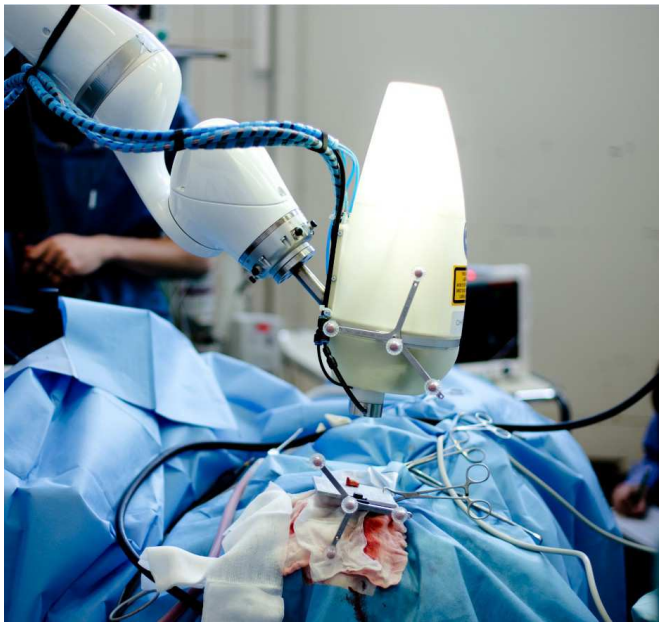

Figure 1: Photo of the current laser head prototype, with all parts integrated, taken during an in-vivo performance in March 2015.

The working distance strongly influences the usability and applicability in an OR environment. A short working distance between the nozzle system and the operating field, i.e. 40mm, leaves no space for other instruments like retractors for soft tissue or aspirator tubes. Furthermore, it limits the space for the laser head positioning and the maneuverability of the robot. Because the robot stops and retracts the laser head from its target when the inner torque sensors detect even

small external forces on the system e.g. due to a gentle collision with the patient. Another drawback of a short working distance is the limited access for the surgeon to actually see the operating area. The working distance is defined by the last focusing optic minus all material afterwards. The tradeoff here is now a long working distance versus a desired spot size, which in turn influences dramatically the cutting performance. A shorter the focal distance, reduces the focus, which leads to a higher energy density for higher cutting efficacy. The size of the nozzle system was engineered to achieve complete visibility on the operating field and at the same time to guarantee a directed and steady vapor onto the target, even for 20mm deep cuts. The desired vapor turns into "fog" after 110mm. Thus, we designed the nozzle system such that it has a distance from the operating area of 75mm, being the working distance.

In this context, the ergonomics must also be mentioned. One of the biggest hurdles a new system for an operating room has to overcome is the integration into it. The medical personal and the devices being already in the operating room must still have enough space to work unobstructed. The new system must assist and complete the existing ones. The CARLO® system fits nearly seamlessly in the operation routine [14].

The next challenging parameter is the cutting speed. Since we operate with a pulsed laser system, we need to balance the overlapping percentage of the focal spot and the scanning speed to achieve an efficient ablation process. We adapted the scanning speed according to the focal spot size and tissue for each intervention to create a clean and straight cutting line.

Compactness is the key word in nearly all components within the laser head. Not only assists a small laser head the system in terms of ergonomics and visibility, it also allows the robot to maneuver more freely. Furthermore, the weight of the laser head cannot exceed the maximum payload of the robotic arm divided by four according to the regulations for medical devices. Our laser head with dimensions of L=350mm; W=160mm; H=160mm and a weight of 2.5kg fulfills all requirements.

Optics

The optical components in the laser head guide and profile the Er:YAG ablation beam and align it with the depth measurement and VIS beams coaxially. One of the goals is a long photo ablation zone b=20mm at a working distance of 75mm from the end surface of the laser head, here the nozzle system, to the operating area with the necessary energy density to ensure efficient and carbonization free laser osteotomy, see Figure 2.

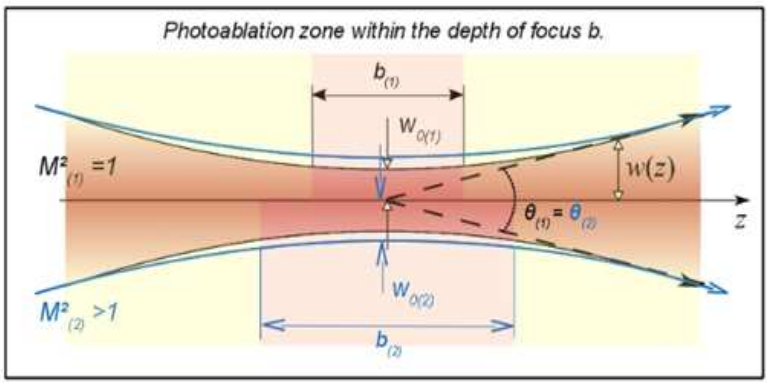

Figure 2: Propagation of a Gaussian beam and a beam with $M^2>1$ after being focused by the same optic along the z-axis.

One of the most important aspects is to minimize the overall losses within the optical system to achieve the highest possible energy density. Our laser head shows overall optical losses of 35%. The average energy density to ablate hard tissue effectively should be higher than 30mJ/cm^2. We achieve energy densities of 70±15mJ/cm^2.

Laser Sources

We have three different laser sources being coaxially aligned and integrated in the laser head. The ablation laser is a pulsed Er:YAG with a wavelength of 2940nm. It is a custom made laser system for osteotomies and operates with an

energy range from 150mJ to 600mJ and pulse rates from 5Hz to 35Hz. We can vary these parameters to achieve osteotomic cuts of 650µm to 1000µm width. The biggest benefit of this particular laser system is the compact design of its laser source (L=155mm; W=35.5mm; H=48.5mm), which can be integrated into the laser head independently from its controller, cooling system and power supply.

The depth control system is OCT based with a state of the art swept source in the near IR, which is integrated in the trolley of the CARLO® device. A single mode fiber, the measuring arm, guides the light into the laser head where it is coupled into a collimator.

The last laser is a visible laser diode with a wavelength of 530nm, which is integrated within the OCT system and coupled via a beam splitter into the measuring arm. The beam splitter ensures few losses for the measuring beam and an output power of the green laser of lower than 1mW, to keep the system as a class I laser device and ensure safety for the user. We use it to reference the laser head to the navigation system and to simulate the desired cuts. Furthermore, it provides an additional safety feature to our system by showing the beam path' of all laser sources and allows the surgeon to survey the process optically.

The green laser and OCT laser are delivered coaxially aligned to each other into the laser head. Therefore, we can use the visible light to align all three beams coaxially via a dichroic mirror.

Monitoring Cameras

The current laser head has two high resolution CCD-cameras integrated at the front within the laser head. The very compact design (L=19.1mm; W=26.4mm; H=26.4mm) and weight of 26g makes these cameras ideal for our application. Out coupling windows of BK7 glass and smart positioning of the cameras ensure a clear view on the operation area on which the objective is focused. We are using them to calibrate the laser head and to monitor and record the cutting process in real-time.

Tissue Conditioning

In order to avoid carbonization during the ablation process, a nozzle array around the ablation beam was designed to cool and moisturize the ablated tissue with normal saline solution. Three dual nozzles are oriented in 120° to each other and integrated in a housing of L=51mm, an outer diameter of Ø=44mm and an inner bore diameter of Ø=20mm for beam propagation. Each dual nozzle is operated with 5ml/min to 20ml/min and 0.5bar to 3bar. The precise setup is highly depended on the laser parameters and the targeted tissue itself. It is fixed at the out-coupling window of the laser head. The spraying angle and orientation of each individual nozzle is optimized with respect to the working distance and the focus point of the treatment laser. This arrangement ensures an optimal and homogeneous cooling and moisturizing effect on the target tissue area at all cutting angles. The external mixture mechanism of the dual nozzles makes the precise control of droplet size and speed possible. This way we can optimize the vapor for the present cut to ensure droplet penetration in depth. Such a precise control of water applied to the cut enables us also to use a minimum amount of water to minimize absorption losses in it and to be able to keep the cut clean with the high pressure applied.

Scanner

The scanner is a fast steering mirror with low noise, high accuracy (angular resolution <0.6 to <1.2µrads rms), high acceleration/step speed (<5ms for a 1mrad step) and high angular range (±3° mechanical). The mentioned parameters and its compact size of L=41.4mm; W=40.64mm; H=40.64mm make it ideal for our application. Our working distance is 75mm from the laser head to the target tissue and the resulting scan area is 191mm^2.

Robot

Machines are often of great help, especially in terms of accuracy and speed. However, using an autonomous controlled robot is a lethal threat for every human in its reachable range. Therefore, our medical application demands highest standards in terms of robot safety and robot control. The KUKA lightweight robot iiwa, originally developed for space

travels, meets these requirements. Each of its seven joints has a built-in sensitive torque measurement sensor. Even a weak collision leads to an immediate stop of the robot. Further, we specify maximum velocities and forbidden spatial 3D ranges, which adherence is watched on a special hardware close security layer on the robot.

System Control

The positioning of the laser is crucial. Each light pulse has to hit its corresponding destination at the first time. This problem has been tackled by introducing a 2-axes controllable scanner to deflect the laser beam towards its target. We operate in a two step positioning mode, the deflected mirror responds extremely fast to small changes, whereas the robot handles wide moves. To bring the robot, the laser head and the patient into a same coordinate system, the stereo optical tracking solution is used. In particular, an optical marker is attached to the patient and the laser head. By applying highly sophisticated calibration methods [16], a target registration error of 0.5mm on the patient is reached.

In-vitro Experiments

We conducted these in-vitro experiments to demonstrate the possibilities of the CARLO® system performing functional cuts and showing its potential for advanced osteotomies. We conducted the following experiments without a depth control and CT-data based preoperative planning. We converted three geometries with unique shapes into our planning software and projected them on the target area.

The pig shaped geometry has smooth and sharp edges. Furthermore, we choose its size to be L=30mm and H=16mm so it exceeds the scanning range of the scanner. To cut the whole shape, we divided it in six segments (see Figure 3). This means, that after the laser cuts a segment, the robot has to reposition the laser head in space to cut the next one. The Pig gives an overall impression for the two step positioning mode and demonstrates the repositioning precision of the system.

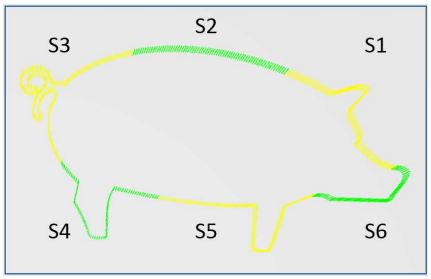

Figure 3: Pig figure with six segments representing the cutting steps. Planned and projected on a prepared bone sample.

The diamond shaped geometry as show in Figure 4, demonstrates the repeatability and precision for angles and sharp edges. The horizontal cut through the middle of the diamond shape is divided in three pieces to avoid deformation at the corners and deeper cuts at the intersection points with the main shape. We cut three groups, each consisting of two diamond shapes, located at a defined gap of 3mm next to each other. Whereas the laser head was repositioned for each diamond shape.

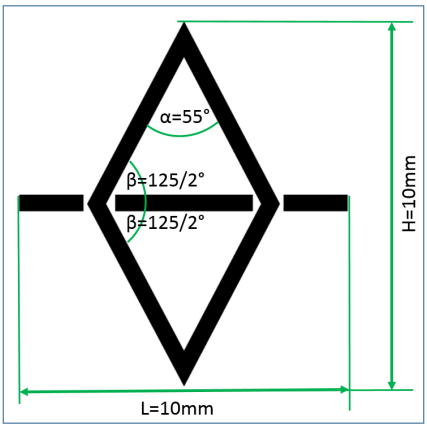

Figure 4: Diamond figure with its dimensions and angles. Planned and projected on a prepared bone sample

For these experiments we produced discs out of cortical cow bone having a mostly homogeneous material to work with. We used a hollow drill with an inner diameter of $Ø_{inner}$=40mm in order to extract the disc from the upper leg of a fresh cow cadaver. Afterwards, we grinded them with a single-disc sanding machine to create discs with thicknesses of 5mm to 8mm and plane-parallel surfaces.

We placed an aluminum target plate with an optical tracking marker being attached to it on a small table and positioned CARLO® next to it, similar to where it would be during a CMF-surgery if the target plate would be the patients head. Then, we fixed the bone disc on that target plate and referenced the target area on the bone discs surface with three point positioning using an in house developed pointer tool. First we simulated the cutting path with the green laser making sure that the figures fit to the size of the disc and that they are positioned at the right place. The laser osteotomy was performed using normal saline spray to avoid carbonization and executed seven scans per geometry/segment.

After cutting, the bone samples were photographed with a digital CCD camera for microscopes, the INFINITY2 from Lumenera. The microscope magnified the picture four times and we evaluated them with the Infinity Analyse software. We calibrated the software according to our microscope. Due to the measurement procedure within the Infinity Analyse software, a manual allocation of the measurement points, an overall measurement error of ±15µm for distances and ±2.5° for angles is expected. Outer dimensions of the geometries are measured with a digital caliper.

3. RESULTS

Pig

Figure 5 shows the cut pig geometry. The overall impression is promising. The shape is clearly defined and in the expected dimensions, L=30.8mm and H=16.65mm. The difference of the dimensions (0.8mm and 0.65mm respectively) to the planned pig size is due to the cutting width with a mean value of 920.51±113.82µm. The rather big standard deviation originates from the positioning inaccuracy. We position the focus point of the treatment laser usually on the surface of the target. Here, the positioning error of the navigation system results in an offset of the focus point away from the target surface and ultimately in a wider cut. Whereas, we cannot determine the direction of that offset with this experimental setup. Even though, details like the tail or neck are clearly cut out as expected.

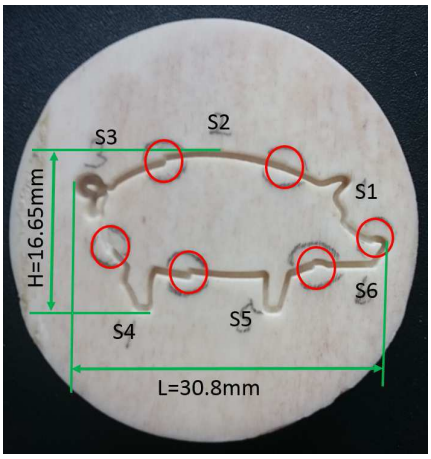

Figure 5: Cut pig geometry with its outer dimensions and segment connecting points marked with red circles.

An unexpected outcome is the big shift of the connection points between segments S2 to S3 and segments S4 to S5. The cause of this shift is the positioning precision of the navigation system, which originates from the calibration of the laser head. It is unusual that one axis shows such a big shift respectively to the others. Figure 6 shows examples of the evaluation and measurements with the Infinity Analyse software.

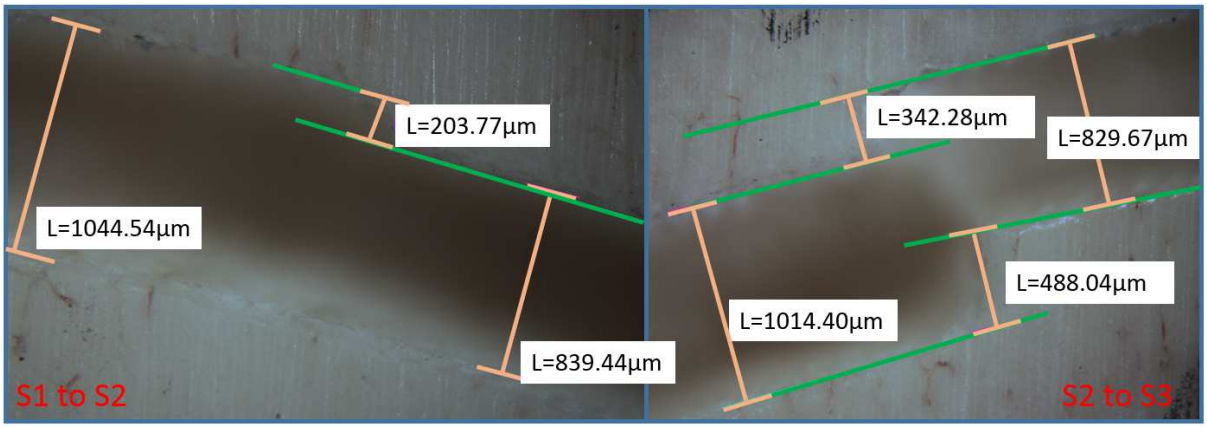

Figure 6: Evaluation of the shifts between the segments with the Infinity Analyze software. Left the connection between segments S1 to S2 and right the connection between segments S2 to S3.

Figure 6 also shows the influence of the focal point offset on the overall shift. If the cutting width would stay stable, the lower and upper shift of the connection points between segments S2 and S3 would be the same. But the measurements show a difference of 145.76µm between the lower and upper shift, which is too big to be explained by measurement errors. Thus, the shifts originate from a positioning error in space. The spatial repositioning error can also be in such a way that it creates a shift in only one direction as for segments S1 and S1. Table 1 shows all measured shifts.

Table 01: Connecting point shifts for the segments of the pig geometry.

Connection Point	S1_S2	S2_S3	S3_S4	S4_S5	S5_S6	S6_S1
Upper shift [µm]	203.77	342.28	189.91	309.33	161.29	138.48
Lower shift [µm]	not visible	488.04	210.90	640.80	229.85	295.7

Diamond

Figure 7 shows the cut pattern with the grouped diamonds. For the evaluation, we measured the cut width of each site of every diamond shape, resulting in 36 measurements. Furthermore, all created angles, six per diamond were taken into account. Whereas the angles of α=55° for the tip of the shapes were evaluated separately (two per diamond shape) from β=62.25° at the bottom (four per diamond shape).

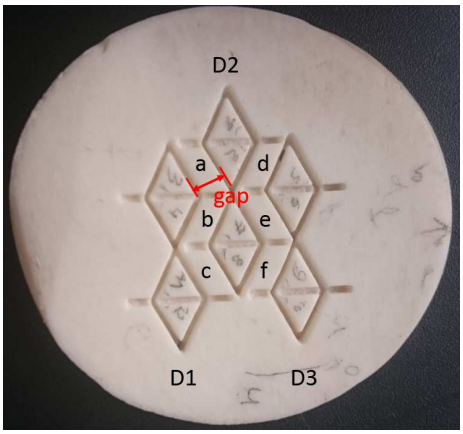

Figure 7: Labelled diamond geometries on the achieved cuts. The marked gap in red shows the measured span for the positioning of the diamond groups.

The outer dimensions of the cut diamond shapes fit with L=10.26±0.14mm and H=10.09±0.07mm very well to the planned ones. It seems minimal to small if we subtract the cutting width of 857.79±66.59µm. Still the relatively small standard deviation indicates a good repeatability.

The measured angles support the above results for the good repeatability with α=53.87±2.59° for the tips and β=61.21±1.70° for the bottoms. Figure 08 shows an example of the angle measurement of a tip and the width of a cut. It also shows the capability to cut sharp edges in the inner path of the laser beam and slightly round ones on the outer path.

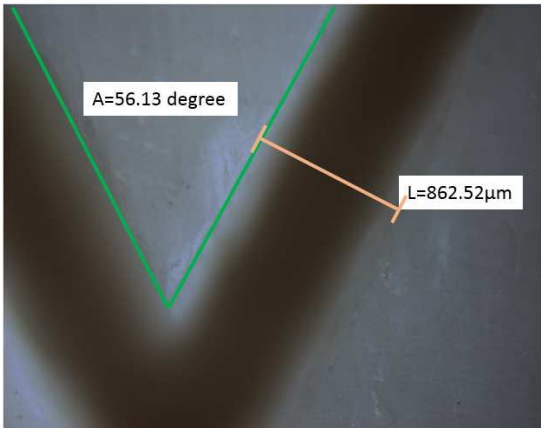

Figure 8: Example for angle and cut width measurements with the Infinite Analyse software for the cut diamond geometries.

In order to evaluate the repositioning precision for this experiment, we measured the gaps between the diamond groups as shown in Figure 7. Whereas gap a, b and c defines the repositioning of D1 to D2 with a mean value of 3.14±0.04mm and gap d, e and f the repositioning from D2 to D3 with a mean value of 3.03±0.02mm. With these values we achieved a very accurate repositioning of the planned 3mm.

4. DISCUSSION

The results of these experiments demonstrate the capabilities and performance of CARLO® very well. The achievements bring us closer to a CARLO®, which performs geometry-free, 3D navigated osteotomy of <1mm cutting width and achieves maximum precision compared to conventional tools. Thanks to the miniaturization of the system, a simple translation into an operating room environment for a surgical intervention is realistic. Also a controlled, safe and precise transfer of pre-operatively planned osteotomy patterns to the surgical site is made possible. With real-time intraoperative navigation of the operation area any unexpected changes of the anatomical situation can be corrected immediately.

Previous studies reported better bone healing after laser osteotomy. We established the hypothesis that this phenomenon was because of the missing "smear layer" on the bone surface [12,13]. This mechanical detrimental effect reduces bone bleeding and covers completely the bone surface. On the contrary, after laser osteotomy fresh bone bleeding with the anatomically open and biologically active surface, promoting the healing process, has been seen in histological evaluation.

In summary by using the CARLO® device, new perspectives open up: Osteotomies with higher freedom in the design of cut geometries, such as dove-tails, can be carried out with a maximum of accuracy on properly planned anatomical regions. Such functional cuts not only offer better wound healing than mechanical tools or piezo surgery but consequently reduce the morbidity of patients. Thanks to the optimum fit of the bone edges to each other, higher stability is achieved and thus a less rigid and stable plates are needed for osteosynthesis. The reconstruction is expected to be significantly higher than with straight cuts. So that after decades of straight osteotomies and osteosynthesis with strong plates, a rethinking of fracture treatments according to the biomechanics could be reconsidered.

We will continue further to optimize the system in the future with a more compact laser head by introducing blocks of optical alignments and the miniaturization of the housing itself. The nozzle system will be developed towards a sterile class 1s, single use medical product and will be further miniaturized in the process. A real time depth control system will assist in an overall better performance due to an active feedback regarding the laser head position and consequently the focus point positioning. Together with some changes on the optics we should be able to achieve cut widths of 500µm. There is also room for improvement regarding the calibration of the laser head. Just by optimizing the position of the marker fixed to the laser head we can increase the overall positioning precision further.

REFERENCES

[1] Barone, CM. et al.: "Analysis of bone formation after cranial osteotomies with a high-speed drill" J CraniofacSurg 8:466, (1997)

[2] Kondo, S. et al.: "Thermological study of drilling bone tissue with a high-speed drill" Neurosurgery 46: 1162, (2000)

[3] Jääskeläinen, SK., Teerijoki-Oksa, T., Forssell, K., V.ah.atalo, K., Peltola, JK., Forssell, H.: "Intraoperative monitoring of the inferior alveolar nerve during mandibular sagittal-split osteotomy" Muscle Nerve 23: 368–375, (2000)

[4] Eggers, G. et al.: " Piezosurgery: An ultrasound device for cutting bone and its use and limitations in maxillofacial surgery" Br J Oral Maxillofc Surg. 42:451-3, (2004)

[5] Pearson, GJ., Schuckert, KH.: "The role of lasers in dentistry: present and future" Dent Update. 30(2):70–74, (2003)

[6] Anic, I., Miletic, I., Krmek, SJ., Borcic, J., Pezelj-Ribaric, S.: "Vibrations produced during erbium:yttrium-aluminum-garnet laser irradiation" Lasers Med Sci.24(5):697–701, (2009)

[7] Lo, DD. et al.: "Femtosecond plasma mediated laser ablation has advantages over mechanical osteotomy of cranial bone" Lasers Surg Med. 44:805-14, (2012)

[8] Spencer, P. et al.: "Effective laser ablation of bone based on the absorption characteristics of water and proteins" J Periodontol. 70:68-74, (1999)

[9] Akyol, UK., Güngörmüs, M., Gündogdu, C., Erdem, H.: "Histologic evaluation of the effects of Er:YAG laser on bone ablation" J Contemp Dent Pract. 10(5):65–72, (2009)

[10] Kang, HW., Oh, J., Welch, AJ.: "Investigations on laser hard tissue ablation under various environments" Phys Med Biol. 53(12):3381–3390, (2008)

[11] Fried, D., Ragadio, J., Akrivou, M., Featherstone, JD., Murray, MW., Dickenson, KM.: "Dental hard tissue modification and removal using sealed transverse excited atmospheric-pressure lasers operating at lambda=9.6 and 10.6 microm" J Biomed Opt. 6(2):231–238, (2001)
[12] Stübinger, S. et al. : "Comparison of Er:YAG laser and piezoelectric osteotomy: An animal study in sheep" Lasers in Surgery and Medicine 42:743–751, (2010)
[13] Baek, KW., Deibel, W., Marinov, D., Griessen, M., Dard, M., Bruno, AE., Zeilhofer, H-F., Cattin, PC., Juergens, P.: "A comparative investigation of bone surface after cutting with mechanical tools and Er:YAG laser" Lasers in Surgery and Medicine 47:426–432, (2015)
[14] Baek, KW., Deibel, W., Marinov, D., Griessen, M., Bruno, AE., Cattin, PC., Juergens, P.: "Clinical Applicability of Robot-guided Contact-free Laser Osteotomy in Cranio-Maxillo-Facial Surgery: In-Vitro Simulation and In-Vivo Surgery in Minipig Mandibles" British Journal of Oral & Maxillofacial Surgery – Accepted (2015)
[15] Stübinger, S.: "Advances in bone surgery: the Er:YAG laser in oral surgery and implant dentistry" Clinical, Cosmetic and Investigational Dentistry 47-62, (2010)
[16] Schneider, A., Petzold, S., Baek, KW., Marinov, D., Cattin, PC.: "Simultaneous Intrinsic and Extrinsic Calibration of a Catadioptric Laser Photoablation System" Medical Image Computing and Computer Assisted Interventions - MICCAI15. – Accepted (2015)

Chapter 4

Spray Cooling Systems

Laser osteotomy is based on thermal-mechanical interaction induced by the laser beam into the targeted tissue. Cooling and moisturizing mechanisms must be put in place during such interventions to prevent dehydration and pulpal heating, the main causes of thermal damage and reduced tissue ablation [48]. Kang et al. [32] investigated laser hard tissue ablation under various environments, i.e. dry, wet (500 µm thick water layer), wet (500 µm thick perfluorocarbon layer) and spray ablation ($8\,\mathrm{ml\,min^{-1}}$). The authors concluded that the ablation was optimal during water spray cooling, i.e. particularly clean with no thermal damage, and suggested spray cooling systems as a feasible technology for laser osteotomy which should enable high cutting efficiencies. Such water sprays are considered to be high heat flux cooling systems and are used for very demanding applications such as multi-chip cooling and laser-diode array cooling [49]. During laser osteotomies, hard tissue does not reach as high superheat temperatures as in the previously mentioned applications. Superheat occurs when the temperature of a liquid cooled heated surface exceeds the saturation temperature of the liquid, see also Figure 4.6. However, during laser ablation, local energy deposition in tissue happens repeatedly within a micro seconds regiment. Therefore, a fast removal of the induced heat must be guaranteed such that the heat does not accumulate in the surrounding tissue causing thermal damage. In his doctoral thesis Glassman [50] researched spray cooling systems for different applications and compiled a general overview of comparative cooling technologies and the respective heat fluxes and heat transfer coefficients. Glassman [50] concluded that

using the right parameters and alignment, spray cooling systems are superior to all other methods. Yan et al. [51] agrees with Glassman [50] on his results.

Spray cooling is considered as an experimental technology since not all mechanisms and interactions of the spray and the heated target are fully understood [52]. Hence, for each application a specific nozzle system must be designed and optimized. The development of a suitable nozzle is based on general knowledge about the main parameters and an optimization process. This chapter gives an overview of the most influential parameters for spray cooling systems and their interaction with the laser light cutting process of hard tissue.

4.1 Types of Spray Cooling Systems

The discussions in his sub-chapter are mainly based on the information found in the book *Zerstäubungstechnik: Prinzipien, Verfahren, Geräte* [53] Chapter 5 published by the Axel Springer publishing house. Other sources are referenced individually.

There are two basic types of spray cooling systems or nozzles, categorized by their means of vapor generation.

The first utilizes the kinetic energy of a high-pressure liquid jet passing through the nozzle orifice and hence creating a pressure differential which vaporizes the liquid. This process is known as pressure atomization (PA). Main characteristics of such sprays are discharge velocity, shape and droplet size which depend strongly on the pressure differential, the rheological properties of the liquid and the geometrical design of the nozzle itself. The limitations lie in dynamic vapor customization and creating a spray with low flow rates using higher viscose liquids.

The second spray cooling type employs a high velocity gas mass flow to provide the energy needed for vapor generation. This process is known as secondary gas assisted atomization (SA). Thereby, the mass flow ratio between the mass flows of gas and liquid plays a major roll.

$$\mu = \frac{\dot{m}_g}{\dot{m}_l} \tag{4.1}$$

μ: mass flow ratio
$\dot{m}_g$ [kg s^{-1}]: mass flow of gas
$\dot{m}_l$ [kg s^{-1}]: mass flow of liquid

Usually, the droplets of the vapor get finer as the mass flow ratio rises. Furthermore, a high mass flow ratio enables better control of the individual mass flows of liquid and gas, which results in a more constant droplet size.

SA nozzles do not have the limitations of the PA spray systems going to low mass flow, but a higher complexity in design and application. Furthermore, they cannot be used in closed spaces due to the permanent influx of high volumes of gas. The SA spray systems are further divided into two categories; nozzles with external mixture and nozzles with internal mixture of gas and liquid.

For nozzles with external mixture, the gas and the liquid interact outside of the nozzle body with each other to create the desired vapor. In the most common case, the liquid exits the nozzle in its center with nearly no pressure. That orifice is surrounded by a ring channel which carries the high-pressure gas that creates a vacuum at its exit around the orifice. Through this negative pressure, the liquid is stretched out as a lamella across the orifice's profile until it hits its tear-off edge and gets vaporized by the high mass flow of gas. The higher the mass flow ratio, the thinner the lamella gets, which in turn results in a finer spray with smaller droplets. However, the influence of the mass flow has an upper limit, above which the droplet size of the spray does not get any smaller. Figure 4.1 illustrates a SA nozzle with external mixture.

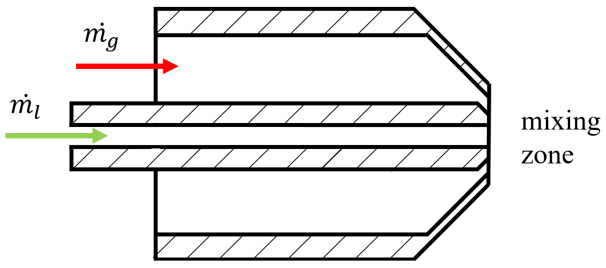

Figure 4.1: Schematic of a secondary gas assisted atomization nozzle with external mixture.

For nozzles with internal mixture, the gas and the liquid interact within the

nozzle body, in a mixing chamber, to create the desired vapor. The technical implementation of such nozzles is usually individually adapted, depending on the gas and liquid used. The mass flows of gas and liquid must be tuned to each other, which results in a higher expense to control the nozzle compared to a nozzle with external mixture. Further, the desired vapor pattern is influenced by the design. One option is a Y-jet nozzle [54], which is commonly used for heavy fuel oil vaporization with steam as the atomizing gas, see Figure 4.2a. The fine mixing of steam and oil within the Y-jet provides an intense heat transfer. This lowers the viscosity of the oil and hence its surface tension, which results in a finer vapor. The finer the vapor the better the combustion of the oil. Another option is a so called plain jet nozzle [55]. This specific model has a pre-chamber within the mixing chamber, see Figure 4.2b. This leads to the following characteristics; a low viscosity, a low surface tension and a small mass flow ratio. This again leads to a finer spray with smaller droplets.

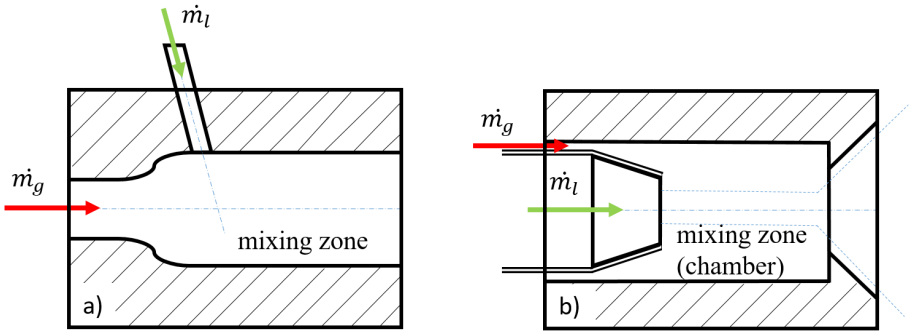

Figure 4.2: Schematic of a secondary gas assisted atomization nozzle with internal mixture. a) Y-jet nozzle. b) Plain-jet nozzle.

4.2 Main Parameters of Spray Cooling Systems

This section describes the main parameters of a nozzle and their influence on the spray cooling process. Furthermore, pressure atomization (PA) and secondary gas assisted atomization (SA) for spray cooling systems are compared.

4.2.1 Heat Transfer

The heat transfer coefficient is one of the main values in heat transfer by convection or phase transition between a fluid and a solid.

$$h = \frac{q}{\Delta T} \; [\mathrm{W/m^2K}] \tag{4.2}$$

h: heat transfer coefficient
q [W/m^2]: heat flux
ΔT [K]: temperature difference

It is a proportionality constant between the heat flux and the temperature difference between the solid surface and the liquid.

The following discussion and figures are based on the work of Yan et al. [51], further sources are referenced specifically. The authors describe the mechanisms involved in spray cooling systems. As a base of the evaluation they take a heated surface with the heat flux propagating against the direction of the droplet motion of the cooling spray. In the case of laser ablation, the original heat source, i.e. the laser beam, propagates with the direction of the cooling spray. However, the medium to be cooled is the bone which gets heated locally during the ablation process. Hence, it can be looked at as a heated surface with a heat flux in "all" directions, where the mechanisms described by Yan et al. [51] apply.

Not all heat transfer mechanisms are fully understood and established. There are several theories and simulations that attribute the main heat transfer to different mechanisms. Furthermore, the mechanisms interact and affect each other which makes it difficult to distinguish them. Here, only the four major mechanisms that are agreed on by several authors based on numerous independent studies are described:

- Liquid film evaporation off the heated surface.
- Forced convection arising from droplet impingement on heated surface.
- Enhancement of nucleation sites on the heated surface.
- Presence of secondary nucleation sites on the surface of spray droplets.

Liquid Film Evaporation off the Heated Surface One of the main mechanisms of spray cooling is the evaporation from the surface of a liquid film on a heated target. The heat is conducted from the heated surface through the liquid film to the vapor. Such a thin liquid film is about 300 µm to 500 µm thick and is formed at the beginning of the spray cooling process. The film creates a small effective thermal resistance, which is lowered through the convection achieved by mixing the impinging spray droplets with the liquid film. This interaction improves the heat transfer substantially and is considered as an enhancement for heat transfer, see Figure 4.3. The liquid film itself is attributed with bad heat transfer properties according to Silk et al. [49]. The cooling effect of the heated surface with the full evaporation of a liquid film on it is inferior to a spray cooling with moderate evaporation efficiency.

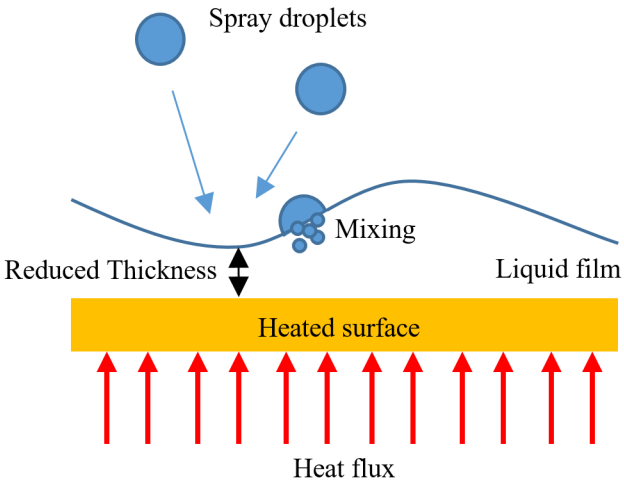

Figure 4.3: Impingement of droplets and a possible generated mixing lower the total thermal resistance on a liquid film.

Forced Convection Arising from Droplet Impingement on Heated Surface In our case, forced convection is the transport mechanism of thermal energy through fluid motion, generated by the spray droplets impinging the thin liquid film and thus creating convection, see Figure 4.4. This mechanism transports the majority of thermal energy for single phase spray cooling due to the absence of nucleation, under 99 °C for water. For the two-phase region at the period of low

heat flux and surface superheat, forced convection is the dominant effect. In the case of spray cooling, a two-phase region is where liquid and heated gas in form of vapor bubbles coexist. The forced convection mechanism applies during the ablation of hard tissue if the mass flow ratio is not optimized and hence a liquid film is created on the bone surface.

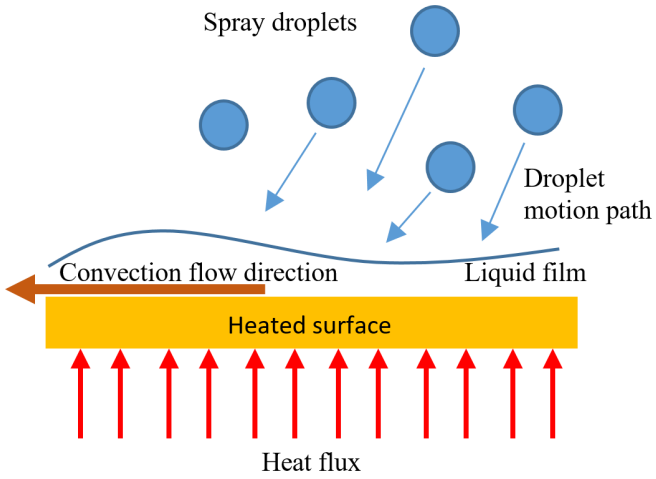

Figure 4.4: Forced convection principle caused by droplet impinging.

Enhancement of Nucleation Sites on Heated Surface Nucleation for spray cooling systems on a heated surface describes the process that occurs during the formation of vapor bubbles at fixed positions which are called nucleation sites. These are cavitations on the heated surface which support vapor bubble growth. If the local nucleation site reaches a saturation temperature due to thermal energy absorption, the liquid at the surface undergoes a phase change and a vapor bubble is created. This vapor bubble continuous to grow by absorbing more and more thermal energy and hence cooling its surroundings, i.e. the heated surface. This is also why such vapor bubbles do not form close by an existing nucleation site; the necessary temperature for the phase change is not reached since the initial nucleation site absorbs the necessary thermal energy and hence hinders the creation of another vapor bubble. This mechanism is known as pool boiling and is slow compared to spray cooling. First, it takes some time for the vapor bubbles to gain the needed buoyancy force at a certain diameter to overcome gravity and

break through the liquid film's surface tension in order to escape. Second, the nucleation site needs time to recover from the heat loss and reach the saturation temperature to be able to create a new vapor bubble. Spray cooling on the other hand breaks up the vapor bubbles faster and more frequently. The droplets impinge through the liquid film, hitting the heated surface and breaking up the vapor bubbles on the active nucleation sites. The same impingement results in a better heat transfer and a forced convection of the liquid film, which can remove the vapor bubbles from the nucleation sites, as discussed above. All three interactions together result in smaller vapor bubbles and are shown in Figure 4.5. This enables the formation of more vapor bubbles simultaneously, thereby enhancing the total heat transfer to almost a magnitude higher than with pool boiling.

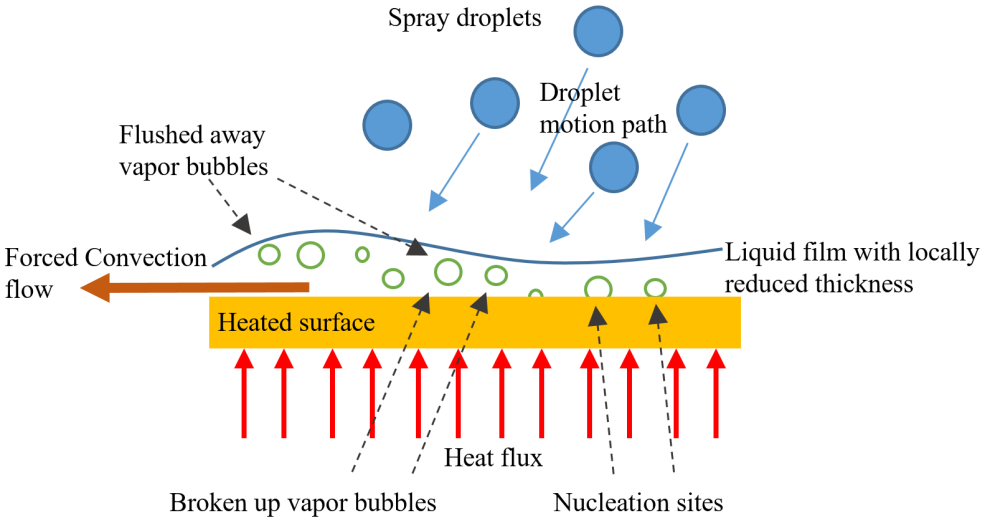

Figure 4.5: Nucleation sites and vapor bubble states on heated surface under the effect of droplets impingement.

Presence of Secondary Nucleation Sites on the Surface of Spray Droplets
Vapor bubbles that are not flushed away by forced conviction can burst above the liquid film. Spray droplets can then mix with the vapor and hence entrap vapor bubbles within them. When such spray droplets penetrate the liquid film, the entrapped vapor bubbles start to act as secondary nucleation sites creating new vapor bubbles, which contribute to the heat transfer. Further vapor bubbles can grow from the remains of former vapor bubbles inside the liquid film [56].

A similar effect occurs during pool boiling. However, spray cooling can produce three to four times more vapor bubbles then pool boiling which consequently enhances the overall heat transfer.

4.2.2 Critical Heat Flux

For two phase heat flux interactions between a heated surface and a liquid, the heat transfer is dominated by the latent heat absorption of evaporation as discussed above. This creates a very efficient heat transfer with the upper boundary called the critical heat flux (CHF). The CHF is basically a boiling limitation where the liquid film is replaced by a vapor film across the heated surface. This results in a drastic reduction of the heat transfer which leads to a physical burnout of the materials of the heated surface [49]. For laser osteotomy, exceeding the CHF first leads to drying of the surrounding tissue and consequently results in the carbonization of bone, introducing permanent damage and preventing further ablation of tissue. Figure 4.6 shows the basic interactions of boiling and condensation for the heat transfer between a heated surface and a liquid.

The critical heat flux is a measure of the spray systems cooling capacity. The higher the CHF the more thermal energy can be transferred efficiently from the heated surface. The following discussion is based on the work of Sehmbey et al. [57] who reviewed experimental spray cooling research focused on electronics up to the year 1995. Figure 4.7 shows the heat transfer characteristics for gas assisted atomization (SA) and pressure atomization (PA) water spray, G is the water flow rate.

The graphs shown in Figure 4.7 are obtained with preconditioned water, subcooled for the PA spray system and heated nearly to saturation for the SA spray systems. Thus, the plots show the heat flux q against the surface temperature T_{sur}. The marked regimes are:

1. Single phase forced convection, with a moderate heat transfer coefficient.
2. Two phase nucleate boiling, with a high heat transfer coefficient.
3. Flattening of the curve approaching CHF.

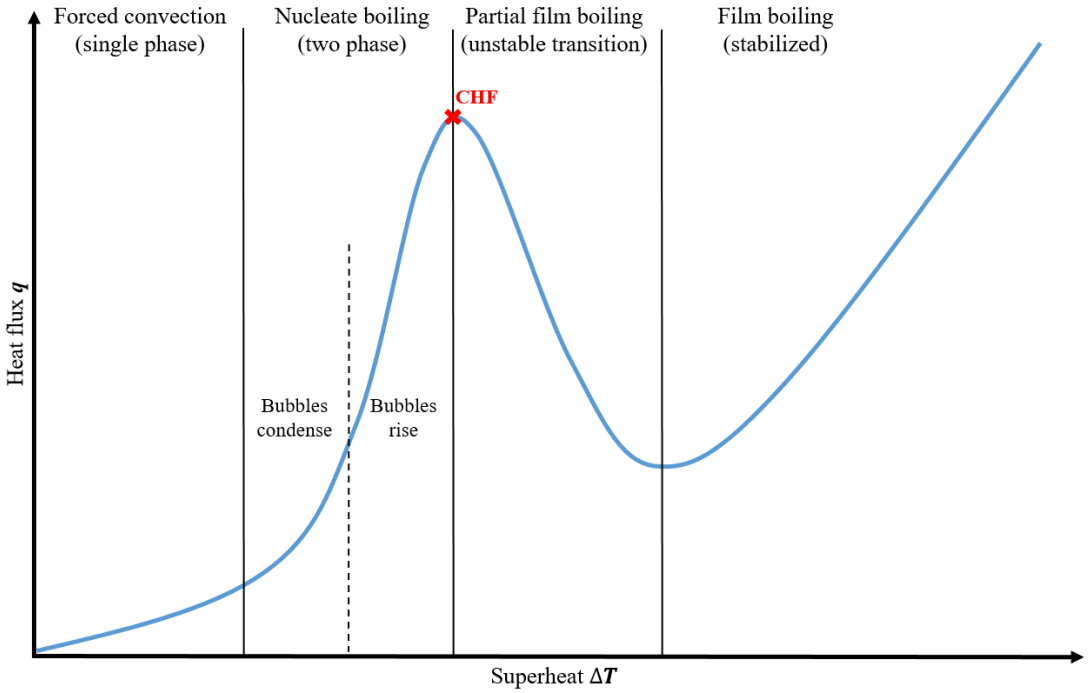

Figure 4.6: A typical boiling curve for a liquid cooled heated surface which temperature exceeds the saturation temperature of the liquid, i.e. it is in the superheated state; $\Delta T = T_{sur} - T_{sat}$.

The plots also illustrate that the CHF′s and heat transfer coefficients are similar for both spraying systems. Whereas, the water flow rate of the PA spray systems was more than ten times higher compared to the one of the SA spray system.

4.2.3 Target Surface

The influence of the target surface's topography has been researched in various studies with the conclusion that it has a big impact on the overall cooling effect during spray cooling. However, it behaves differently for pressure atomization (PA) and gas assisted atomization (SA) spray systems [57]. Using PA spray systems on very smooth surfaces (i.e. average roughness smaller 0.1 µm), increases the heat transfer coefficient tremendously. While for SA spray systems an increase in surface roughness resulted in a higher heat flux [57]. Baek et al. [58] compared bone cut faces after osteotomies performed with Er:YAG lasers and then with

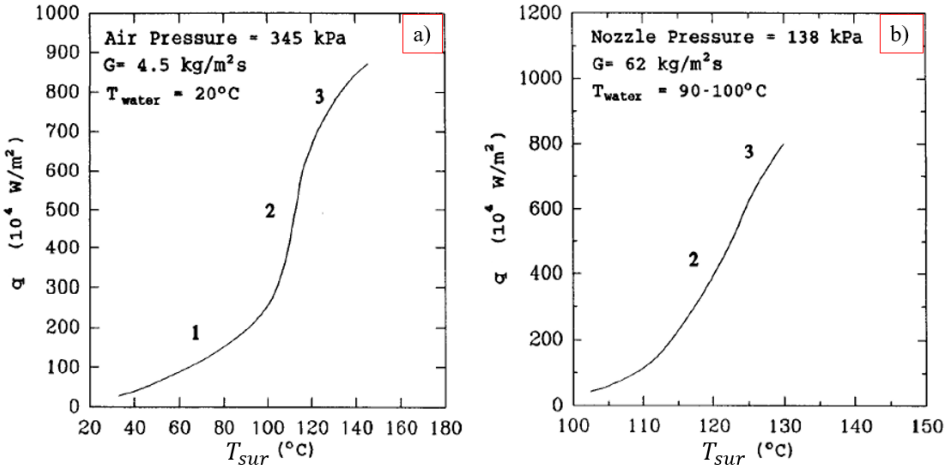

Figure 4.7: Spray cooling heat transfer characteristics [57]. a) SA: Gas assisted atomization water spray. b) PA: Pressure atomization water spray.

state-of-the-art mechanical tools, i.e. congenital drill and piezo osteotome. Their investigation showed that the cut face created by laser osteotomy presents a high structural analogy to the surfaces of original untouched bone that has open structures creating a large effective surface area and hence increases the critical heat flux for SA [59]. Figure 4.8 shows such a bone surface with clearly visible average surface roughness bigger than 5 µm (this is an estimated value and was not given by the authors).

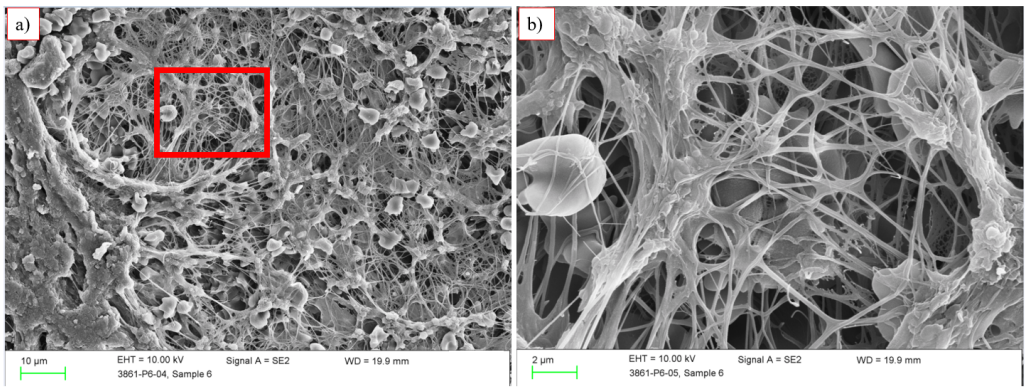

Figure 4.8: SEM image of a bone cut face created by laser osteotomy [58]. a) Original Image of Baek et al. b) Magnified cutout indicated by red box in 8a.

4.2.4 Droplet Size

Tilton [60] found out that the reduction of the spray droplet diameter leads to an increase of the heat transfer coefficient. Further, the evaporation efficiency rises for spray cooling systems due to the increase of the CHF with increasing flow rates and/or decreasing droplet diameter as concluded by Visara and Mudawar [61]. Both of these studies confirm that a smaller droplet size of the spray leads to superior cooling.

The droplet size range for SA spray systems is variable due to two independent and controllable parameters, firstly the gas differential pressure which determines the gas mass flow and secondly the liquid differential pressure which determines the liquid mass flow. The droplet size range is a function of the mass flow ratio μ.

For PA spray systems, all changes on the liquid differential pressure Δp lead to a simultaneous change of the mass flow and the droplet size range.

4.2.5 Spray Density

For low flow density, the overall cooling effect is determined by the liquid flow rate since the spray droplets evaporate as soon as they hit the hot surface. When spray cooling transits from low density mist cooling to high density spray cooling, the CHF and the heat transfer coefficient show no dependence on flow rate [57]. At this point the excessive liquid creates a film on the heated surface. The higher the liquid flow rate, the thicker the film on the surface, which lowers the evaporation efficiency on the liquid surface and hence counteracts the increased convection [62]. This suggests that there is an optimum film thickness which can be optimized for the heat transfer effects discussed above. The liquid flow rate itself depends on the geometrical design of the nozzle and operational parameters. The SA spray system enables us to continuously control the mass flows of gas and liquid from zero to their limit values. Whereas for PA, a minimum differential pressure must be created to start vaporizing.

4.2.6 Droplet Velocity

The influence of spray velocity for low density spray cooling are negligible since most of the droplets evaporate at CHF. However, for high spray densities, an increase of droplet velocity results in an increase of the heat transfer coefficient and the CHF, as for SA spray systems [57]. Chen et al. [63] attributed a dominant influence to the droplet velocity. During their experiments the authors isolated the effects of the velocity by keeping the liquid flow rate at a narrow range of 5 %. They found out, that an increase in droplet velocity by a factor four, results in an increase of the heat transfer coefficient by up to 40 %, and the CHF by up to 50 %. Hence, they concluded that a low density spray with high droplet velocity is more effective than a dense spray with low velocity. SA spray systems can usually have up to ten times higher droplet velocities compared to PA spray systems.

4.3 Nozzle Alignment

The main parameters to achieve the desired cooling effect with a nozzle system used are; geometrical design, the sprays alignment and orientation to the target surface, and a possible interaction with other sprays. The following subsections describe the main parameters and effects thereof.

4.3.1 Inclination Angle

In laser osteotomies, the laser beam should hit the target tissue vertically. Since the spray cooling cannot be aligned co-axially with the optical path of the laser beam, it must be aligned next to the beam path and the nozzle itself inclined so that the center of the spray cone hits the cut. Figure 4.9 shows the basic alignment of one nozzle to the cutting laser beam and the resulting inclination angle α.

Visaria and Mudawar [64] studied the effects of spray inclination on two-phase spray cooling and critical heat flux. The highest CHF was achieved with an inclination angle of 0°, i.e. vertical spray direction on the heated surface, for all nozzle variations, flow rates and sub-coolings used. An increase of the inclination

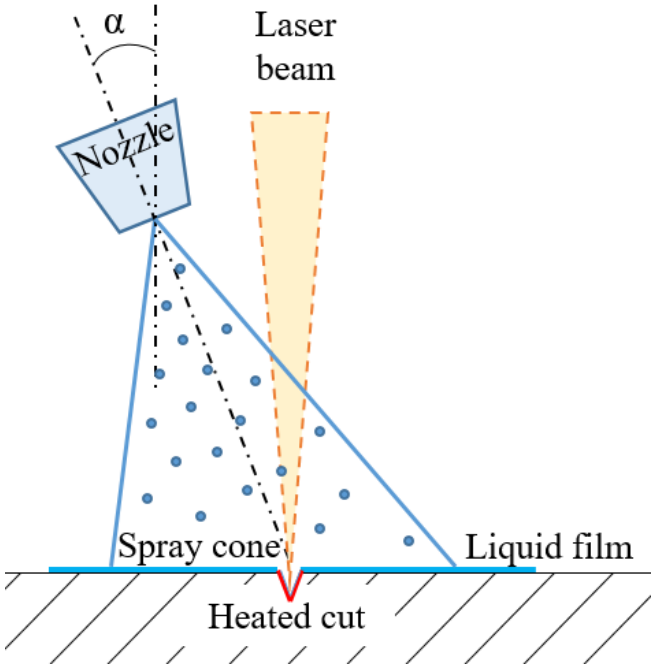

Figure 4.9: Nozzle alignment for laser osteotomy with resulting inclination angle α in respect to the tissue surface.

angle not only decreases the CHF but also changes the spray area from circular to elliptic, which reduces the spray density per area. As a result, tissue dehydrates at lower CHF compared to vertical sprays, and further decrease with increasing inclination angles [65]. Furthermore, a lateral liquid flow downstream over the surface is created which increases forced convection. This flow does not impact the outer region of the spray ellipse at its minor axis, and hence leads to less cooled points where the CHF occurs first [64]. The above described effects are only relevant if the laser beam is pivoted especially in the less cooled areas, i.e. cutting across the whole spray area. When the whole cutting system is moved simultaneously, i.e. laser beam and spray cone locked in position to each other, then the laser beam will always be at the same spot of the spray cone.

4.3.2 Nozzle-to-Surface Distance

Horacek et al. [66] studied spray cooling for multiple nozzles. The authors found out, that an increase of the nozzle-to-surface distance leads to a higher removal of

thermal energy and a more uniform heat flux distribution. They speculate that there should be an optimum distance to achieve a uniform heat flux distribution, which does not necessarily have to be the same nozzle-to-surface distance found for maximum net heat removal rate. In their work, the distance from nozzle to heated surface was varied between 7 mm to 17 mm. For the small nozzle-to-surface distances, the non-uniform heat flux distribution is attributed to the insufficient surface coverage by the spray (using multiple nozzles on a large heated surface). However, too big of a distance reduces the number of droplets per unit area and hence lowers the heat transfer. Therefore, the optimum nozzle-to-surface distance must be evaluated for a given nozzle design and alignment geometry. These shortcomings can be neglected, if the nozzle spray always covers the whole surface and if the liquid flow rate can be adjusted accordingly.

4.3.3 Multiple Nozzles

Multiple nozzles create stagnation zones where their sprays intersect. These zones create fluid domes that have a lower fluid momentum but a greater mass flow as the original spray cones, hence a lower CHF [49]. Lin et al. [67] attributed a reduction of the overall heat transfer performance by 30 % to such stagnation zones as more nozzles were used to cover bigger areas. Figure 4.10 shows a schematic of this phenomenon.

Multiple nozzles make less efficient use of the cooling fluid compared to single nozzles [68]. However, they achieve higher peak heat fluxes since the heated surface is cooled through a liquid flow without any evaporation, i.e. no phase transition during the cooling process. Overall the multiple nozzle array was inefficient due to the creation of stagnation zones. The authors found out, that fluid domes can be avoided, if the nozzle array was inclined towards the heated surface, this supports fluid drainage. Silk et al. [69] managed to increase the CHF by 23 % going to an inclination angle of 15 °C .

Horacek et al. [66] concluded that the average heat flux for the spray cooled regions was the same for single- and two-nozzle cases, with a measurement uncertainty of 5 %. They assumed that the reason was the relatively dilute sprays investigated. Fluid mass flows of 11 ml min^{-1} to 30 ml min^{-1} for each nozzle where

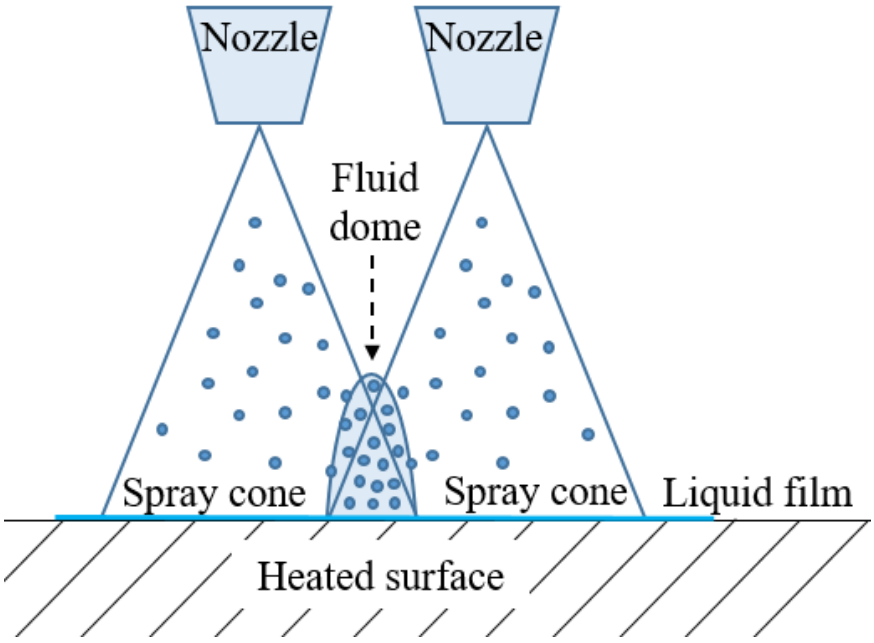

Figure 4.10: Spray cone stagnation zone phenomena; fluid dome created by two nozzles.

only half of the spray of each nozzle impacted the heated surface, at a nozzle-to-surface distance of 7 mm to 17 mm. The sprays overlap close to the heated surface and far from the nozzle orifice. Here, where the droplet density of each spray is small enough not to collide with the other sprays droplets and so alter the overall spray pattern; fluid domes can be avoided.

4.4 Spray Interaction with Laser Cutting

The cooling liquids used during laser osteotomy with the CARLO device are water based, i.e. NaCl 0.9 % and Ringer's lactate solution since these liquids are established in invasive surgery, e.g. for open wound irrigation. Hence, the discussions in the following sub-chapters are based on the work of Kang et al. [48] who used water as cooling liquid to investigate the main mechanisms for hard tissue ablation while cooling with a spray system. Further sources are referenced specifically. The setup in the study has two major differences to the application

of the CARLO device; the laser source used and the targeted tissue itself, which depend on each other.

The authors used an Er,Cr:YsGG (yttrium, scandium, gallium, garnet) laser, with a central wavelength of λ=2.79 µm, compared to our research using an Er:YAG laser, λ=2.94 µm. The reasons lie in the composition of the target tissue itself, dental enamel on one hand and cortical bone on the other. Table 4.1 shows the main building blocks of the compared hard tissues [70]. The absorption coefficient of water at λ=2.79 µm (α=5300 cm^{-1}) is only about half of the absorption coefficient at λ=2.94 µm (α=12 500 cm^{-1}). But hydroxyapatite has an absorption peak for Er,Cr:YsGG laser radiation which makes it a good alternative for dental enamel tissue ablation. Whereas, the Er:YAG laser has clear advantages for bone ablation, i.e. cortical bone and especially trabecular bone. The general mechanisms of hard tissue ablation while cooling with water spray are suitable for both laser systems with their target tissues.

Component	Collagen [%]	Water [%]	Hydroxyapatite [%]	Fett [%]
Dental enamel	0.5	4.5	95	0
Cortical bone	25.5	13.5	60	1
Trabecular	34	30.5	34	1.5

Table 4.1: Composition of hard tissue; dental enamel, cortical bone and trabecular bone [70].

4.4.1 Water Spray Flow Rate

The ablation volume in hard tissue increases with higher energy densities applied and decreases with higher flow rates for all applied energy densities. The ablation volume at an energy density of 52 $\mathrm{J/cm^2}$ was reduced by 17 % using the highest water volume flow (22.8 $\mathrm{ml\,min^{-1}}$) compared to the lowest (2.8 $\mathrm{ml\,min^{-1}}$).

4.4.2 Ablation Threshold

The ablation thresholds were measured as 1.2 $\mathrm{J/cm^2}$ for uncooled samples and as 2.1 $\mathrm{J/cm^2}$ for spray cooled samples using 8 $\mathrm{ml\,min^{-1}}$ water volume flow. During laser ablation cooled with the water spray, part of the laser light gets absorbed

by water droplets and hence does not reach the target tissue. The higher the water volume flow during such a procedure, the higher the ablation threshold. This effect has a smaller relative influence on the ablation efficiency going to high laser energy densities.

4.4.3 Transmission

The incident and transmitted radiant exposure through water spray show a linear relationship. However, a transmission can only be measured after the incident radiant exposure reaches a certain level, e.g at $2\,\mathrm{J/cm^2}$ for a flow rate of $8\,\mathrm{ml\,min^{-1}}$. Kang et al. [48] state that this minimum incident energy density, for the given coolant flow rate, is necessary to create a vapor channel through the water spray along the laser beam, so that the remaining energy of the initial laser pulse can reach the target tissue and start the ablation process.

4.4.4 Ablation Efficiency and Volume

Bone ablation using water spray cooling creates clean craters without any thermal damage compared to charred, deformed and cracked craters created through ablation without spray cooling. However, using a water flow rate of $8\,\mathrm{ml\,min^{-1}}$ and applying ten pulses for spray cooling ablation resulted in a wider crater with a total ablation volume up to twice as big as for dry ablation. Continuous and fast water vaporization induces an ablative momentum on the tissue surface, called hydro-kinetic effect. The water droplets are accelerated by the photons and cause a secondary bombardment of the targeted tissue [71], resulting in a higher ablation rate. Furthermore, when a liquid layer is present on the target tissue, the strong absorption of the laser light and the following recoil of the water, mechanically ablates any loose non-apatite phases [72].

Kang et al. [48] also measured the acoustic energy during spray cooling assisted ablation compared to dry ablation. They speculated, that the additional effects associated with spray cooled ablation augment the peak acoustic amplitude with longer pressure durations, which results in an enhanced ablation efficiency.

4.4.5 Laser Cut Shape

When a laser beam hits water droplets, photons can not only be absorbed but are also scattered. Kang et al. [32] believe that a scattering in the forward direction dominates, especially for water particles larger than the laser wavelength, and hence creates narrow, sharp cone cuts, i.e. the droplet directs the photons forward, imitating a focusing lens. This effect is called Mie scattering [48]. As implied, small droplets are favorable to prevent Mie scattering and enable a parallel cut. Furthermore, a high energy density of the applied laser pulse vaporizes the droplets faster (more light gets absorbed), so that Mie scattering is minimized.

4.4.6 Spray cooling Effect

Water spray cooling efficiently removes thermal energy before it can accumulate and damage the surrounding tissue. Water has a 30 times higher thermal conductivity than air and induces a rapid heat diffusion through vaporization and convection processes. In case of liquid films on the target tissue and high superheat, nucleate boiling can be induced.

4.5 Summary

Spray cooling systems are crucial during laser ablation of hard tissue. The spray cools and moisturizes the target surface in order to prevent heat accumulation and consequently thermal damage to the surrounding tissue, while even enhancing the ablation efficiency. Furthermore, the water flow binds and removes debris, keeping the cut clean for further ablation [48]. Basically, spray cooling enhances the heat flux during the ablation process allowing tight temperature control with optimized mass flow rates of liquid, and in the case of SA nozzles gas flow rates [49]. Highest peak heat fluxes are obtained when phase change is avoided [68]. Chen et al. [73] stated that it is desirable to select nozzle systems that produce the smallest droplet size possible with as high velocities as possible to achieve maximum CHF while using the minimal amount of coolant. In agreement with the authors and conclusively from the evaluation here, SA spray systems are most desirable for applications in laser osteotomy in an open environment. Such spray

cooling systems provide the best overall cooling effect while being versatile in their spray parameters for different applications and bone structures.

Chapter 5

Development of a Spray Cooling System for Laser Osteotomy

This chapter shortly describes the research and development process to build the optimum nozzle system for hard tissue ablation, which led to a European patent (No. EP3127501 A1). The patent is included in the last section of this chapter. Not all claims of the patent are integrated yet. The nozzle system is still under further development in order to achieve higher flexibility, usability and the integration of further claims. The goal is the certification of the nozzle system as a class 1s medical device according to the Medical Device Directive (93/42/EEC). This further development is outside the scope of this thesis. The described nozzle systems in this work were applied in various in-vivo and in-vitro experimental studies. The results and evaluations of these were incorporated into the development and design of the nozzle systems.

The first three nozzle systems were designed by Thomas Richter, CEO of IBR Zerstäubungtechnik, Germany and Co-Inventor of the patent. The development was focused on basic functionality and alignment. The last nozzle system described, was designed by Rafael Bätscher, founder and owner of rabatec Engineering GmbH, Switzerland. Here, integration and usability were in focus.

5.1 Basic Secondary Gas Assisted Atomization Nozzle

The first spray system was a dual nozzle with external mixture. A so called perfume atomizer. Figure 5.1 shows the designed nozzle.

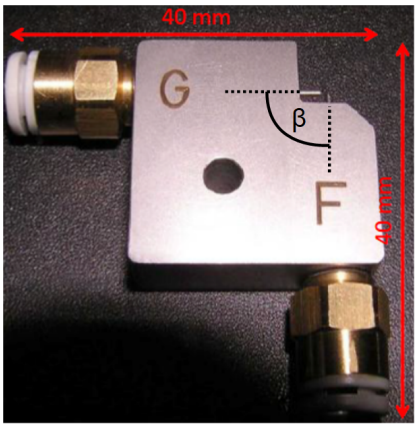

Figure 5.1: Designed perfume atomizer with a bore for alignment and fixation. Supply tubes for liquid and gas are connected through integrated stud fittings. The volume flow was $1\,\mathrm{ml\,min^{-1}}$ to $5\,\mathrm{ml\,min^{-1}}$, the maximum gas pressure 5 bar with a spray angle of $\Theta = 20 - 25°$.

The gas and liquid are guided in separate tubes through the nozzle. Such perfume atomizers are used for applications with small liquid volume flows like air brush spray guns. It is possible to achieve droplet sizes down to several micro-meters in diameter. The properties of such systems depend mostly on its geometrical design and the liquid used;

- The higher the gas pressure, the smaller the mean droplet diameter at a constant liquid flow (until the minimum spray droplet diameter is reached).
- A smaller inclination angle β of the liquid tube leads to a smaller mean droplet size (in our case $\beta = 90°$, i.e. liquid tube perpendicular aligned to the gas tube).

The liquid volume flow was controlled with a syringe pump. If the supply tube for the liquid is just within a liquid reservoir, i.e. no liquid volume flow control,

the negative pressure created by the gas volume flow at the tubules orifice of the nozzle conveys the liquid. As soon as a droplet forms at the tip of the tubule, the gas vaporizes it. In this case, an increase of gas flow results in a higher liquid flow.

This nozzle with liquid flow control was the first basic SA nozzle and attached to an alignment on an x-y-stage, see Figure 5.2. It was used to perform basic experiments such as "necessity of a cooling spray system", see Figure 5.3, and to find "optimal cooling parameters" for the laser system used at that time.

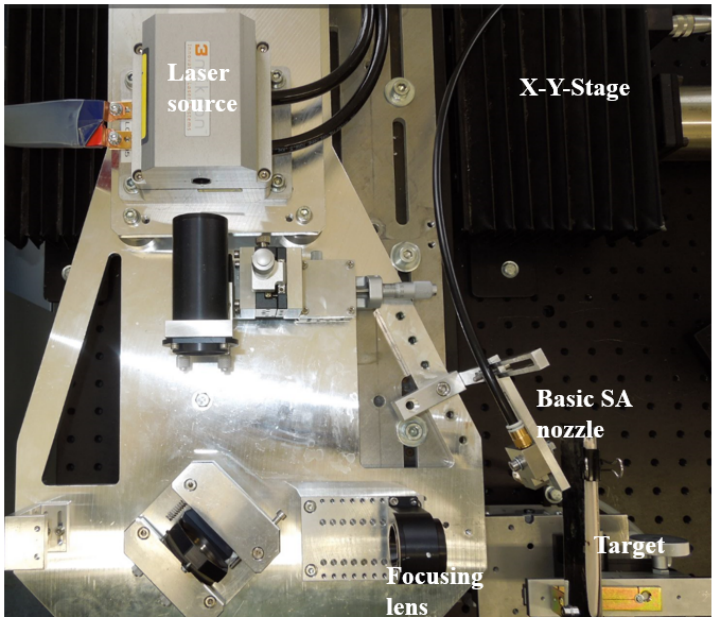

Figure 5.2: Bone cutting alignment on x-y-stage with basic SA nozzle.

Following up, the basic SA nozzle was integrated into the first laser head of the CARLO device, see Figure 5.4, and used to evaluate cutting techniques. After the first experiments showed promising results, the nozzle concept was miniaturized and adapted to the next laser head generation in order to enable in-depth studies for osteotomies.

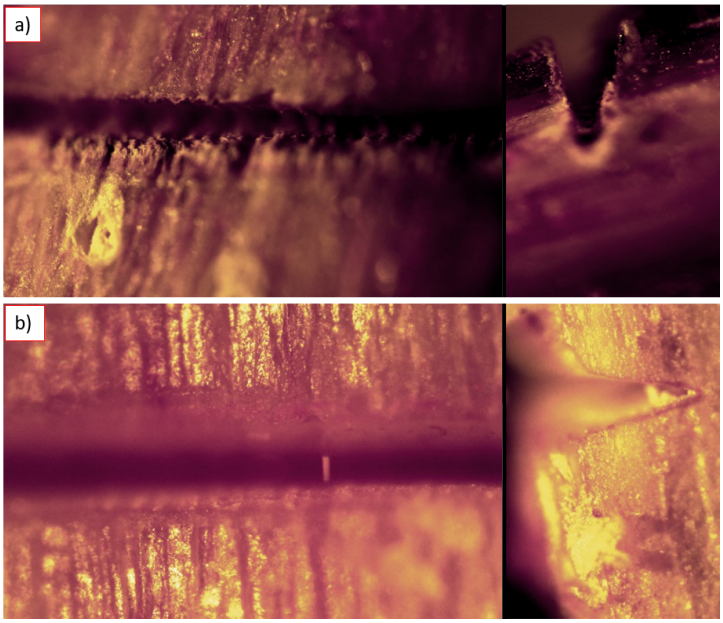

Figure 5.3: Laser osteotomy cuts in cortical porcine bone performed with a diode pumped Er:YAG laser. 40 times magnified under a microscope and captured with an Infinity Light camera from Lumera in top and side view. a) Cut performed without spray assisted cooling resulted in rough edges and obvious thermal damage on the cut and surrounding tissue. b) Cut performed with spray assisted cooling resulted in precise and clean cut without thermal damages to it or the surrounding tissue.

5.2 Nozzle Array of two Secondary Gas Assisted Atomization Nozzles

The next step in the development was to minimize the SA nozzle design and to integrate it into the next generation laser head to enable more complex experiments/cuts. But, it was still necessary to keep a certain flexibility for the alignment to enable variation and optimization of operational parameters for the laser osteotome without losing cooling performance. This was realized by designing the SA nozzle according to the principle shown in Figure 4.1. Further, studies showed that a second SA nozzle was necessary to cover the full working area for various cutting angles in order to keep the intervention carbonization free, see Figure 5.5. The orifice of each nozzle spray was aligned depending on the work-

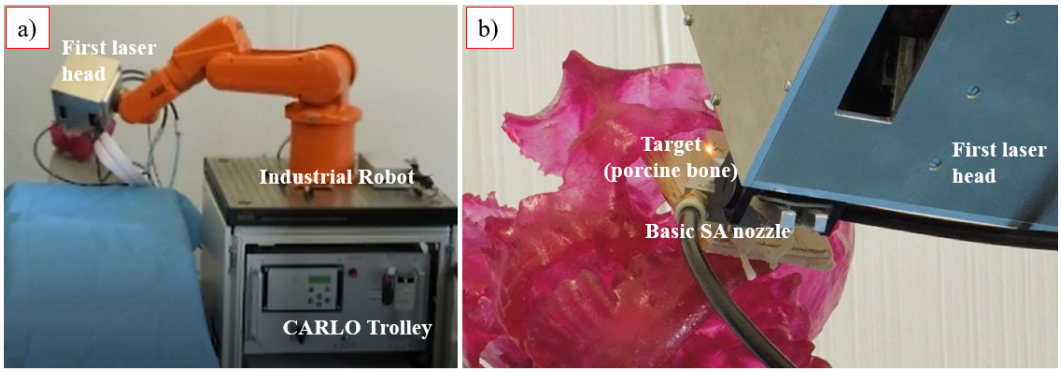

Figure 5.4: The CARLO device during a performance demonstration. a) CARLO device overview. b) Close-up of laser head with basic SA nozzle.

ing distance and working area of the laser beam. The spray of both nozzles covers a working area of 20 mm in diameter, creating a homogeneous spray pattern and cooling conditions across the whole working area. This concept was so successful that the first live animal study could be done with the developed laser osteotome; a part of its evaluation was published by Baek et al. [58].

5.3 Nozzle System of three Secondary Gas Assisted Atomization Nozzles

The next development steps were initiated by challenges faced when cutting cortical bone with higher density. Further, more complex cutting patterns, increase of working distance and the first features towards a single use medical device had to be taken into account. The next generation was realized by adding a third SA nozzle, orientated symmetrically to each other, in order to create an even more homogenous spray pattern on the target surface. All three SA nozzles were integrated into one embodiment with individual liquid supply channels and one common gas supply. The inclination angle α was minimized to achieve a high droplet penetration into the cut cavity. It also improved the homogeneity of the spray pattern by minimizing the elliptical shape of the individual sprays on the target area, which enabled further optimization of the liquid mass flow. Figure 5.6 shows the designed nozzle system.

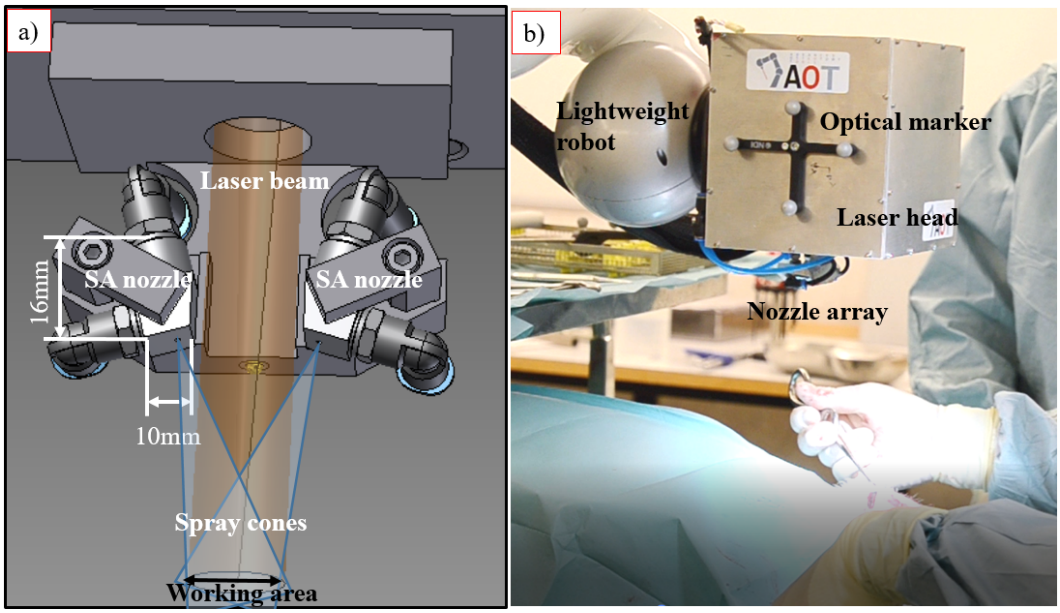

Figure 5.5: Concept of the two SA nozzle array for functional cuts. a) CAD design. b) CARLO with integrated SA nozzle array during the first animal study.

This nozzle system was the basis for the mentioned European patent and already fulfilled claims 1, 3, 4, 5 and 7. Comments on the claims can be found in the patent itself and the next chapter.

5.4 Fully Integrated Nozzle System with three Secondary Gas Assisted Atomization Nozzles

The next development step was focused on integration, usability and improvement of the overall performance. The main goals were the "industrialization" of the nozzle system and the applicability as a universal cooling spray system for laser osteotomies. Main functions include the sealing of the laser head during interventions, keeping the optics clean within the laser head, establishing the sterile zone between the laser osteotome and the operating field, fast attachment and removal of the nozzle system and enabling cutting of bone tissue regardless of surrounding conditions like massive blood and debris flows. This version of the

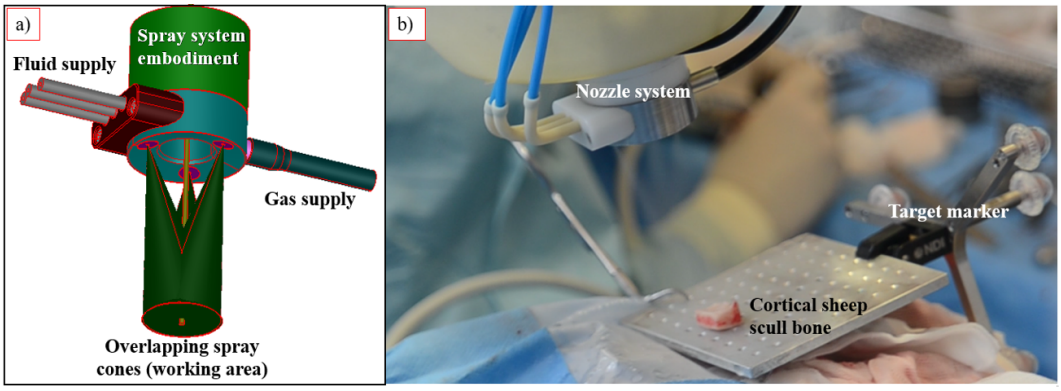

Figure 5.6: Nozzle system design of three SA nozzles integrated into one embodiment and optimized for deep cuts in cortical bones. a) CAD Design. b) Performance during the second animal study, while cutting cortical sheep scull bone.

nozzle system was tested in cadaver and in vitro studies. The next nozzle system generation was then used in an animal study. Figure 5.7 shows the latest version relevant for this thesis and gives an overview of all incorporated claims according to Chapter 3. Comments and descriptions of all claims are found on the following pages, grouped as incorporated and not incorporated claims. The discussions are based on the main idea behind each claim, which does not exclude other uses or applications.

5.4.1 Implemented Patent Claims

This section describes the already implemented patent claims within the nozzle system and their main functionality. The claims are listed as in the patent itself and not by order of development.

Claim 1 A multi-nozzle system within one body, which has a bore for laser beam propagation, mountable onto a laser medical device with the nozzle systems arranged around the laser beam. Here, the specific nozzle alignment minimizes their inclination angle, which optimizes the overall spray pattern on the target, the droplet penetration in depth. Also, the spray cones of the individual SA nozzles overlap/interact as close as possible to the target surface to minimize absorption

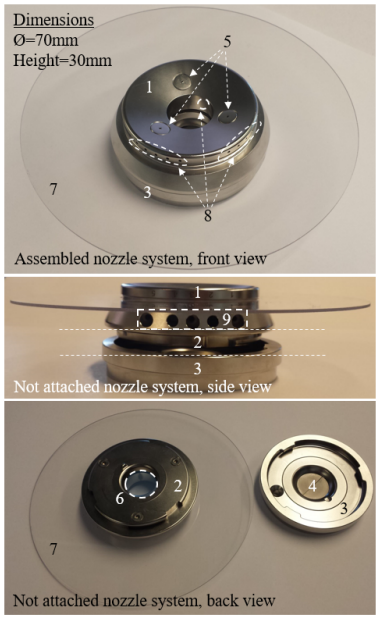

Figure 5.7: Fully integrated nozzle system with three SA nozzles; overview of all incorporated claims.

of the laser light by the droplets, i.e. the light travels longer unhindered.

Claim 3 Regular arrangement of multiple nozzles around the laser exit, here three. Creating a homogeneous spray pattern to optimize cooling properties.

Claim 4 Used nozzles are SA spray nozzles for enhanced and optimized cooling performance, through precise control of the mass flow rate of each SA nozzle.

Claim 5 The nozzle body comprises of multiple stacked plates, here three. This feature enables a customization according to the spray cooling properties and other features needed in the application of interest. It also makes it easier to produce, assemble and integrate the whole nozzle system, i.e. each stack can be produced in the most efficient/necessary material and way.

Claim 7 A liquid supply plate with a liquid chamber for each individual nozzle and individual liquid emission channels, which enables a controlled supply of each

SA nozzle with the liquid needed for the application of interest, e.g. medical drugs or wound washing.

Note: The current nozzle has individual liquid supply channels. Nevertheless, the liquid is pumped by the same peristaltic pump out of a common reservoir of cooling solution. The administration of different solutions and/drugs is not researched/necessary yet.

Claim 13, 14 and 15 An individual number of suction and/or blowing opening(s), depending on the need and the facilities during the given intervention, are applied to the inner transfixion of the nozzle system to protect the inner optics, e.g. out-coupling window, of the laser head. Further openings are directed outwards of the nozzle system for suction- and/or blowing, depending on the need and the facilities during the given intervention. Such openings can be directed 360° to each area of interest, e.g. integrated cameras in the laser head, to protect these from debris.

Claim 16 and 17 The nozzle base has an interface to the medical device. This interface opens the medical device mechanically when the nozzle system is attached, and hence creates a path for the laser beam towards the operation field. The design of this interface is asymmetrical so that only one position of the nozzle system in respect to the medical device is possible, which is crucial for liquid and gas tube guidance, draping positioning and overall handling regarding safety. When the nozzle system is removed, the opening of the medical device closes mechanically again.

Claim 18 A window is integrated within the inner bore of the laser system to protect the optics of the medical device, while the nozzle system is attached to it. This is crucial, since the inner optics and electronics must stay clean to guarantee functionality of the medical device. Furthermore, the inner optics are not sterile and would compromise the sterile zone. Therefore, the window functions also as a barrier to establish the sterile zone.

Claim 19 The described window in claim 18 consequently seals the device. It is more than 99 % transparent for all laser wavelength used. Hence, to avoid back reflections into the medical device, the window is tilted respectively to the axis of the laser beam and the nozzle systems inner bore.

Claim 20 Usually the nozzle system is used within a sterile zone. Thus, either a fixation option for the draping or a full integration onto the nozzle system is necessary. The benefits of the full integration are that the nozzle system is the last element for the system when build up and hence seal and establishes the sterile zone. Furthermore, all supply channels for gas and air can be integrated within it, saving time for installation and fixation for other solutions.

5.4.2 Not Implemented Patent Claims

This section describes the not yet implemented patent claims within the nozzle system and their main functionality. These claims and functions can be implemented as needed for specific regulatory or treatment specific requirements.

Claim 2 A dynamic adjustment of the spray direction of each individual nozzle is not necessary yet and one of the most challenging features in terms of minimization, integration, control and cost efficiency for a single use device. This feature can enable optimized cooling for all cutting techniques and patterns by following the ablation laser beam and/or selective cooling and cleaning of tissue.

Claim 6 Each SA nozzle has an own gas supply. In some interventions it is crucial to be able to bring the vaporization into a pulsing mode or to stop it completely, e.g. to clean the operation area or reposition the laser head. There are two basic concepts for such an option, which can be implemented in the individual nozzle systems as required. In both cases fast pressure regulation valves are required to achieve necessary opening times, e.g. 0.2 s, to be able to pulse the vapor, e.g. between depth measurements and cutting process. These methods presume that the initial gas supply stays intact without any pressure loss at all times. Furthermore, we are able to open and close each dual nozzles gas supply at will. This brings the advantage to be able to regulate the vapor

through variable valve timing and to stop each single dual nozzle if needed, e.g. if several solutions are used.

Claim 8 and 9 Gas and liquid supplies are controlled individually for each nozzle with valves. The implementation enables claims 6 and 7. Fast valves enable also a fluid pulsing mode, where the fluid supply, or gas and liquid separately, is turned on and off in a given frequency, e.g. to dry the cut between laser cutting and depth control measurement.

Claim 10 Here internal central valves for the liquid and gas supply are described, respectively. These are incorporated, but not exactly as claimed. The peristaltic pump which supplies all three SA nozzles could be used as an external central valve. The gas supply has also an external central valve with an integrated manometer.

Claim 11 Target luminescence integrated within the nozzle system. In most indications the target tissue must be illuminated very well, so that the surgeon can see the operating area. Furthermore, cameras in the laser head (and other monitoring devices) can monitor the intervention in higher quality. Which eliminates further illuminating devices. The current laser head has such a feature integrated in itself.

Claim 12 An RFID chip is integrated for quality assurance. This nozzle system will operate in a sterile zone. The RFID chip is integrated according to the corresponding detectors position at the nozzle system fixation on the medical device, to ensure that each nozzle system is only used for one patient. Furthermore, the consumption can be monitored and each nozzle system traced back if needed.

5.5 European Patent No. EP3127501 A1

(19) Europäisches Patentamt
European Patent Office
Office européen des brevets

(11) EP 3 127 501 A1

(12) EUROPEAN PATENT APPLICATION

(43) Date of publication:
08.02.2017 Bulletin 2017/06

(21) Application number: **15180233.7**

(22) Date of filing: **07.08.2015**

(51) Int Cl.:
A61B 18/20 *(2006.01)* ***A61B 18/22*** *(2006.01)*
A61B 17/3203 *(2006.01)* ***A61C 1/00*** *(2006.01)*

(84) Designated Contracting States:
AL AT BE BG CH CY CZ DE DK EE ES FI FR GB GR HR HU IE IS IT LI LT LU LV MC MK MT NL NO PL PT RO RS SE SI SK SM TR
Designated Extension States:
BA ME
Designated Validation States:
MA

(71) Applicant: **Advanced Osteotomy Tools - AOT AG**
4057 Basel (CH)

(72) Inventors:
- **Deibel, Waldemar**
  34474 Wrexen/Diemelstradt (DE)
- **Richter, Thomas**
  48147 Münster (DE)
- **Bruno, Alfredo E.**
  4105 Biel-Benken (CH)

(74) Representative: **Latscha Schöllhorn Partner AG**
Austrasse 24
4051 Basel (CH)

(54) CONDITIONING A LASER-TISSUE CONTACT SURFACE

(57) A nozzle device (1) comprises a plurality of multi-fluid nozzles (5) and a body (2) with a bore (8). The bore (8) has a laser entrance (82) and a laser exit (81). The nozzle device (1) is adapted to be mounted to a laser medical device such that a laser beam generated by the laser medical device enters the laser entrance (82) of the bore (8) of the body (2) and exits the laser exit (81) of the bore (8) of the body (2). The body (2) houses the multi-fluid nozzles (5) and the multi-fluid nozzles (5) are arranged around the laser exit (81) of the bore (8) of the body (2). The nozzle device (1) allows to conditioning a tissue at and near where it is cut or drilled by the laser beam of the laser medical device. Thus, the nozzle device (1) is particularly suitable for a laser osteotomic device allowing to minimize collateral damages of the tissue when being cut or drilled.

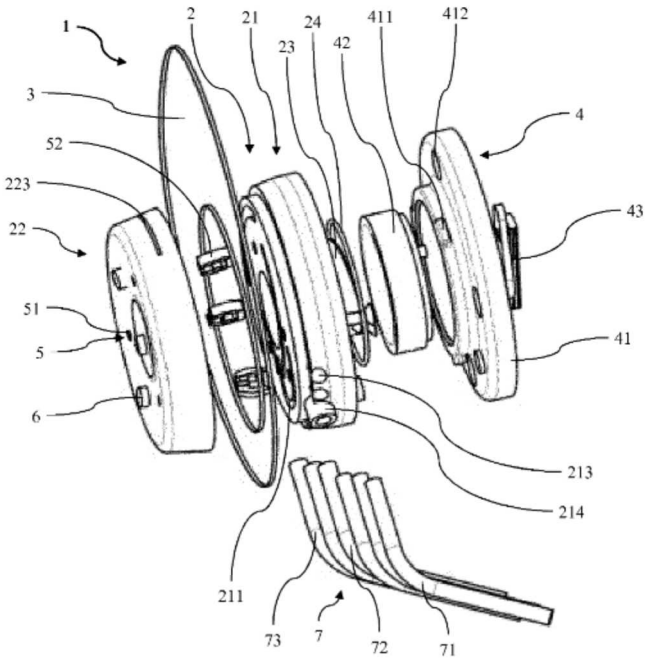

Fig. 1

EP 3 127 501 A1

Description

Technical Field

[0001] The present invention relates to a nozzle device for a laser medical device and a respective nozzle device set. Such devices and sets can be used for conditioning a laser-tissue contact surface in a process of treating the tissue by means of a laser beam delivered by the laser medical device. In particular such treating can relate to cutting a bone or a similar human or animal hard tissue.

Background Art

[0002] For cutting and drilling materials in various technical fields it has become increasingly popular to use apparatuses which apply a laser beam to the material. Today, in industrial applications such laser cutting or drilling is widespread since it allows for efficiently and flexibly process work pieces at high precision. Also, for cutting human or animal hard or soft tissue such like bones, cartilages or the like laser cutting and drilling with laser is more and more applied. For example, in computer assisted surgery it is known to use a laser beam as cutting instrument. More particularly, e.g., in WO 2011/035792 A1 a computer assisted and robot guided laser osteotomic medical device is described which allows for precise and gentle drilling and cutting of bone and other human or animal hard and also soft tissue.

[0003] Within such laser drilling and cutting particularly in the medical field conditioning the material or tissue in an area where it is hit by the laser beam can be of importance. For example, to guarantee an efficient and clean controlled execution of robot-guided laser cuts in hard and soft tissue it is crucial to achieve as few dehydration of the tissue around the drill or cut from the ablation as possible. Also, dissipation of the heat from the cut into the tissue structure can have disadvantageous effects such as melting which are aimed to be prevented as far as possible.

[0004] In this context, there is a need for a device or system allowing to condition the tissue or material at and near where the tissue is treated by a laser beam in order to minimize collateral damages of the tissue and material. In particular, there is a need for such a device or system which can be used in laser osteotomic devices.

Disclosure of the Invention

[0005] According to the invention this need is settled by a nozzle device as it is defined by the features of independent claim 1 and by a nozzle device set as it is defined by independent claim 20. Preferred embodiments are subject of the dependent claims.

[0006] The gist of the invention is the following: A nozzle device for conditioning a laser-tissue contact area comprises a plurality of multi-fluid nozzles and a body with a bore. The bore has a laser entrance and a laser exit. Thereby, the nozzle device is adapted to be mounted to a laser medical device such that a laser beam generated by the laser medical device enters the laser entrance of the bore of the body and exits the laser exit of the bore of the body. The body houses the multi-fluid nozzles and the multi-fluid nozzles are arranged around the laser exit of the bore of the body.

[0007] The term "tissue" in the context of the invention can relate to hard or soft human or animal tissue. Particularly, it can relate to bone tissue, finger or toe nail tissue, cartilage tissue or the like.

[0008] The laser medical device can particularly be a laser osteotome. By the laser beam entering the laser entrance of the bore and exiting the laser exit of the bore the laser beam passes the bore of the body. The bore can particularly be a straight bore. Thus, the laser beam can straightly pass the bore and the body.

[0009] The term "laser-tissue contact area" as used herein relates to an area of the tissue at and around which it is hit by the laser beam when the laser medical device is operated. For being mountable to the laser medical device in order that a laser beam generated by the laser medical device can pass the bore, the body can be connected to the laser medical device with the laser entrance of the bore facing towards the laser medical device and the laser exit of the bore projecting away from the laser medical device. Therefore, the laser medical device can have a mounting structure securing the nozzle device at the laser medical device in a precise predefined position.

[0010] The multi-fluid nozzles can particularly be two-fluid nozzles. They typically can be spray nozzles facilitating dispersion of a liquid such as water or a 0.9% NaCl-solution and a gas such as air into a spray. Like this, the nozzles can efficiently moisturize and cool the laser-tissue contact area. Generally, spray nozzles can be categorized based on the energy input used to breakup of the liquid into drops. They can have one or more outlets wherein a multiple outlet nozzle can be referred to as a compound nozzle.

[0011] By providing the nozzle device with a plurality of multi-fluid nozzles around its laser exit it can efficiently condition the laser-tissue contact area. In this context the term "conditioning" can particularly comprise moisturizing and cooling the tissue at the laser-tissue contact area. The plurality of nozzles is advantageously uniformly distributed around the laser exit and adjusted to be focused on the laser-tissue contact area. Advantageously, they are positioned and oriented such that the sprays generated are focused at or near the laser-tissue contact area.

[0012] The nozzle device according to the invention allows for an intervention such as a cut or a drill to the tissue with minimum or no carbonization around the area of intervention. Dehydration of the tissue around the intervention can be minimized or eliminated by moisturizing the ablation zone and the surrounding tissue. Furthermore, the nozzle device can prevent heat to dissipate further away from the intervention area through the cooling effect introduced by the kinetic energy of the nozzles'

sprays or vapor and the absorption of excessive energy through the cooling liquid itself. Like this, the nozzle device allows to conditioning the tissue at and near where it is cut or drilled by the laser beam of the laser medical device. Thus, the nozzle device is particularly suitable for a laser osteotomic device and allows to minimize collateral damages of the tissue.

[0013] Preferably, the multi-fluid nozzles have a spray direction which is adjustable. In this connection the term "spray direction" can relate to a main or central direction a spray is ejected from the respective multi-fluid nozzle. It is understood that multi-fluid nozzles generally generate a spray with droplets travelling in varying directions over a certain angle. Nevertheless such a spray has a main orientation being the spray direction.

[0014] By having a flexibly adjustable spray direction the sprays of all of the multi-fluid nozzles can be focused on the laser-tissue contact area in variable environments. For example, the tissues can be placed at different places in front of the nozzle device and the nozzles can be adjusted to the respective distance between the tissue and the nozzle device. This allows for using the same nozzle device types for different work distances. Or, the focus of the sprays of the nozzles can be adjusted with increasing ablation of the tissue. This can particularly be beneficial when comparably deep drills or cuts are applied.

[0015] For adjusting the spray direction of the nozzles the nozzle device can have a control unit. Such control unit allows for precisely adjusting the nozzles. Also, an automated adjustment is possible.

[0016] Preferably, the plurality of multi-fluid nozzles comprises three, four, five or six multi-fluid nozzles regularly arranged around the laser exit of the bore of the body. When the bore of the body has a circular cross section the multi-fluid nozzles can be 120°, 90°, 72° or 60° offset to each other depending on the number of nozzles included. Such a number of multi-fluid nozzles allows for evenly and efficiently conditioning the laser-tissue contact area.

[0017] The multi-fluid nozzles can generate a spray by distributing or atomizing the liquid which can be caused by the interaction of high velocity gas and liquid. Thereby, compressed air can conveniently be used as the atomizing gas but steam or other gases are also possible. The multi-fluid nozzles can be internal mix nozzles in which the fluids, typically a gas and a liquid, contact inside the nozzle. Shearing between high velocity gas and low velocity liquid can disintegrate the liquid stream into droplets producing a comparably high velocity spray.

[0018] However, preferably the multi-fluid nozzles are external-mix multi-fluid nozzles. Typically, in external-mix nozzles fluids contact outside the nozzle itself. This type of spray nozzle may require more atomizing air and a higher atomizing air pressure drop because the mixing and atomization of liquid takes place outside the nozzle. The liquid pressure drop can be lower for this type of nozzles, sometimes drawing liquid into the nozzle due to the suction caused by the atomizing air nozzles. This spray may be shaped to efficiently produce a variety of different spray patterns. For example, a flat pattern can be formed with additional air to flatten or reshape the circular spray cross-section discharge. Such external-mix nozzles allow for a comparably precise and flexible adjustment of the provided spray.

[0019] The multi-fluid nozzles of the nozzle device according to the invention are built for a precise regulation of the volume flows of gas and liquid. A fluid increase at constant pressure enlarges the droplets of the resulting vapor or spray and hence produces a bigger moisturizing effect. Bigger droplets could also be used to enhance the purge qualities of the vapour or spray. A constant spray with a higher pressure produces finer droplets. This results in a bigger cooling effect through the increased kinetic energy stored in the finer droplets. Such a spray also enables a better uncontested penetration in thinner cuts or drills, thus preventing a water film and ensuring a constant tissue cooling.

[0020] Preferably, the body comprises a plurality of stacked plates. Such plates can be rings or ring-like shaped. They can be manufactures of any suitably material such as a robust plastic or metal. Different plates can be made of different materials. A body formed of stacked plates allows for a flexible assembling of the nozzle device. Also it allows for efficiently providing a nozzle device adapted to a specific application, i.e. a convenient customization of the nozzle device or system. Further, the stacked plates embodiments of the nozzle device allow for easily integrate a variety of functions into the system.

[0021] Thereby, the plurality of stacked plates preferably comprises a gas supply plate. This gas supply plate has a gas chamber for each of the multi-fluid nozzles, a gas supply channel for each of the gas chambers, and a through bore being part of the bore of the body. Thereby, the through bore of the gas supply plate comprises the laser exit of the bore of the body, each of the gas supply channels is connected to one of the gas chambers, and each of the gas chambers has an outlet being the outlet of the respective multi-fluid nozzle. As mentioned above the gas can particularly be air. Such gas supply plate allows for easily and efficiently integrate the function of supplying a gas into the multi-fluid nozzles. Such gas supply can be required for producing and tuning the sprays of the nozzles.

[0022] Also, the plurality of stacked plates preferably comprises a liquid supply plate. This liquid supply plate has a liquid chamber or homogenizer chamber for each of the multi-fluid nozzles, a liquid supply channel for each of the liquid chambers, a liquid emission channel, and a through bore being part of the bore of the body. Each of the liquid supply channels is connected to one of the liquid chambers, each of the liquid chambers is connected to one of the liquid emission channels, and each of the liquid emission channels extends through one of the gas chambers of the gas supply plate to the outlet of said one of the gas chambers of the gas supply plate. Like this, the

function of supplying liquid to the multi-fluid nozzles can efficiently be integrated. Also, by the liquid emission channels extending through the gas chambers external mix multi-fluid nozzles can efficiently be provided in the nozzle device. The liquid emission channels can also be single part set into the liquid chambers.

[0023] In some interventions it is crucial to be able to bring the vaporization or spraying into a pulsing mode or to stop it completely, e.g., to clean the operation area or to reposition the laser head of the laser medical device. In this context, each of the multi-fluid nozzles preferably comprises a gas supply equipped with a valve. The valves can be fluently or stepwise controllable or they can be simple on/off valves. All of the gas supplies of the multi-fluid nozzles together can have one single valve such that all multi-fluid nozzles are equipped with the same single gas supply valve. Alternatively, each of the multi-fluid valves can be equipped with its own valve such that the number of gas supply valves is identical to the number of multi-fluid nozzles. It is also possible that some of the multi-fluid nozzles are equipped with a single valve such that groups of multi-fluid nozzles are built by single gas supply valves. Also, individual gas supply valves can be combined with one central gas supply valve such that the gas supply can be adjusted in the individual multi-fluid nozzles as well as the gas supply can centrally be controlled such as stopped.

[0024] In embodiments of the nozzle device including a gas supply plate the gas supplies can be formed by the gas supply channels. By means of one or plural gas supply valves an efficient adjustment of the gas stream in the multi-fluid nozzles can be achieved. For example, by closing a gas supply valve the spray of the associated multi-fluid nozzle(s) can rapidly be stopped which can be beneficial in various applications. The gas supply valves can be precisely adjusted by a control unit.

[0025] The gas supply valves advantageously are fast pressure regulation valves which allow to achieve necessary opening times, e.g. 0.2 seconds, to be able to pulse the vapour or spray. For example, the spray can be pulsed between drill or cut depth measurements and the cutting process. These methods presume that the initial gas supply stays intact without any pressure loss at all times.

[0026] Preferably, each of the multi-fluid nozzles comprises a liquid supply equipped with a valve. Similar as described herein before in connection with the gas supplies all of the liquid supplies of the multi-fluid nozzles together can have one single valve such that all multi-fluid nozzles are equipped with the same single liquid supply valve. Alternatively, each of the multi-fluid valves can be equipped with its own valve such that the number of liquid supply valves is identical to the number of multi-fluid nozzles. Such individual liquid supply valves allow for using different solutions in one set up or intervention. For example, this allows for varying the ratio between a cooling solution and another solution which can be enriched with drugs for wound cleaning.

[0027] It is also possible that some of the multi-fluid nozzles are equipped with a single valve such that groups of multi-fluid nozzles are built by single liquid supply valves. In embodiments of the nozzle device including a liquid supply plate the liquid supplies can be formed by the liquid supply channels. By means of one or plural liquid supply valves an efficient adjustment of the liquid stream in the multi-fluid nozzles can be achieved. The liquid supply valves can be precisely adjusted by a control unit which can be a central control unit.

[0028] By being able to open and close the multi-fluid nozzle liquid supply at will and to any extent the spray or vapor of the nozzle device can be regulated through variable valve timing. In some embodiments, each single multi-fluid nozzle can individually be stopped if needed. This can, e.g., be beneficial when several solutions are used in the several multi-fluid nozzles. Or, it also allows for only providing gas if needed at a specific stage of the ablation or cutting process. The valves also allow for a comparably fast opening and closing. Like this, a fluid pulsing mode can be provided where the fluid supply is repeatedly turned on and off in a given frequency which, e.g., can be beneficial to dry the cut or drill between laser intervention and a depth control measurement.

[0029] In particular, the nozzle device preferably comprises a valve control for opening and closing the valves of the gas supply and the valves of the liquid supply independent from each other.

[0030] Preferably, the nozzle device comprises a plurality of light sources arranged around the laser exit of the bore of the body. The light sources can particularly comprise light emitting diodes (LED). In many applications, the target tissue must be well illuminated, so that the operator or surgeon can see the operating area. Furthermore, frequently cameras or other monitoring devices are used in the laser head of the laser medical device in order to monitor the intervention in high quality. By providing the light sources in the nozzle device the need for additional illuminating devices which can be cumbersome to place or precisely operate in many applications can be eliminated. Advantageously, the number of light sources of the nozzle device is chosen to achieve an even and sufficient illumination of the tissue intervention area.

[0031] Preferably, the body comprises a RFID chip. Thereby, the acronym RFID relates to radio-frequency identification. In many applications the nozzle device can be operated in a sterile zone. The RFID chip can then ensure that each nozzle device is only used for one application or patient. For example, the laser medical device can have a corresponding detector with which it can identify the mounted nozzle device. Furthermore, the RFID chip allows for monitoring the consumption and for tracing each nozzle device. This can particularly be beneficial for supporting the use of nozzle devices and the like.

[0032] Preferably, the nozzle device comprises a gas stream inlet/outlet arranged to suck or blow debris induced by the laser beam generated by the laser medical

device. The gas can particularly be air. Such gas stream inlet/outlet allows for removing debris generated by ablation. Particularly, sensitive parts like the optics of the laser medical device, cameras in the laser head, an outcoupling window of the laser medical device or the like can be protected from the debris. Thus, the quality of intervention can be maintained during ablation of the tissue.

[0033] Thereby, the plurality of stacked plates preferably comprises a debris protection plate. This debris protection plate has a through bore being part of the bore of the body, an open inner gas chamber directed to the through bore, and a gas stream channel. The through bore of the gas supply plate comprises the laser entrance of the bore of the body and the gas stream channel is connected to the inner gas chamber. In turn, the gas stream channel can be connected to blowing or suction means. Thereby, the debris protection plate preferably comprises an open outer gas chamber oriented to the laser-tissue contact area, wherein a further or the already mentioned gas stream channel is connected to the outer gas chamber. Such a plate within the stacked plates arrangement of the nozzle device allows for an efficient implementation of a debris protection.

[0034] Preferably, the nozzle device comprises a base having a through bore, a closure, a laser medical device fixture and a mounting structure. Thereby, the closure is adjustable from a closed position in which it closes the through bore to an open position in which the through bore is open, the laser medical device fixture is arranged to fix the nozzle device to the laser medical device and the mounting structure is arranged to be mounted the body. Such a base allows for conveniently mounting and demounting the body to and from the laser medical device. Also, it is possible that the same base is used for mounting different bodies depending on the needs of the respective application. The closure allows for protecting the laser medical device when the nozzle or its body is demounted. Thereby, the closure preferably is configured such that it is in its closed position when the body is demounted from the base and in its open position when the body is mounted to the base.

[0035] Preferably, the nozzle device comprises a window which closes the bore between the laser entrance and the laser exit. Thereby, the window preferably is inclined in relation to an axis of the bore. Like this, a laser beam travelling through the bore does not hit the window in a right angle. Thus, reflection of light into the direction of the laser medical device can be prevented.

[0036] Exemplary technical specifications of a possible nozzle device can be the following: outer diameter of 44 mm; inner diameter (bore diameter) of 20 mm, height 50 mm; orientation of the nozzles adjusted for a distance of 75 mm to an operating field and centered on a focal spot of the laser medical device; fluid volume flow from 3 ml per min to 30 ml per min; spray angle of the multi-fluid nozzles of 20° to 25° and a tolerable gas pressure of 0.5 bar to 3.5 bar.

[0037] Another aspect of the invention relates to a nozzle device set comprising a nozzle device as described above and a drape. The drape sterilely covers the nozzle device. Thereby, such covering can be a complete or partial covering of the nozzle device. In particular, at least exits of the multi-fluid nozzles though which sprays are ejectable out of the multi-fluid nozzles preferably are outside the drape. Also, other associated devices or parts thereof can be covered by the drape together with the nozzle device. For example, a laser head and/or a robot arm of the laser medical device can be included in the drape together with the nozzle device which, e.g., can be mounted to the laser head.

[0038] In many applications the nozzle device can be used within a sterile zone. Thus, either a fixation option for a drape or an integration of the nozzle device in the drape can be beneficial. Benefits of the integration into the drape can be that, since the nozzle device and eventually associated parts can be the last element for the intervention system when being built up, it can be provided in a seal and sterile manner allowing to establish the sterile zone. Furthermore, all supply channels for gas and air can be integrated within the drape, saving time for installation and fixation for other solutions.

Brief Description of the Drawings

[0039] The nozzle device and nozzle device set according to the invention are described in more detail herein below by way of an exemplary embodiment and with reference to the attached drawings, in which:

- Fig. 1 shows perspective exploded view of an embodiment of a nozzle device according to the invention;
- Fig. 2 shows a front view of the nozzle device of Fig.1;
- Fig. 3 shows a cross sectional view along the line A-A of Fig. 2;
- Fig. 4 shows a side view of the nozzle device of Fig. 1; and
- Fig. 5 shows a perspective view of the nozzle device of Fig. 1.

Description of Embodiments

[0040] In the following description certain terms are used for reasons of convenience and are not intended to limit the invention. The terms "right", "left", "up", "down", "under" and "above" refer to directions in the figures. The terminology comprises the explicitly mentioned terms as well as their derivations and terms with a similar meaning. Also, spatially relative terms, such as "beneath", "below", "lower", "above", "upper", "proximal", "distal", and the like, may be used to describe one element's or feature's relationship to another element or feature as illustrated in the figures. These spatially relative terms are intended to encompass different positions and orientations of the nozzle device in use or operation in

addition to the position and orientation shown in the figures. For example, if the device or a specific part thereof in the figures is turned over, elements described as "below" or "beneath" other elements or features would then be "above" or "over" the other elements or features. Thus, the exemplary term "below" can encompass both positions and orientations of above and below. The device may be otherwise oriented (rotated 90 degrees or at other orientations), and the spatially relative descriptors used herein interpreted accordingly. Likewise, descriptions of movement along and around various axes includes various special device positions and orientations.

[0041] To avoid repetition in the figures and the descriptions of the various aspects and illustrative embodiments, it should be understood that many features are common to many aspects and embodiments. Omission of an aspect from a description or figure does not imply that the aspect is missing from embodiments that incorporate that aspect. Instead, the aspect may have been omitted for clarity and to avoid prolix description.

[0042] In this context, the following applies to the rest of this description: If, in order to clarify the drawings, a figure contains reference signs which are not explained in the directly associated part of the description, then it is referred to previous or following description sections. Further, for reason of lucidity, if in a drawing not all features of a part are provided with reference signs it is referred to other drawings showing the same part. Like numbers in two or more figures represent the same or similar elements.

[0043] Fig. 1 show an exploded view of an embodiment of a nozzle device 1 according to the invention. The nozzle device 1 comprises a plurality of ring-like shaped and stacked plates as well as other parts which in Fig. 1 are disassembled from each other. In particular, the nozzle device 1 includes a nozzle device base 4 and a body 2. The nozzle device base 4 comprises a flange like base plate 41, a ring shaped diaphragm ring 42 and diaphragm wings 43. The base plate 41 has flat ring section provided with axial screw bores 412 as laser medical device fixture and a rim section. At an outer peripheral surface of the rim section of the base plate 41 male parts 411 of a bayonet fixing are provided as mounting structure.

[0044] The body 2 of the nozzle device 1 comprises an essentially ring shaped liquid supply and debris protection plate 21 (in the following referred as LSDP plate 21) neighboring the nozzle device base 4 and an essentially ring shaped gas supply plate 22. At an outer peripheral surface the LSDP plate 21 is equipped with gas ports 213, a power port 214 and liquid ports 215 (not visible in Fig. 1). At a side of the LSDP plate 21 facing the gas supply plate 22 liquid chambers 211 are formed into the LSDP plate 21.

[0045] The gas supply plate 22 of the body 2 comprises an inwardly inclined front side of the nozzle device 1 which is equipped with three LEDs 6 as light sources and three openings establishing spray outlets 51 of three two-fluid nozzles 5 as multi-fluid nozzles. Each of the two-fluid nozzles 5 further includes a liquid emission channel 52 and, as showed in more detail below, one of the liquid chambers 211 of the LSDP plate 21. At a peripheral outer surface of the gas supply plate 22 slits 223 are provided being the open end of outer gas chambers 215 arranged in the LSDP plate 21 (not visible in Fig. 1).

[0046] Between the nozzle device base 4 and the body 2 an O-ring 24 and a window 23 and between the LSDP plate 21 and the gas supply plate 21 a draping holder 3 are provided. The draping holder 3 basically has an uneven rounded form and is provided with an eccentric round bore. It is made of glass. The nozzle device 1 further comprises a set of media supply lines 7 with gas supply lines 71, a power line 72 and liquid supply lines 73.

[0047] As can be seen in Fig. 2 in which the nozzle device 1 is shown in an assembled state towards its front end, the gas supply lines 71 are connected to the gas ports 213 of the LSDP plate 21, the power line 72 to its power port 214 and the liquid supply lines 73 to its liquid ports 215. Thereby, the gas ports 213, the power port 214 and the liquid ports 215 lie in one straight line.

[0048] The nozzle device 1 has a straight bore 8 extending from its front side at the LSDP plate 22 to the back side at the nozzle device base 4. At the front side of the nozzle device 1 the bore 8 ends in its laser beam exit 81. The spray outlets 51 of the three two-fluid nozzles 5 are regularly arranged around the laser beam exit 81 of the bore 8. Like this, the spray outlets 51 are arranged along a circle in an angle of 120° offset from each other. Centrally between each two neighboring spray outlets 51 one of the LEDs 6 is placed. Thus, also the LEDs 6 are arranged along a circle in an angle of 120° offset from each other.

[0049] In Fig. 3 a cross section of the assembled nozzle device 1 is shown. The diaphragm ring 42 is inserted into an opening of the base plate 41. Thereby, the diaphragm ring 42 is turnable inside and relative to the base plate 41. It is further coupled to the diaphragm wings 43 such that turning the diaphragm ring 42 relative to the base plate 41 induces a movement of the diaphragm wings 43. Thereby, the diaphragm wings 43 open and close a laser beam entrance 82 of the bore 8 depending on the turning of the diaphragm ring 42.

[0050] At its end side facing the nozzle device base 4, the LSDP plate 22 of the body 2 has a rim recess in which the rim section of the base plate 41 is arranged. More particularly, the rim recess of the LSDP plate 22 has a female portion 216 of the bayonet fixing at a inner ring circumferential surface. By turning the body 2 relative to the nozzle device base 4 around a longitudinal axis of the nozzle device 1 when being arranged on the rim section of the base plate 41 the female portion 216 of the bayonet fixing of the LSDP plate engages the male portion 411 of the bayonet fixing of the base plate 41. Thereby, the body 2 can be locked and unlocked on the nozzle device base 4.

[0051] The diaphragm ring 42 is coupled to the LSDP plate 21 when the body 2 is arranged on the nozzle device

base 4. Like this, when turning the LSDP plate 21 relative to the base plate 41 the diaphragm ring 42 is also turned relative to the base plate 41. Thereby, the diaphragm wings 43 are opened or closed, respectively. More particularly, when the body 2 is locked on the nozzle device base 4 by turning the LSDP plate 21 relative to the base plate 41 the diaphragm ring 42 is turned to the identical extent and the diaphragm wings 43 are moved apart such that the laser beam entrance 82 of the bore 8 is opened. Vice versa, when the body 2 is unlocked from the nozzle device base 4 by turning the LSDP plate 21 in an opposite direction relative to the base plate 41 the diaphragm ring 42 is turned to the identical extent and the diaphragm wings 43 are moved towards each other such that the laser beam entrance 82 of the bore 8 is closed. In Fig. 2 the body 2 is shown unlocked from the nozzle device base 4 and the laser beam entrance 82 are closed by the diaphragm wings 43 accordingly.

[0052] When the body 2 is mounted to the nozzle device base 4 the O-ring 24 is clamped between the LSDP plate 21 and the base plate 41. The O-ring 24 has an elasticity allowing for sealing the connection of the LSDP plate 21 and the base plate 41. Additionally, the O-ring 24 damps movements of the LSDP plate 21 and the base plate 41 relative to each other along a longitudinal axis 11 of the nozzle device 1.

[0053] Furthermore, between the LSDP plate 21 and the base plate 41 the window 23 is arranged. Thereby, the window 23 is inclined relative to the longitudinal axis 11 of the nozzle device 1. More specifically, the window 23 and the longitudinal axis 11 lie in an angle of about 84° relative to each other. Like this, it can be prevented that light of a laser beam provided through the bore 8 of the nozzle device 1 is reflected and travelling back to the laser medical device. Rather, laser beam light would be deflected by 12° when being reflected by the window 23 such that it is not sent back to the laser medical device.

[0054] As can be seen in Fig. 3 the LSDP plate 21 comprises an inner gas chamber 212 which ends in an opening provided at in inner cylindrical surface of the LSPD plate 21. The inner gas chamber 212 is connected to one of the gas supply lines 71 via one of the gas ports 213 and via a gas stream channel (not visible in Fig. 3). It is further oriented such that gas provided by the respective gas supply line 71 and exiting the opening of the gas chamber 212 hits the window 23. Like this, the window can efficiently be cleaned. In particular, debris generated by ablation can be removed from the window 23 such that provision of the laser beam can be kept at a constant high quality during a ablation process.

[0055] The liquid chambers 211 formed in the end side of the LSDP plate 21 facing the gas supply plate 22 are connected to the liquid supply lines 73 via the liquid ports 213 and liquid supply channels (not visible in Fig. 3) such that they can be provided with a liquid to be sprayed by the two-fluid nozzles 5. Each of the liquid supply lines 73 as well as each of the gas supply lines 71 are provided with a valve. The valves can be adjusted and, particularly be switched on and off. By means of the valves, the gas and liquid supply into the two-way nozzles 5 can be controlled.

[0056] The gas supply plate 22 comprises gas chambers 221 each being part of one of the two-fluid nozzles 5. The gas chambers 221 connect the spray outlets 51 with the liquid chambers 211. Each of the gas chambers 221 is connected to the gas supply lines 71 via a gas supply channel (not visible in Fig. 3) of the gas supply plate 22 and is provided with one of the liquid emission channels 52. When the two-fluid nozzles are provided with liquid and gas the liquid is pushed via the liquid chambers 211 through the liquid emission channels 52 out of the spray outlet 51. In the meantime the gas is forwarded through the gas chambers 221 out of the spray outlet 51. Outside the two-fluid nozzles 5 the gas stream hits the liquid stream and according sprays are produced. By adjusting the pressure and flow of the gas and the liquid characteristics of the sprays can precisely be defined.

[0057] The end side of the gas supply plate 22 has a surface which is inwardly inclined towards the laser beam exit 81. Like this, two-fluid nozzles 5 are directed towards a focal spot. Thus, in a situation where the two-fluid nozzles 5 produce a straight spray the sprays meet in the focal spot. In order that the two-fluid nozzles 5 do not have to be adjusted, the focal spot is preferably located where the laser beam hits the tissue to drill or cut.

[0058] The LSDP plate 21 is further equipped with the outer gas chambers 215 which are connected to the slits 223 in the gas supply plate 22 and to the gas supply lines 71 via the gas ports 213 and a gas stream channel (not visible in Fig. 3). As can be seen in Fig. 4 showing the nozzle device 1 from a side and in Fig. 5 showing the nozzle device in a perspective there are two slits 223 neighboring each other. The outer gas chambers 215 are connected to the gas supply lines 71. By providing gas through the outer gas chambers 215 and out of the slits 223 a gas stream can be produced around a front side of the nozzle device 1. Like this debris produced by ablation can be removed from around the nozzle device 1 and from the laser-tissue contact area.

[0059] This description and the accompanying drawings that illustrate aspects and embodiments of the present invention should not be taken as limiting the claims defining the protected invention. In other words, while the invention has been illustrated and described in detail in the drawings and foregoing description, such illustration and description are to be considered illustrative or exemplary and not restrictive. Various mechanical, compositional, structural, electrical, and operational changes may be made without departing from the spirit and scope of this description and the claims. In some instances, well-known circuits, structures and techniques have not been shown in detail in order not to obscure the invention. Thus, it will be understood that changes and modifications may be made by those of ordinary skill within the scope and spirit of the following claims. In particular, the present invention covers further embodiments

with any combination of features from different embodiments described above and below.

[0060] The disclosure also covers all further features shown in the Figs. individually although they may not have been described in the afore or following description. Also, single alternatives of the embodiments described in the figures and the description and single alternatives of features thereof can be disclaimed from the subject matter of the invention or from disclosed subject matter. The disclosure comprises subject matter consisting of the features defined in the claims or the exemplary embodiments as well as subject matter comprising said features.

[0061] Furthermore, in the claims the word "comprising" does not exclude other elements or steps, and the indefinite article "a" or "an" does not exclude a plurality. A single unit or step may fulfil the functions of several features recited in the claims. The mere fact that certain measures are recited in mutually different dependent claims does not indicate that a combination of these measures cannot be used to advantage. The terms "essentially", "about", "approximately" and the like in connection with an attribute or a value particularly also define exactly the attribute or exactly the value, respectively. The term "about" in the context of a given numerate value or range refers to a value or range that is, e.g., within 20%, within 10%, within 5%, or within 2% of the given value or range. Components described as coupled or connected may be electrically or mechanically directly coupled, or they may be indirectly coupled via one or more intermediate components. Any reference signs in the claims should not be construed as limiting the scope.

Claims

1. Nozzle device (1) for conditioning a laser-tissue contact area, comprising a plurality of multi-fluid nozzles (5) and a body (2) with a bore (8), wherein
the bore (8) has a laser entrance (82) and a laser exit (81),
the nozzle device (1) is adapted to be mounted to a laser medical device such that a laser beam generated by the laser medical device enters the laser entrance (82) of the bore (8) of the body (2) and exits the laser exit (81) of the bore (8) of the body (2),
the body (2) houses the multi-fluid nozzles (5), and
the multi-fluid nozzles (5) are arranged around the laser exit (81) of the bore (8) of the body (2).

2. Nozzle device (1) according to claim 1, wherein the multi-fluid nozzles (5) have a spray direction which is adjustable.

3. Nozzle device (1) according to claim 1 or 2, wherein the plurality of multi-fluid nozzles (5) comprises three, four, five or six multi-fluid nozzles (5) regularly arranged around the laser exit (81) of the bore (8) of the body (2).

4. Nozzle device (1) according to any one of the preceding claims, wherein the multi-fluid nozzles (5) are external-mix multi-fluid nozzles (5).

5. Nozzle device (1) according to any one of the preceding claims, wherein the body (2) comprises a plurality of stacked plates (21, 22).

6. Nozzle device (1) according to claim 5, wherein the plurality of stacked plates (21, 22) comprises a gas supply plate (22) having
a gas chamber (221) for each of the multi-fluid nozzles (5),
a gas supply channel (222) for each of the gas chambers (221), and
a through bore being part of the bore (8) of the body (2), wherein
the through bore of the gas supply plate (22) comprises the laser exit (81) of the bore (8) of the body (2),
each of the gas supply channels (222) is connected to one of the gas chambers (221), and
each of the gas chambers (221) has an outlet being the outlet (51) of the respective multi-fluid nozzle (5).

7. Nozzle device (1) according to claim 6, wherein the plurality of stacked plates (21, 22) comprises a liquid supply plate (21) having
a liquid chamber (211) for each of the multi-fluid nozzles (5),
a liquid supply channel for each of the liquid chambers (211),
a liquid emission channel (52), and
a through bore being part of the bore (8) of the body (2), wherein
each of the liquid supply channels is connected to one of the liquid chambers (211),
each of the liquid chambers (211) is connected to one of the liquid emission channels (52), and
each of the liquid emission channels (51) extends through one of the gas chambers (221) of the gas supply plate (22) to the outlet of said one of the gas chambers (221) of the gas supply plate (22).

8. Nozzle device (1) according to any one of the preceding claims, wherein each of the multi-fluid nozzles (5) comprises a gas supply (71) equipped with a valve.

9. Nozzle device (1) according to any one of the preceding claims, wherein each of the multi-fluid nozzles (5) comprises a liquid supply (73) equipped with a valve.

10. Nozzle device (1) according to claim 8 and 9, comprising a valve control for opening and closing the

valves of the gas supply (71) and the valves of the liquid supply (73) independent from each other.

11. Nozzle device (1) according to any one of the preceding claims, comprising a plurality of light sources (6) arranged around the laser exit (81) of the bore (8) of the body (2).

12. Nozzle device (1) according to any one of the preceding claims, wherein the body (2) comprises a RFID chip.

13. Nozzle device (1) according to any one of the preceding claims, comprising a gas stream inlet/outlet (212, 223) arranged to suck or blow debris induced by the laser beam generated by the laser medical device.

14. Nozzle device (1) according to any one of claims 5 to 12 and 13, wherein the plurality of stacked plates comprises a debris protection plate (21) having
a through bore being part of the bore (8) of the body (2),
an open inner gas chamber (212) directed to the through bore (8), and a gas stream channel, wherein the gas stream channel is connected to the inner gas chamber (212).

15. Nozzle device (1) according to claim 14, wherein the debris protection plate (21) comprises an open outer gas chamber (215) oriented to the laser-tissue contact area, wherein a gas stream channel is connected to the outer gas chamber (215).

16. Nozzle device (1) according to any one of the preceding claims, comprising a base (4) having a through bore, a closure (42, 43), a laser medical device fixture (412) and a mounting structure (411), wherein the closure (42, 43) is adjustable from a closed position in which it closes the through bore to an open position in which the through bore is open and wherein the laser medical device fixture (412) is arranged to fix the nozzle device (1) to the laser medical device and the mounting structure (412) is arranged to mount the body (2) to the base (4).

17. Nozzle device (1) according to claim 16, wherein the closure (42, 43) is configured such that it is in its closed position when the body (2) is demounted from the base (4) and in its open position when the body (2) is mounted to the base (4).

18. Nozzle device (1) according to any one of the preceding claims, comprising a window (23) which closes the bore (8) between the laser entrance (82) and the laser exit (81).

19. Nozzle device (1) according to claim 18, wherein the window (23) is inclined in relation to an axis (11) of the bore (8).

20. Nozzle device (1) set comprising a nozzle device (1) according to any one of the preceding claims and a drape, wherein the drape sterilely covers the nozzle device (1).

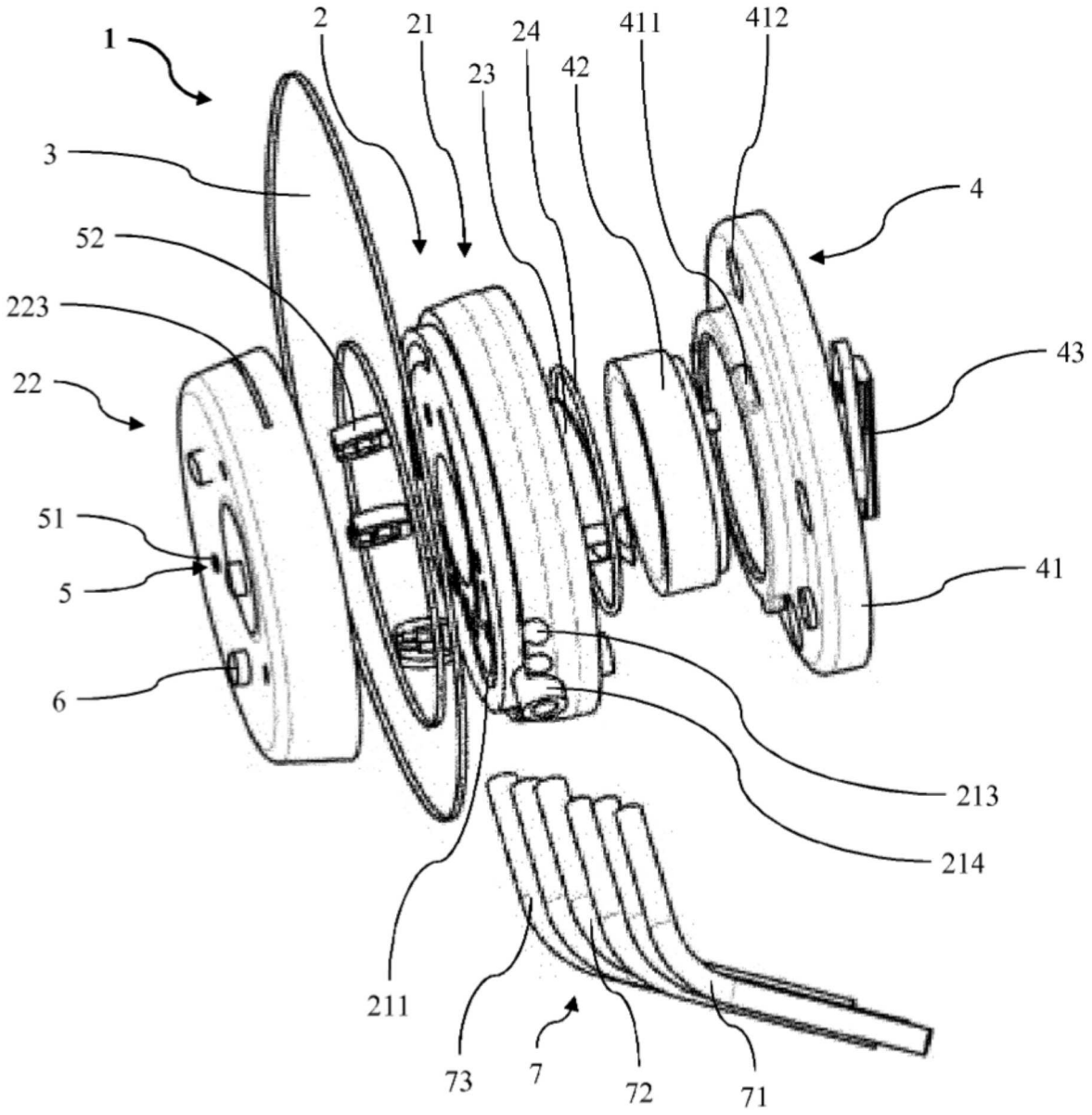

Fig. 1

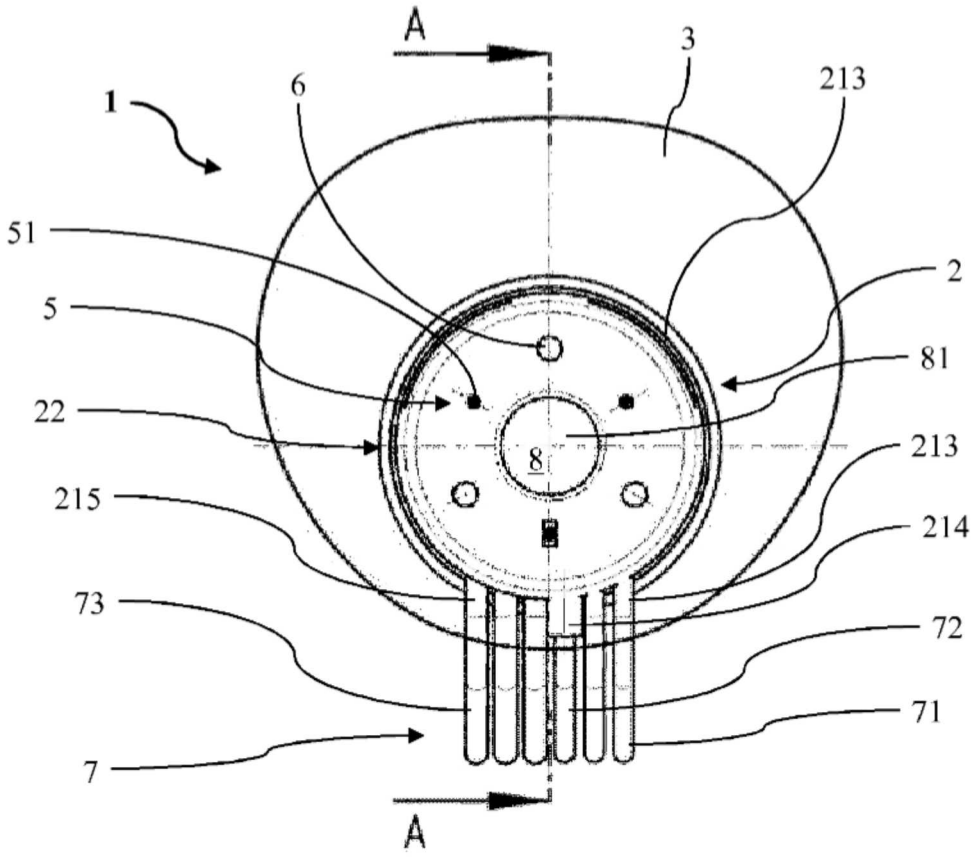

Fig. 2

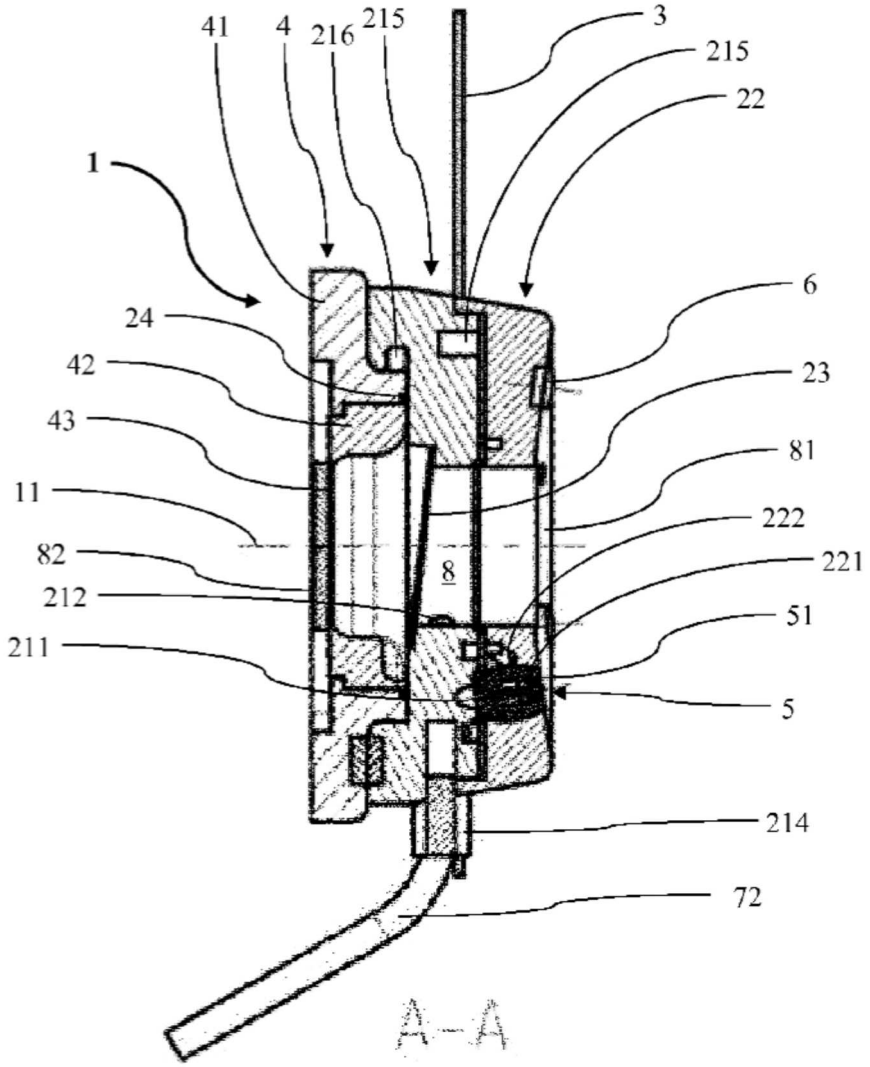
41
4
216
215
3
215
22
1
6
24
42
23
43
81
11
222
82
8
221
212
51
211
5
214
72
A-A

Fig. 3

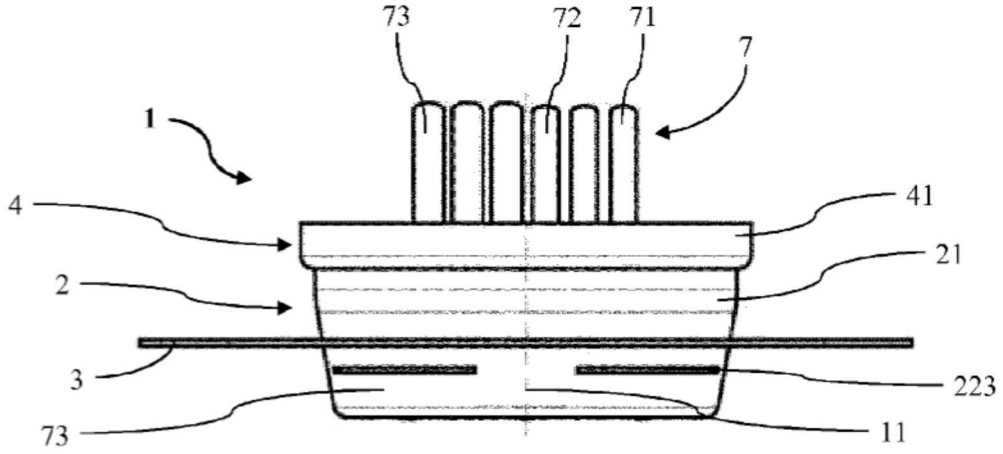
73
72
71
7
1
41
4
21
2
3
223
73
11

Fig. 4

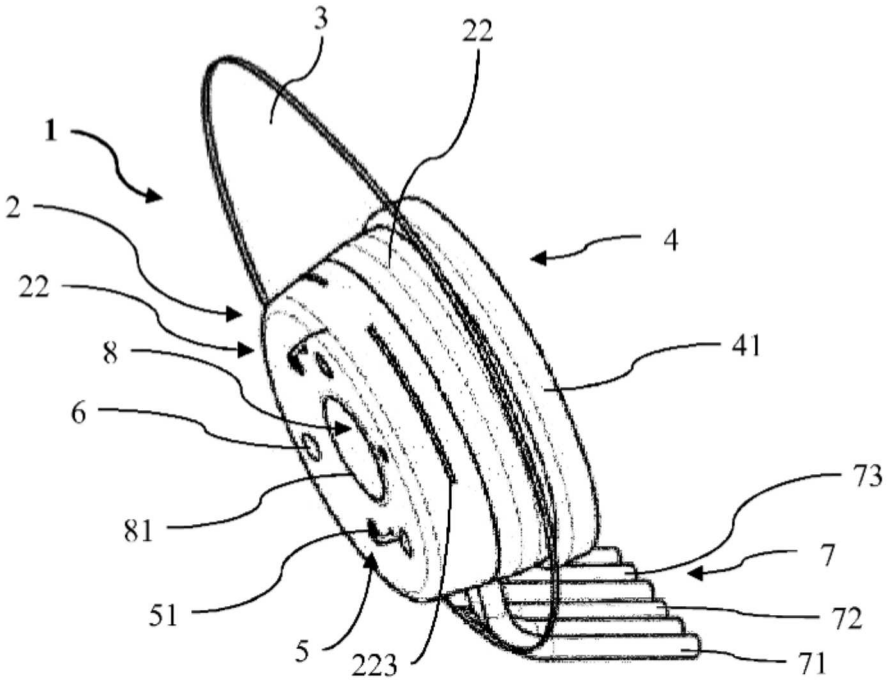

Fig. 5

Europäisches Patentamt
European Patent Office
Office européen des brevets

EUROPEAN SEARCH REPORT

Application Number
EP 15 18 0233

DOCUMENTS CONSIDERED TO BE RELEVANT

Category	Citation of document with indication, where appropriate, of relevant passages	Relevant to claim	CLASSIFICATION OF THE APPLICATION (IPC)
X	US 2005/256517 A1 (BOUTOUSSOV DMITRI [US]) 17 November 2005 (2005-11-17)	1-5, 8-11, 13-20	INV. A61B18/20 A61B18/22 A61B17/3203 A61C1/00
Y	* paragraphs [0006], [0020] - [0024], [0028] - [0029], [0044] - [0047]; figures 4,5 *	6,7,12	
Y	US 2014/257254 A1 (BOUTOUSSOV DMITRI [US] ET AL) 11 September 2014 (2014-09-11) * paragraph [0011] - paragraph [0014]; figures 1,2 *	6,7	
Y	US 2009/143773 A1 (GOSSE ALBAN [FR] ET AL) 4 June 2009 (2009-06-04) * paragraph [0131] *	12	

TECHNICAL FIELDS SEARCHED (IPC)
A61B
A61C

The present search report has been drawn up for all claims

Place of search	Date of completion of the search	Examiner
Munich	3 February 2016	Gentil, Tamara

CATEGORY OF CITED DOCUMENTS

X : particularly relevant if taken alone
Y : particularly relevant if combined with another document of the same category
A : technological background
O : non-written disclosure
P : intermediate document

T : theory or principle underlying the invention
E : earlier patent document, but published on, or after the filing date
D : document cited in the application
L : document cited for other reasons

& : member of the same patent family, corresponding document

EPO FORM 1503 03.82 (P04C01)

ANNEX TO THE EUROPEAN SEARCH REPORT ON EUROPEAN PATENT APPLICATION NO. EP 15 18 0233

This annex lists the patent family members relating to the patent documents cited in the above-mentioned European search report. The members are as contained in the European Patent Office EDP file on
The European Patent Office is in no way liable for these particulars which are merely given for the purpose of information.

03-02-2016

Patent document cited in search report	Publication date	Patent family member(s)	Publication date
US 2005256517 A1	17-11-2005	EP 1748743 A2	07-02-2007
		EP 2329785 A1	08-06-2011
		ES 2400185 T3	08-04-2013
		ES 2407672 T3	13-06-2013
		SI 1748743 T1	30-04-2013
		SI 2329785 T1	31-07-2013
		US 2005256517 A1	17-11-2005
		US 2010185188 A1	22-07-2010
		WO 2005070034 A2	04-08-2005
US 2014257254 A1	11-09-2014	EP 2967752 A1	20-01-2016
		US 2014257254 A1	11-09-2014
		WO 2014164737 A1	09-10-2014
US 2009143773 A1	04-06-2009	EP 2237731 A1	13-10-2010
		FR 2924327 A1	05-06-2009
		US 2009143773 A1	04-06-2009
		US 2010305554 A1	02-12-2010
		WO 2009071592 A1	11-06-2009

Chapter 6

Heat Induction during Laser Bone Ablation: Thermal Imaging Measurements

This paper was submitted in Mai 2019 to the *Wiley Online Library* under the online magazine *Lasers in Surgery and Medicine* and is currently under review. It is expected to be published after the submission of this thesis.

In this paper, heat induction and relaxation within the tissue during laser osteotomies are investigated. During multiple in-vitro experiments on cortical cow bone discs, several cuts were performed with the develoed laser osteotome. The procedures were recorded and analyzed with a thermal camera.

It was shown that heat accumulates during laser bone ablation within the tissue if the procedure is not assisted with an external spray cooling. This leads consequently to thermal damages of the treated and surrounding tissue, and consequently to carbonization.

In this research we could show that using the in-house developed nozzle system, the maximum temperatures for the induced heat were much lower. Furthermore, the induced heat relaxed out of the tissue before the next laser pulse hit, preventing heat accumulation. Finally, a spatial evaluation at the time of maximum induced heat showed a symmetrical temperature distribution for the heat motion perpendicular to the laser beam propagation direction.

Heat Induction during Laser Bone Ablation: Thermal Imaging Measurements

Waldemar Deibel[1,2], Marcello Augello[3,4], Adrian Schneider[2], Michael Peyer[2], James Jockel Leuenberger[2], Alfredo Bruno[2], Philipp Juergens[3,4,*], Philippe C. Cattin[1,2,*]

[1]Department of Biomedical Engineering, University of Basel, Switzerland
[2]Advanced Osteotomy Tools AG, Basel, Switzerland
[3]Hightech Research Centre of Cranio-Maxillofacial Surgery, University of Basel, Switzerland
[4]Department of Cranio-Maxillofacial Surgery, University Hospital Basel, Switzerland
***Note:** Both authors contributed equally to this paper.

Abstract.
Objectives Understanding all interactions between laser light and hard tissue is crucial if laser osteotomes should one day replace conventional osteotomy tools. One of the expected dangers is thermal damage caused by the incident light. Here, heat induction and relaxation within the tissue during such procedures are measured, analyzed and discussed to better understand the overall process.
Methods Several osteotomy cuts were performed on cortical cow bone discs with the laser osteotome CARLO. The procedures were recorded and analyzed with a thermal camera.
Results Heat accumulates during laser bone ablation within the tissue if the procedure is not assisted with an external spray cooling. Furthermore, a symmetrical temperature distribution for the heat induction perpendicular to the laser beam propagation direction was shown.
Conclusion Under the proper conditions, thermal damage can be avoided during laser bone ablation. These results will help the laser osteotome to become a real alternative to conventional tools such as the piezoelectric saw or drills since it executes arbitrary cutting geometries for contact free procedures.

Keywords: laser, bone ablation, heat induction, imaging, thermal damage

1 Introduction

Since its development in the 1960s, the laser was always seen as a fascinating and promising technology. It is not surprising that it found many applications in different industries and private households, varying from CD players to huge metal cutting machines. Sure enough, it also found its way into many medical fields such as ophthalmology or dermatology. The first experiments for laser hard tissue ablation were performed by Goldman et al. [1] as early as 1964 with a ruby

laser at a wavelength of 694 nm. They used teeth to demonstrate that the laser could be used as a surgical tool. Unfortunately, that treatment induced severe thermal damage to nerve fibers and caused tooth cracking. In 1972 Stern et al. [2] started to investigate the CO_2 laser (carbon dioxide laser) as a possible light source for hard tissue treatment. However, the results did not improve much compared to Goldman et al. [1], so Stern et al. [3] concluded two years later that the laser would never be an applicable tool for dentistry when the caused thermal effects are not eliminated. Nevertheless, research with CO_2 lasers for osteotomy purposes continued and started to produce better results in terms of efficiency, safety and thermal damage avoidance [4][5][6]. In 2010 Burgner et al. [7] demonstrated a prototype system for roboter-assissted osteotomy. They used CT data for the preoperative planning and executed the osteotomies by using an articulated robot-guided mirror arm for beam delivery. The authors concluded that apart from the rather slow cutting speed, the complexity and size of such a system are the major hurdles to overcome before it could be considered a real option for osteotomies under OR conditions. In parallel, other laser systems were developed for hard tissue ablation, which present today a viable option. In 1989 Hibst and Keller introduced the Er:YAG laser (erbium-doped yttrium aluminum garnet laser) for hard tissue ablation [8], arguing that its wavelength of 2.94 µm with an absorption peak in water would enhance the ablation process, resulting in high efficiency. The strong absorption in water defined the ablation effect as a thermomechanical interaction [9]. The water content in the hard tissue evaporates (thermal effect) and instantly builds pressure (mechanical effect), resulting in micro explosions that break up the hydroxyapatite structure. In 1994 Frentzen et al. [10] found that those micro explosions created small fissures or cracks in the hard tissue. They proposed an external cooling of the treated tissue to reduce such negative side effects. In 2008 Kang et al. [11] investigated laser hard tissue ablation under various environments, i.e. dry, wet (500 µm water layer), wet (500 µm perfluorocarbon layer) and spray ablation ($8\,\mathrm{ml\,min^{-1}}$). They concluded that the ablation was optimal during water spray cooling, i.e. particularly clean with no thermal damage, and suggested spray cooling systems as a feasible technology for laser osteotomy. In 2015 Baek et al. [12] showed that under the right conditions, the Er:YAG laser system has even some advantages over conventional mechanical tools for laser osteotomy. They conducted several osteotomies in minipig mandibles during an animal study. On one side a state-of-the-art piezoelectric osteotome (PZE) was used to create the defect, on the other, a laser osteotome. The extracted bone samples were analyzed with scanning electron microscopy (SEM). Samples from the laser osteotome showed biologically open cut surfaces. In contrast, samples from the PZE "*showed a flattened tissue structure over the cut surface, resembling the smear layer from tooth preparation*". Furthermore, the laser osteotome cut surfaces showed no cracks in the hard tissue compared to the cut surfaces from the PZE. In the same year, Baek et al. [13] demonstrated that the previously introduced Er:YAG laser osteotome can be integrated into an OR to function as an unobtrusive tool for the

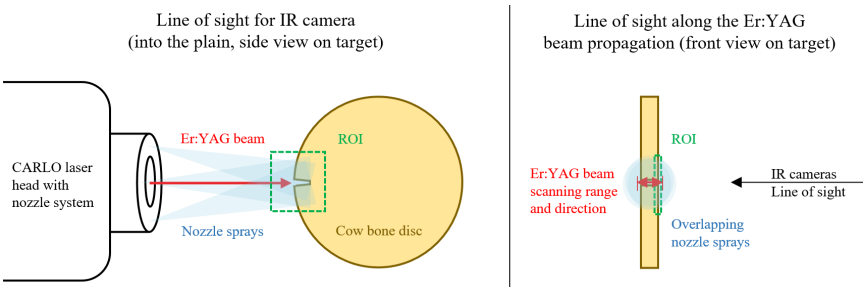

Fig. 1: Experimental setup for thermal effects measurements during laser bone ablation, with CARLO as the cutting tool and a cow bone disc as the target tissue. The working distance between the nozzle system and the bone disc was 70 mm. The field of view for the IR camera is the region from which the measurements were evaluated, its actual field of view is larger.

surgeons. Hence, eliminating the drawbacks of the more complex and bulkier CO_2 laser-based osteotome [7].

This paper investigates the interaction of light and hard tissue during laser ablation. The hypothesis is that thermal damage can be excluded for laser osteotomy and that this technology could find its way into the OR as a reliable tool for complex surgeries.

2 Material and Methods

2.1 Experimental Setup

The experiments were performed with the following main components; a laser osteotome CARLO (Cold Ablation Robot-guided Laser Osteotome, AOT AG, Basel, Switzerland), cow bone discs as target tissue, a thermal camera and a computer which recorded the thermal images during the cutting procedures. Figure 1 shows the experimental setup.

The CARLO is an automated laser osteotome developed by Advanced Osteotomy Tools AG (www.aot.swiss). It comprises of four major parts [14]. A trolley for mobility that stores all control units and has the user interface and. A robotic arm which is mounted on the trolley and holds the cutting tool, the laser head. Lastly, an optical navigation system that guides the movements of the robot with respect to the operating field for safe and precise cut execution. The built-in laser system is a solid state Er:YAG laser with a central wavelength of 2.94 µm. It was set up for 4.5 W operating at 10 Hz (450 mJ per pulse) and a pulse length of 250 µs. This resulted in a 1 mm wide focal spot with an energy density of 70.7 J/cm^2 on the target tissue. The cuts were planned by referencing the starting point of the line to be cut via a pointer tool. The CARLO robot then positioned the laser head accordingly. For the cut execution, its built-in fast steering mirror with low noise, high accuracy (angular resolution <0.6 µrad s to

$<1.2\,\mu\text{rad}\,\text{s}$ RMS), high acceleration/step speed (5 ms for a 1 mrad step) and high angular range ($\pm 3°$ mechanical) scanned the laser beam along that cutting line across the entire bone disc profile in the range of 5 mm to 8 mm. The turning point of the scan was set just outside the sample to avoid increased pulse application where the beam halted to change its direction. An infrared (IR) camera recorded the heat induction into the bone sample during the whole cutting procedure. Whereas for the evaluation, only measurements of the cutting procedure directly at the edge of the bone sample facing towards the IR camera were taken, i.e. just before the laser beam exited the sample's edge at the turning point and when it started to cut again on its way back. The scanning speed was set to $1.3\,\text{mm}\,\text{s}^{-1}$, resulting in a beam spot overlapping percentage of 87 %, which ensured a smooth cut as it would be setup for an osteotomy. The high beam spot overlapping percentage also ensured that several good visible pulses on the edge of the bone disc could be recorded and a potential heat accumulation detected before the measurements could be damped or obscured by surrounding tissue. The measurements for the evaluated pulses were taken over the course of eight to ten consecutive full range scans. The cooling of the target tissue was realized with tap water by the built-in nozzle system with a total water mass flow of $12\,\text{ml}\,\text{min}^{-1}$ at 3 bar produced by the three secondary gas-assisted atomization nozzles with external mixture. This setup proved to be ideal in previous experiments and is comparable to optimized parameters published by Kang et al. [15] for spray-assisted hard tissue ablation with a similar system (Er,Cr:YsGG laser with a wavelength of 2.79 µm, energy density of $52\,\text{J}/\text{cm}^2$, optimized total water mass flow of $8\,\text{ml}\,\text{min}^{-1}$). The high-pressure nozzle spray prevents the building of a potential water layer within the cut, as it pushes out excess water over the edges on both sides of the bone sample. With this setup, only a thin layer of the nozzle spray remains between the ROI and the IR camera. We judge the influence of this fast-moving layer neglectable for the overall results of this experiment since the nozzle spray droplets have a very small mass and are distributed in a low density. The temperature measurements were taken just after a pulse, when water is evaporated, and the debris carries out excessive material. With the Er:YAG laser having its absorption peak in water, a potential water layer evaporates first, then the radiation penetrates the tissue for its interaction. The maximum temperature measurements were taken when the light just evaporated all water and interacted with the tissue. In that moment, the debris also counteracts the nozzle spray's forward motion and prevents the water droplets from entering the cut, see Figure 2. The set high beam spot overlapping percentage also ensured that several good visible pulses and a potential heat accumulation at the edge of the bone disc could be detected.

The camera used for recording and measuring was the IR FLIR A655sc thermal camera. It has a Vanadium Oxide (VoX) microbolometer detector which provides 14-bit data up to 50 frames per second at full frame 640×480 pixel resolution. For these experiments, its high speed windowing mode with an increased frame rate output up to 200 Hz at 640×120 pixel was used to have the highest temporal resolution possible. The temperature ranges are $-40\,°\text{C}$ to

150 °C and 100 °C to 650 °C with an accuracy of 2 °C. A setup with a frame rate of 200 Hz results in 5 ms steps measurements. While the heat induction is generated during a 250 µs pulse. Hence, such a setup cannot guarantee that the highest thermal point is measured. Since thermal effects are rather slow though, the measured maximum temperature should not be 200 times higher as a calculation for the thermal load for a 5 ms average indicates. The thermal high should be rather close to the measured maximum temperature. Also, the more important value is the thermal low, which indicates a potential heat accumulation over the course of several pulses. Since the pulses are applied 100 ms apart, the measured thermal low is accurate. The thermal camera was mounted on a tripod and aligned to record the heat induction into the sample and its thermal propagation during the cutting processes. The camera recorded the cutting procedure from a perpendicular line of sight to the bone sample surface and the incident cutting beam, see Figure 1. The measurements were recorded with the FLIR ResearchIR software (v 4.30.1) with different temperature ranges according to the heat induced into the bone discs. All measurements were evaluated with the FLIR ResearchIR software for the ROI within our recorded data.

2.2 Sample Preparation

These experiments targeted bovine cortical discs. They were produced out of fresh cow femur, bought at a local abattoir, to have mostly homogeneous material to work with. A hollow drill with an inner diameter of 40 mm was used to extract the discs and grind them afterwards with a single-disc sanding machine. As a result, cortical bone discs with a diameter of 40 mm and a thickness of 5 mm to 8 mm with nearly plane-parallel surfaces were obtained. These samples were then stored in a deep freezer at −18 °C. Before the experiments they were unfrozen in room temperature tap water for two hours. These discs were then used to perform basic studies of heat induction and heat propagation within the bone tissue during laser ablation with and without water spray cooling.

3 Results

Heat induction by laser radiation was evaluated during its interaction with hard tissue and its 2D spatial propagation was quantified. Thermal images for laser bone ablation were acquired with and without spray assisted cooling. The experiments with the highest measured temperatures during one pulse are presented in Figure 2 and Figure 4. The temperatures were measured during a full range scan for one pulse or pulse train as it would behave during an osteotomy. Hence, the measured values are influenced by the previous pulse(s) and tissue conditioning. When the tissue is not adequately cooled down before the next pulse is applied heat accumulates and the next pulses T_{min} or baseline is increasing.

The maximum temperatures measured (T_{max}) during bone laser ablation without spray cooling for six cuts ranged from 204 °C to 231 °C, the minimum

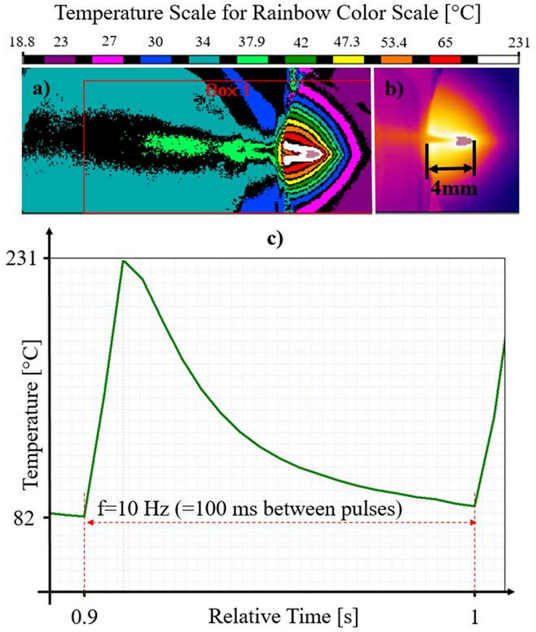

Fig. 2: Measured temperatures $T_{max} = 231\,°C$ and $T_{min} = 82\,°C$ during laser osteotomy on a bone disc without spray assisted cooling. a) Temperature segmented figure with the rainbow color scale. b) Fusion image with smooth transitions for the temperature measurements. c) Temporal plot for one whole laser pulse.

temperatures measured (T_{min}) ranged from 68 °C to 98 °C. As an example, Figure 2 shows the pulse with the highest T_{max} measured, here 231 °C and T_{min} = 82 °C. It is important to note that T_{min} rises by 4.9 °C for the next pulse. In general, for all measurements, T_{min} rose for each consecutive pulse by two to seven degrees, see Figure 3, which confirms that the tissue is being constantly heated with each new laser pulse applied. As soon as the last water vaporizes, the tissue starts to carbonize at temperatures of 100 °C to 300 °C [16].

The maximum temperatures measured (T_{max}) during osteotomies with spray cooling for six cuts ranged from 93 °C to 150.1 °C, the minimum temperatures measured (T_{min}) ranged from 21 °C to 23 °C. As an example, Figure 4 shows the pulse with the highest measured T_{max}, here 150.1 °C, which is also in the carbonization region. But the white segment in Figure 4a shows a temperature regime from 150 °C to 29 °C, with a heat penetration of approximately 0.5 mm within the hard tissue. Tissue outside the white segment experienced temperatures under 29 °C, hence no thermal damage induction is possible. Furthermore, the temperature fell down to 21 °C even before the next pulse was applied. Therefore, the tissue cannot accumulate heat over the course of several pulses.

To gain additional information, the spatial heat distribution was evaluated further. A square-shaped temperature measurement cursor was introduced in

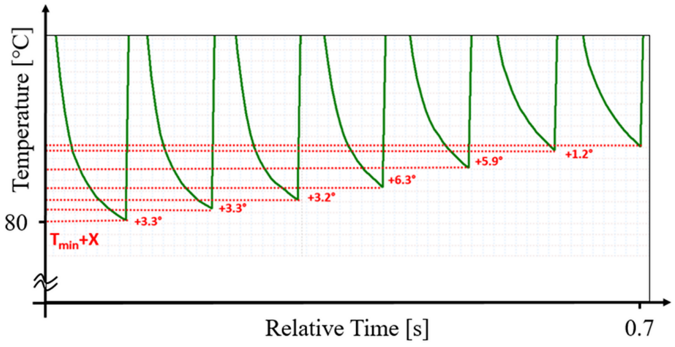

Fig. 3: Example of heat accumulation for each consecutive pulse during bone ablation without spray cooling.

Figure 4a at the position of $T_{max} = 150\,°C$, which was defined as the starting position, see Figure 5. To measure the spatial distribution, the square-shaped cursor was moved by 0.5 mm to the up, down and front positions, respectively. The software indicates temperatures of the square-shaped cursors center, the maximum and minimum values within its area. Table 1 shows the measured results at different positions.

	Starting Point	Front Position	Up Position	Down Position
$T_{Maximum}$[°C]	150	97.34	82.8	79.1
T_{Center}[°C]	150	54.6	45	43.3
$T_{Minimum}$[°C]	150	45	33.1	33.3

Table 1: Measured temperatures for the square-shaped courser area introduced in Figure 5 at different positions.

The temperature decreased with increasing distance to the center of the starting position. Furthermore, the up and the down positions show similar temperature values, indicating a symmetrical temperature distribution for the heat motion perpendicular to the laser beam propagation direction. A slightly higher temperature was measured at the front position. This asymmetric temperature distribution is probably due to the ejection of the debris. The debris removes excessive heat in the form of kinetic energy, reducing heat accumulation drastically within the surrounding tissue [16]. It was difficult to interpret and measure the exact spatial distribution on and within the bone tissue, since the cut itself was conical with a cutting width of 1 mm at the surface, down to a cutting width of 0.8 mm at its bottom. Based on the positioning steps of the square-shaped cursor, it was assumed that the walls of the cut were not exposed to more than 45 °C or 43.3 °C, respectively. It was not possible to clearly define the borders of

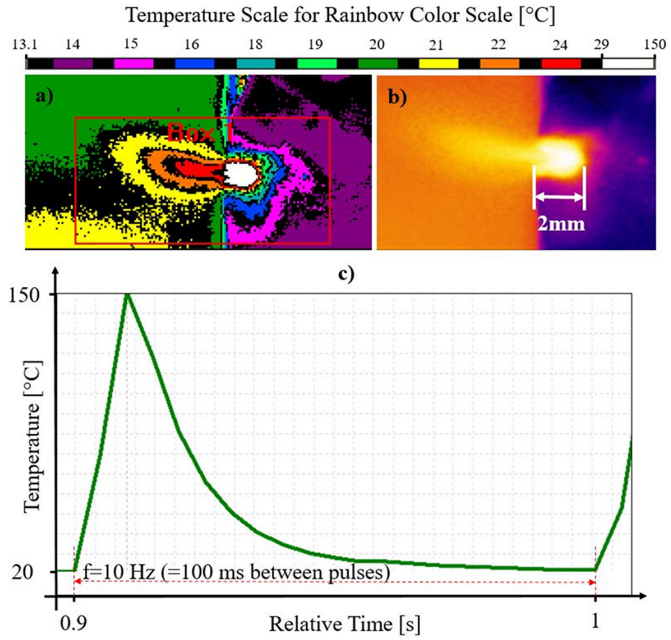

Fig. 4: Measured temperatures $T_{max} = 150\,^{\circ}\mathrm{C}$ and $T_{min} = 21\,^{\circ}\mathrm{C}$ during laser osteotomy on a bone disc with spray assisted cooling. a) Temperature segmented figure with the rainbow color scale. b) Fusion image with smooth transitions for the temperature measurements. c) Temporal plot for one whole laser pulse.

the walls. This might be relevant for very sensitive applications and should be investigated with a better measurement system in the future. The most critical region though is where the laser beam hits the bone perpendicular and penetrates deepest. Therefore, further measurements were conducted to evaluate the temporal heat penetration and its distribution within the bone at the bottom of the cut. Figure 6 shows the three measurement points used within the bone. All of them are positioned along the beam propagation direction and centered on the middle axes of the cut itself. The first brown one (C1) was positioned directly over the bottom of the cut to catch the maximum measured temperature as described above. The second was blue (C2) and positioned 0.4 mm within the bone to measure the heat penetration to that point during the ablation process. Lastly, a green cross cursor (C3) was positioned 0.8 mm within the bone. Here, the temperature rose by a few degrees, marking the position of C3 very close to the utmost region of the heat penetration.

Figure 7 shows the measured temporal plots of all three cross cursors, experiencing heat induction by the laser ablation process after one pulse (same pulse as in figure 4), until all values decrease under the critical temperature for bone $T_c = 47\,^{\circ}\mathrm{C}$ when applied for more than 60 seconds. T_c is only used as a

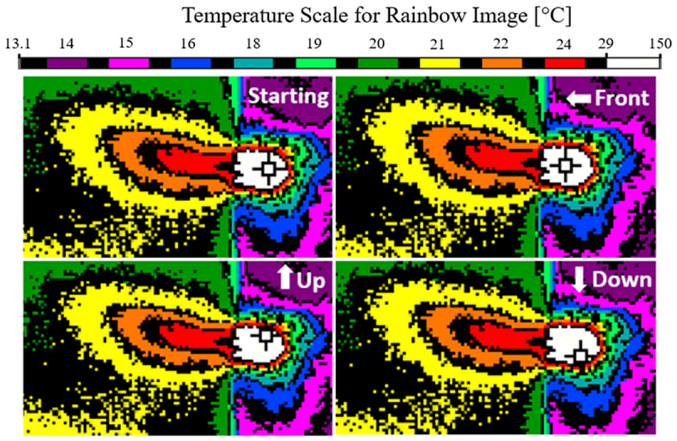

Fig. 5: Heat induction of a pulse during a laser ablation cut in a bovine disc with spray assisted cooling. Temperature segmented figures at the time of T_{max} with a temperature measurement square-shaped cursor at different positions.

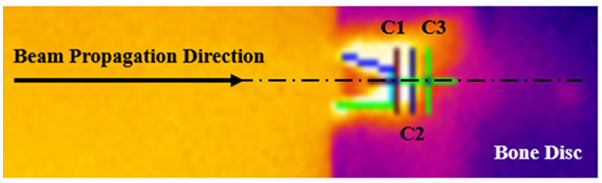

Fig. 6: Fusion image of the achieved cut (before the next laser pulse is applied) with the introduced cross cursors at different positions for spatial heat measurements over time.

reference value where thermal damages can be excluded since the exposure time was magnitudes smaller than defined for T_c.

All three graphs in Figure 7 show a similar progression. The peak values decreased the further the measurement point was within the tissue. This result confirmed that the induced heat propagates and relaxes uniformly within hard tissue. The maximum heat induction for all three cross cursors was measured after 10 ms. T_{max} for C1 was 150 °C and dropped below T_c after 25 ms more to 37.7 °C, total time $t_t = 35$ ms. For C2 at 0.4 mm within the hard tissue $T_{max} = 102.7$ °C was measured, down to 40.5 °C at $t_t = 25$ ms (T_{max} for C1 was 68.2 °C at $t_t = 25$ ms). Lastly, the heat penetrated the hard-tissue up to 0.8 mm, with $T_{max} = 28$ °C for C3.

4 Discussion

Thermal images were acquired during laser ablation on cow bone discs performed with the CARLO device. The occurred heat induction was evaluated and its

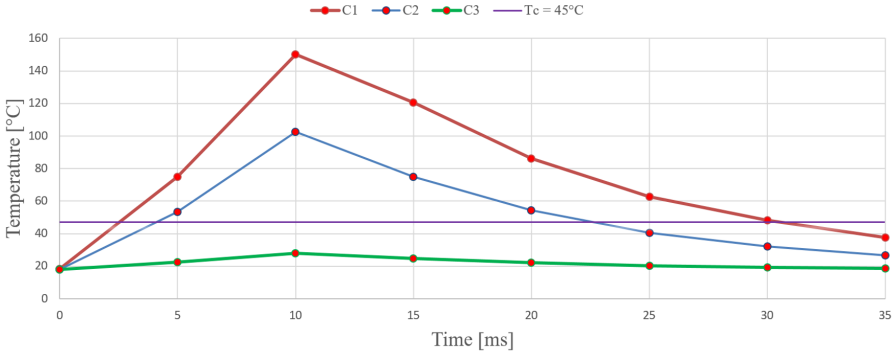

Fig. 7: Temporal plot for three temperature measurement cross cursors positioned spatially apart in 0.4 mm steps within the bone to observe heat induction during one laser pulse.

propagation within hard tissue studied. The first experiments without a cooling system confirmed the results of Kang et al. [11], who showed the importance of spray cooling assistance during laser bone ablation to achieve carbonization free cuts. All other laser bone ablation experiments were performed with spray assisted cooling. It showed lower induced maximum temperatures with $T_{max} = 150\,°C$ and a temperature relaxation to 37.7 °C after 35 ms. The temperature fell to its initial value of $T_{min} = 21\,°C$ before the next pulse was applied. Hence, laser bone ablation was achieved without heat accumulation between the individual pulses, which is most significant factor for inducing tissue damages [16]. A spatial evaluation at the time of T_{max} for spray assisted laser bone ablation showed a symmetrical temperature distribution for the heat motion perpendicular to the laser beam propagation direction. A slightly higher temperature distribution was found in the opposite direction to the beams propagation, which originates from the forward motion of the debris. The region of bone ablation, where the laser beam hits the tissue perpendicular, showed a heat induction up to 0.8 mm in depth. An evaluation of the spatial and temporal heat penetration and its distribution in that region showed the heat propagating and relaxing uniformly. Whereas T_{max} decreased in depth and over time.

These results could be used to optimize laser ablation parameters to achieve a faster cutting by increasing the pulse repetition rate so that the consecutive pulses are applied as soon as the tissue temperature drops to its initial value. Furthermore, knowing the heat induction depths, risks of thermal damage to sensitive tissue beneath the bone could be avoided, e.g. the dura mater located between the skull and brain. In such cases, the applied energy density during the bone ablation could be reduced, to minimize heat induction. For the next step, prolonged cutting experiments with long and deep cuts on fresh cadaver bones should be studied to come closer to real laser osteotomy. The cooling parameters and the possible penetration depth of the cooling droplets would be most interesting to ensure a constant and carbonization-free operation. It is assumed

that during such experiments the found results can be confirmed and further analyzed to find more influential parameters for laser osteotomy. Furthermore, such experiments could be used to analyze different cutting techniques and their influence on heat induction and propagation.

5 Conclusion

Despite the satisfying result that thermal damage can be excluded for laser osteotomies, a device like the CARLO has additional hurdles to overcome before it can be considered a real alternative for conventional osteotomy tools. For one, the price of a laser osteotome will greatly exceed the price for conventional tools like a piezoelectric saw. Another factor is its cutting speed, which might be slower in comparison to a drill or saw. Nevertheless, laser osteotomes have a good chance to make their way into operating rooms. They offer free geometrical and functional cuts, which enable new methods and the possibility to improve established procedures. Especially, complex procedures like cranio-maxillofacial surgeries will benefit from laser osteotomes like CARLO.

References

1. L. Goldman, P. Hornby, R. Meyer, and B. Goldman, "Impact of the laser on dental caries," *Nature*, vol. 203, no. 4943, pp. 417–417, 1964.
2. R. H. Stern, J. Vahl, and R. F. Sognnaes, "Lased enamel: ultrastructural observations of pulsed carbon dioxide laser effects," *Journal of Dental Research*, vol. 51, no. 2, pp. 455–460, 1972.
3. R. H. Stern, "Dentistry and the laser," in *Laser applications in medicine and biology*, pp. 361–388, Springer, 1974.
4. M. Stanislawki, J. Meister, T. Mitra, M. Ivanenko, K. Zanger, and P. Hering, "Hard tissue ablation with a free running er: Yag and a q-switched co 2 laser: a comparative study," *Applied Physics B*, vol. 72, no. 1, pp. 115–120, 2001.
5. M. Ivanenko, R. Sader, S. Afilal, M. Werner, M. Hartstock, C. von Hänisch, S. Milz, W. Erhardt, H.-F. Zeilhofer, and P. Hering, "In vivo animal trials with a scanning co2 laser osteotome," *Lasers in Surgery and Medicine: The Official Journal of the American Society for Laser Medicine and Surgery*, vol. 37, no. 2, pp. 144–148, 2005.
6. J. J. Kuttenberger, A. Waibel, S. Stübinger, M. Werner, M. Klasing, M. Ivanenko, P. Hering, B. von Rechenberg, R. Sader, and H.-F. Zeilhofer, "Bone healing of the sheep tibia shaft after carbon dioxide laser osteotomy: histological results," *Lasers in medical science*, vol. 25, no. 2, pp. 239–249, 2010.
7. J. Burgner, M. Müller, J. Raczkowsky, and H. Wörn, "Ex vivo accuracy evaluation for robot assisted laser bone ablation," *The International Journal of Medical Robotics and Computer Assisted Surgery*, vol. 6, no. 4, pp. 489–500, 2010.
8. R. Hibst and U. Keller, "Experimental studies of the application of the er: Yag laser on dental hard substances: I. measurement of the ablation rate," *Lasers in Surgery and Medicine*, vol. 9, no. 4, pp. 338–344, 1989.
9. M. Frentzen, "Lasertechnik in der zahnheilkunde," *Dtsch Zahnarztl Z*, vol. 46, pp. 443–454, 1991.

10. M. Frentzen, "Bearbeitung der schmelzoberflachen mit gepulster laserstrahlung," *Dtsch Zahnarztl Z*, vol. 49, pp. 166–168, 1994.
11. H. Kang, J. Oh, and A. Welch, "Investigations on laser hard tissue ablation under various environments," *Physics in Medicine & Biology*, vol. 53, no. 12, p. 3381, 2008.
12. K.-w. Baek, W. Deibel, D. Marinov, M. Griessen, M. Dard, A. Bruno, H.-F. Zeilhofer, P. Cattin, and P. Juergens, "A comparative investigation of bone surface after cutting with mechanical tools and er: Yag laser," *Lasers in surgery and medicine*, vol. 47, no. 5, pp. 426–432, 2015.
13. K.-W. Baek, W. Deibel, D. Marinov, M. Griessen, A. Bruno, H.-F. Zeilhofer, P. Cattin, and P. Juergens, "Clinical applicability of robot-guided contact-free laser osteotomy in cranio-maxillo-facial surgery: in-vitro simulation and in-vivo surgery in minipig mandibles," *British Journal of Oral and Maxillofacial Surgery*, vol. 53, no. 10, pp. 976–981, 2015.
14. W. Deibel, A. Schneider, M. Augello, A. E. Bruno, P. Juergens, and P. Cattin, "A compact, efficient, and lightweight laser head for carlo: integration, performance, and benefits," in *Novel optical systems design and optimization XVIII*, vol. 9579, p. 957905, International Society for Optics and Photonics, 2015.
15. H. Kang, I. Rizoiu, and A. Welch, "Hard tissue ablation with a spray-assisted mid-ir laser," *Physics in Medicine & Biology*, vol. 52, no. 24, p. 7243, 2007.
16. M. H. Niemz, *Laser-tissue interactions: fundamentals and applications*. Springer Science & Business Media, 2013.

Chapter 7

Heat Induction during Laser Osteotomies and Piezo Surgery: A Comparative Study with Thermal Imaging Measurements

This paper was submitted in Mai 2019 to the *Wiley Online Library* under the online magazine *Lasers in Surgery and Medicine* and is currently under peer-review. It is expected to be published after the submission of this thesis.

This paper shows that during laser osteotomy, heat induction can be controlled and that under the right conditions no heat damage is caused. Several osteotomy cuts were performed on cadaver sheep heads with the developed laser osteotome and a piezo electrical saw. The procedures were recorded and analyzed with a thermal camera to compare induced heat and heat relaxation within the hard tissue.

It was shown that the efficiency of the spray cooling system determines strongly the outcome of the experiment. During laser osteotomies, the induced heat relaxed in time before the next pulse hit. Hence heat never accumulated from consecutive pulses and thus heat damages an be avoided. The cuts with the piezo electrical osteotome (PZE) in contrast, showed high variability in heat induction. This variance originated from the set-up and the unstable guidance of

the cutting tool itself by the surgeon. It became clear that laser osteotomy is the superior cutting technique compared to piezo surgery. It is less prone to human errors and causes less mechanical and thermal stress to the treated tissue.

Heat Induction during Laser Osteotomies and Piezo Surgery: A Comparative Study with Thermal Imaging Measurements

Waldemar Deibel[1,2], Marcello Augello[3,4], Adrian Schneider[2], Michael Peyer[2], James Jockel Leuenberger[2], Alfredo Bruno[2], Philipp Juergens[3,4,*], Philippe C. Cattin[1,2,*]

[1]Department of Biomedical Engineering, University of Basel, Switzerland
[2]Advanced Osteotomy Tools AG, Basel, Switzerland
[3]Hightech Research Centre of Cranio-Maxillofacial Surgery, University of Basel, Switzerland
[4]Department of Cranio-Maxillofacial Surgery, University Hospital Basel, Switzerland
***Note:** Both authors contributed equally to this paper.

Abstract.
Objectives The hypothesis is that during laser osteotomy heat induction can be controlled and that under the right conditions no heat damage is caused.
Methods Several osteotomy cuts were performed on cadaver sheep heads at the sutura sagittalis with a laser osteotome and a piezo electrical saw as cutting tools. The procedures were recorded and analyzed with a thermal camera to compare induced heat and heat relaxation within the hard tissue.
Results During laser osteotomy, high temperature peaks were induced with each pulse applied to the bone. Through the efficient tissue cooling though, the induced heat relaxed in time before the next pulse hit. Hence heat never accumulated for the consecutive pulses and heat dam-ages were avoided. The cuts with the piezo electrical osteotome (PZE)showed high variability for heat induction. The variance originated from the set up and the unstable guidance of the cutting tool itself.
Conclusions Under the proper conditions, thermal damage can be completely avoided during laser osteotomy. Furthermore, it is the superior cutting technique compared to piezo surgery, since it is less prone to human errors and causes less mechanical and thermal stress to the treated tissue.

Keywords: laser, bone ablation, heat induction, imaging, thermal damage

1 Introduction

Cutting of hard tissues is required in many surgical interventions. As a consequence a lot of research is put into the development of novel cutting tools

to perform these bone cuts more precise, more efficient, less traumatic resulting in an overall better outcome for patients. The most frequently used tools are the conventional drills [1] or surgical saws. The inherent disadvantages of these tools are the increased local temperature of the targeted regions due to frictional heat generation, the deposition of metal shavings, and bacterial decontamination [2]. The next step in the development were piezo electric based tools, especially for delicate procedures such as in oral surgery. They created very small thermal effects, resulting in a better biological outcome [3]. Although all the above mentioned instruments are fitted with an internal cooling system, it is not possible to prevent thermal damage completely as bone tissue is very susceptible to thermal injury [4]. Eriksson and Albrektsson [5] noted that temperature elevations between 44 °C and 47 °C may already lead to tissue damage and in the worst case to necrosis. Such cell death is caused by denaturation of the proteins. Heat and necrosis are directly proportional [6]. Increased areas of necrosis result in tissue breakdown slowing down wound healing. If a certain degree of necrosis of the surrounding differentiated and undifferentiated cells exceeds a certain limit, the body is no longer able to remove the devitalized tissues. This capability is essential, especially with metallic implants, where primer stability depends on vital bone structures close to the osteotomy edge. Investigations have shown that a reduction of heat shortens healing periods and allows a faster integration of osteosynthesis and implant materials [7]. For this purpose several lasers such as Er:YAG (erbium-doped yttrium aluminum garnet laser), Nd:YAG (neodymium-doped yttrium aluminum garnet laser), continuous wave CO_2 (carbon dioxide laser), and pulsed CO_2 have been investigated to perform contact free osteotomies. Photothermolysis analysis by Anderson and Parrish [8] showed that selective damage to structures require highly absorbing particles for the pulsed laser radiation used. For the CO_2 laser with a wavelength of 10.6 µm these particles are the minerals within hard tissue, that makes up 60 % for cortical bone and 34 % for trabecular bone [9]. The CO_2 laser systems were extensively investigated for laser osteotomy purposes by various groups [10][11]. These systems became safer, more efficient and avoided most of the thermal damage associated previously with laser osteotomies. In 2010 Burgner et al. [12] demonstrated a CO_2 laser system for roboter assissted osteotomy. The authors concluded that such a system has to overcome its slow cutting speed, complexity and size before it can be considered a real option for osteotomies under OR conditions. The Er:YAG laser has demonstrated the most promising results with bone tissue [13]. As water is an essential component of hard tissue with 13.5 % for cortical bone and 30.5 % for trabecular bone [9] and the Er:YAG wavelength of 2.94 µm coincides perfectly with the maximum absorption in water.

Previously, our published work focused on the engineering aspects of an Er:YAG laser osteotome in terms of integration, performance and benefits [14] to overcome some of the drawbacks of the CO_2 systems. In a second study, we showed that the laser osteotome produces biologically open cut surfaces, which are more beneficial for the healing process than a flattened tissue structure which is created by cutting bone with a mechanical tool such as a piezo electrical os-

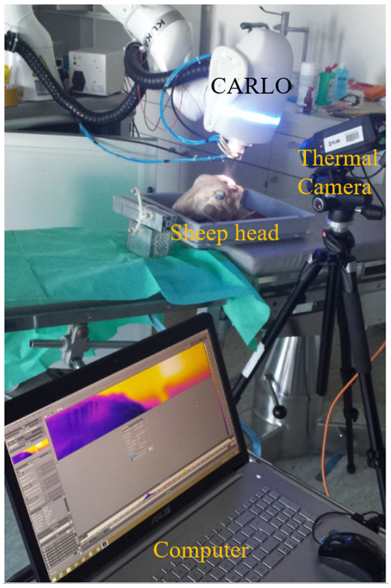

Fig. 1: Experimental setup for thermal effect measurements during osteotomies with the CARLO as the cutting tool and a sheep head as the target tissue.

teotome (PZE) [15]. The aim of this study is to investigate heat induction and its relaxation during laser osteotomy within bone tissue analyzed by means of thermal imaging. The hypothesis is that under the right conditions, thermal damage to the surrounding tissue can be avoided during laser osteotomy. Here, not only the peak values for the induced heat are relevant, but also a potential heat accumulation over time within the tissue. The results are compared to similar evaluations with a PZE as the reference state-of-the-art osteotomy tool.

2 Material and Methods

2.1 Experimental Setup

The experiments were performed with the following main components; two different cutting tools, a laser osteotome CARLO (Cold Ablation Robot-guided Laser Osteotome, AOT AG, Switzerland) and a piezo electrical saw using micro vibrations at an ultrasonic frequency (PIEZOSURGERY, mectron, Italy), sheep heads, a thermal camera (FLIR A655sc) and a computer which recorded the thermal images during the cutting procedures. Figure 1 shows the experimental setup.

CARLO was developed by Advanced Osteotomy Tools AG (www.aot.swiss) and comprises of four major parts [14]. The laser head as the cutting tool is mounted on a robot arm that guides it safely for a precise cut execution. A trolley on which the robot is mounted contains all control units, such as power supplies

and robot controller. The fourth component is the optical navigation system which guides the movements of the robot with respect to the operating field. The laser system used is a solid state Er:YAG laser with a central wavelength of 2.94 µm. For these experiments it was operated at 4.5 W on the sample and a repetition rate with a pulse length of 250 µs. This setup results in an energy density of 70.7 J/cm^2 at the focal spot of the laser with a diameter of 1 mm. The cuts were planned by referencing the starting and the end point of the line to be cut via a pointer tool. The CARLO planning software then connected the points, creating a straight line along which the robot moved the focal spot of the laser head with 1.3 $mm\,s^{-1}$. The cooling of the sample was realized with tap water by the built-in nozzle system with a total water mass flow of 12 $ml\,min^{-1}$ at 3 bar produced by the three build in secondary gas assisted atomization nozzles with external mixture.

The PZE is a state-of-the-art model from mectron, the PIEZOSURGERY. Its function was set to cortical and the maximum water level for cooling. The system was operated by an experienced surgeon from the University Hospital of Basel, Switzerland.

The FLIR A655sc thermal camera was used for thermal imaging. It has a Vanadium Oxide (VoX) micro bolometer detector which provides 14-bit data upto 50 frames per second at full frame 640×480 pixel resolution. It has an option for high speed windowing with an increased frame rate output of up to 200 Hz at 640×120. The optical temperature ranges are $-40\,°C$ to $150\,°C$ and $100\,°C$ to $650\,°C$ with an accuracy of $2\,°C$. Its spectral range is 7.5 µm to 14.0 µm. The thermal camera was mounted on a tripod and aligned to record as much as possible of the heat induction into the sample and its thermal propagation during the cutting processes. The camera recorded the cutting procedure from an angled top down view.

2.2 Sample Preparation

These experiments were targeting sheep heads which were purchased at a local butcher. The heads were frozen at $-18\,°C$ until unfreezing them for the experiments at room temperature for five hours in tap water. They were used to compare heat induction in bone during laser ablation compared to piezo surgery. The sheep were 15 months old, with a skull bone thicknesses of 2 mm to 3 mm at the sutura sagittalis, the region where the experiments were conducted.

2.3 Thermal Imaging Measurements

Thermal imaging measurements were recorded with the FLIR ResearchIR software (V 4.30.1) with different temperature ranges and frame rates. The high speed windowing with a frame rate of 200 Hz was used for all measurements during laser osteotomies to have the highest time resolution possible. The temperature range was adjusted according to the measured temperatures. Thermal imaging measurements for procedures with the PZE were recorded with 50 frames per second to have a bigger field of view. Here, the heat induction into the

sample is continuous, thus time resolution is less crucial. All measurements were evaluated with the FLIR ResearchIR software for a Region of Interest (ROI) within our recorded data.

3 Results and Discussion

Several osteotomy cuts were performed on two sheep heads, at the sutura sagittalis. The CARLO device was used on one sheep head and the PZE on another. All cuts were performed on the same day with few minutes in between each cut for the planning on the respective system. The exchange of cutting systems took 30 minutes, so that the total experiment time was under two hours. All experiments were recorded with the thermal camera. To achieve the potentially largest heat accumulation, only the 2 mm to 3 mm thick cranial bones were cut through. The choice of different sheep heads should have minimal influence, since the animals were at the same age and the heads treated equally postmortem. The following studies are referenced for a thermal damage threshold. Lundskog et al. [6] stated that the exposure time of the applied heat and the damages inflicted by it to the affected area have a linear relationship. They found a crucial threshold at $T_c = 70\,°C$ for exposure times above 30 seconds. Eriksson et al. [5] found a critical damage threshold for bone at $T_c = 47\,°C$ after 60 seconds and reasoned that its origin lied in their different setups and measurement methods. Here, the value from Eriksson et al. $T_c = 47\,°C$ over 60 seconds is used as a damage threshold for accumalated heat, since that paper is more recent and claims to have used superior methods. A temperature-time curve for the induced damage is not given by the source.

The laser ablation of the hard tissue was so efficient that it took usually only a few seconds for the 12 mm long cut to go through the skull. Here, the most significant part of the measurements were evaluated, where the recorded pulse train was clear and the heat induction at maximum values. Seven cuts were performed with the CARLO device, L1-L7. All measurements show a similar progress, see Figure 2 as an example. The values for T_{min} and T_{max} are oscillating around a mean value. T_{min} was measured at the beginning of each laser pulse and T_{max} at its peak. Table 1 shows the calculated mean values and their standard deviations for all seven cuts.

The observed oscillation of T_{min} and T_{max} can have various reasons. The bone could have had locally different properties which leads to slightly different heat relaxations, i.e. more or less dry, cortical or spongious, etc. Another important factor is the margin within the cooling spray effectiveness, e.g. a slight pulsing of the nozzle. But the fact that T_{min} oscillates, rather than rises continuously, indicates that the water spray cooled and moisturized the cutting area sufficiently enough to prevent any heat accumulation above a certain level. The experiments were started with the sheep skull being at room temperature of 21 °C. This means that the mean temperature levels for T_{min} rose by several degrees during the experiments, at the lowest $24.2 \pm 1.6\,°C$ for L3 and up to $35.8 \pm 2.8\,°C$ for L5. It is assumed that these variations are caused by the difference of the local cooling

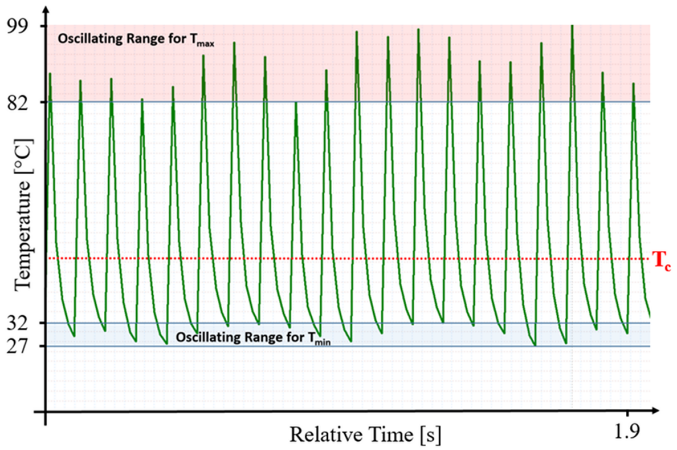

Fig. 2: Temporal plot for the measured heat induction into a sheep skull per pulse by the laser osteotome over 2 seconds for the second cut, L2. The marked blue zone is the measured temperature range for T_{min}, the red zone for T_{max}.

Cut Number	Duration [s]	T_{min}[°C]	T_{max}[°C]
L1	1.7	30.5±1.4	102±5.4
L2	2.0	28.4±1.6	86±5.3
L3	2.5	24.2±1.6	90.4±8.8
L4	1.6	28±1.1	121.4±4.3
L5	3.4	35.8±2.8	108.5±7.9
L6	2.6	29.8±1.6	105.2±6.5
L7	1.6	29±1.7	109.7±3

Table 1: Mean values and their standard deviations for T_{min} and T_{max} during the seven laser osteotome cuts on a sheep head.

efficiency. The cuts on the sheep head where surrounded by hard tissue, so that the spray could only penetrate them from above. When a laser pulse is fired, it creates a vapor channel through the water spray along its propagation direction, losing some of its energy in the process. Then, the remaining energy reaches the target tissue and starts the ablation process [16]. The water content in the bone absorbs the Er:YAG radiation and tries to extend in volume as it vaporizes. This instant pressure increase creates micro-explosions, resulting in the ablation of hard tissue. The outburst out of the ablation area of broken up tissue is called *debris plume*. It also removes excessive heat in the form of kinetic energy, reducing drastically heat accumulation within the surrounding tissue [17]. In between pulses, the coolant absorbs the remaining heat, but is trapped within the cut. Hence, some of the induced temperature stays within and is removed with the next fired laser pulse. Important for spray assisted laser osteotomy is that the T_{min} level never rises above $T_c = 47\,°\text{C}$. T_{max} on the other hand exceeds

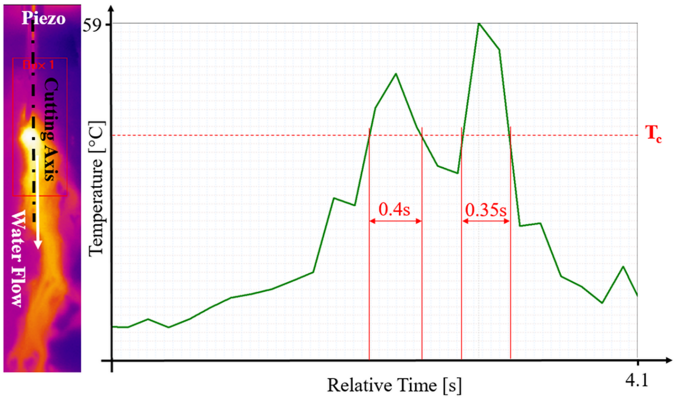

Fig. 3: Measured heat induction into bone during a PZE osteotomy. Cut P1 over 4.1 seconds, with two peaks exceeding T_c. The cutting axis is in line with the cooling water flow.

this threshold with values up to 127.5 °C for L4, but has only exposure times of 50 ms where the temperature rises above 47 °C.

Piezo electrical osteotomy is a continuous cutting process, i.e. heat is continuously induced, in contrast to the consecutive application of pulses during laser osteotomy. Six cuts were performed with the PZE, P1 to P6. It took around 10 seconds to perform a 25 mm long cut. The results vary for the measured induced heat. Figure 3 and Figure 4 show examples of the most relevant measurement parts for cuts P1 and P2, respectively. The measurements show an irregular progression of the heat induction and relaxation over the course of the experiments. Table 2 summarizes the measured temperatures exceeding Tc with respect to the number of measured peaks.

Cut Number	Time above T_c [s]	T_{max}[°C]
P1	0.75	59
P2	5.7	86
P3	4	85
P4	0	42
P5	0.96	82.5
P6	0.075	49.6

Table 2: Measured temperatures above T_c during PZE surgery.

Figure 3 shows P1 as an example where the temperature stayed between 26 °C and 47 °C, except for two peaks that lasted 0.4 seconds and 0.35 seconds. Such short durations above T_c are not enough to induce heat damage.

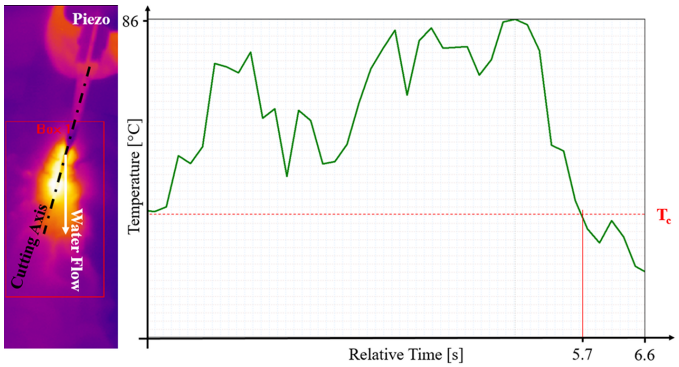

Fig. 4: Measured heat induction into bone during PZE osteotomy for cut P2. The induced heat is higher than T_c for the majority of the experiment. The cutting axis is inclined to the cooling water flow axis.

Figure 4 shows the measurements for heat induction and relaxation for cut P2, performed with the PZE. Here, the average temperature level was considerably higher as compared to P1. The measured temperature exceeds the critical temperature T_c with peak values from 70 °C up to 85.9 °C for 5.7 seconds. This result also does not exceed the critical temperature long enough to induce thermal damage.

It is assumed that the difference in the overall temperature level for the cuts originated from the alignment and guidance of the PZE to the skull surface and the cut itself. The fusion images for the cuts P1 and P2 indicate such differences in Figure 3 and Figure 4. During the experiment of P1, the cutting axis was in line with the exceeding coolant flow over the skull and the cut itself. Furthermore, the PZE was held nearly perpendicular to the cutting axis. The cut and the tip of the PZE got flushed constantly by water, cooling efficiently and creating a layer of water within the cut and around the tip of the PZE. In addition, that layer of water damped the measurement signal to some extend. During the experiment of P2, the alignment was not optimal so that the water flow and the cutting axis did not overlap, leading to more heat accumulation within the tissue. It was not possible to make a quantitative evaluation of these effects with the setup used. More friction, and hence more heat induction, between bone and PZE is created the deeper the blade penetrates or if it gets jammed in the cut. Also, the deeper the cut, the less cooling water penetrates into it. Even if the surgeon is experienced, the cutting speed is never constant or optimized for the given procedure which might create more local heat accumulation. The same holds true for the pressure applied to the PZEs blade. Another general problem is the created bone debris during such procedures, which is generally soaked with cooling water and not only obscures the measurement signal but has also different heat relaxation properties as the bone itself. Another big limitation for accurate results was the measuring method itself. During the cutting process, the PZE blade obstructed the cut and made a direct measurement impossible. The

heat induction was hence measured right after the PZE blade was moved on. In that time, cooling water covered and cooled the tissue. For these experiments, it can be speculated that the actual heat induction was higher than the measured values.

4 Summary and Conclusions

During laser osteotomy on the sheep head, it was discovered, that the efficiency of the spray cooling system determines strongly the outcome of the experiment. A temperature level is induced, around which T_{min} oscillates, for these experiments from 24.2±1.6 °C up to 35.8±2.8 °C. The values for T_{max}, here 86±5.3 °C up to 121.4±4.3 °C, seem to be negligible since the exposure time of these values are in the 50 ms regime. According to Eriksson et al. [5] the critical temperature for bone is 47 °C at exposure times above 60 seconds. Furthermore, most of the excessive heat was extracted from the tissue during laser ablation by the debris plume. Therefore, it can be stated confidently that spray assisted laser osteotomies based on a thermomechanical ablation process as used by the CARLO device, do not induce heat damage during their procedures, given the correct setup.

These results may also help to optimize a laser osteotomy system for laser pulse repetition rate, energy level for ablation volume and a higher ablation efficiency, rendering faster cutting speeds. The optimization of the spray cooling system, i.e. the minimization of its mass flow rate provided that no carbonization is observed, could also bring many advantages since a smaller part of the Er:YAG laser radiation is absorbed by the spray coolant.

The cuts with the PZE showed high variability. In some experiments T_c was not reached. Whereas in others the induced heat often exceeded the critical damage threshold, but likely did not cause thermal damage due to its short application of only a few seconds. Furthermore, the measurements of the heat induction were taken after the blade moved to its next position and exposed the heated area below. Hence, it is assumed that the actual heat induced into the bone is somewhat higher than the measured temperatures.

The PZE surgery outcome is highly dependent on the performance of the surgeon, the topography of the cutting area, the cutting depth and the system setup and its alignment. These factors are difficult to anticipate and balance for tissue safety and cutting consistency. Therefore, a possibility of inducing heat damages during PZE surgeries always remains [18]. It is known that even without heat induction, mechanical damages and hygienic problems might arise [2]. The laser osteotome does not encounter such problems since the procedure is contact free and robot guided, making it a more reliable and consistent system [14][15].

References

1. G. L. Martins, E. Puricelli, C. E. Baraldi, and D. Ponzoni, "Bone healing after bur and Er: YAG laser ostectomies," *Journal of Oral and Maxillofacial Surgery*, vol. 69, no. 4, pp. 1214–1220, 2011.

2. C. M. Barone, D. F. Jimenez, G. J. Yule, and B. Strauch, "Analysis of bone formation after cranial osteotomies with a high-speed drill.," *The Journal of craniofacial surgery*, vol. 8, no. 6, pp. 466–470, 1997.
3. M. Schlee, "Piezosurgery—a precise and safe new oral surgery technique," *Aust Dent Pract*, vol. 2009, pp. 144–8, 2009.
4. C. M. Misch, "Comparison of intraoral donor sites for onlay grafting prior to implant placement.," *International Journal of Oral & Maxillofacial Implants*, vol. 12, no. 6, 1997.
5. R. Eriksson and T. Albrektsson, "The effect of heat on bone regeneration: an experimental study in the rabbit using the bone growth chamber," *Journal of Oral and Maxillofacial surgery*, vol. 42, no. 11, pp. 705–711, 1984.
6. J. Lundskog *et al.*, "Heat and bone tissue. an experimental investigation of the thermal properties of bone tissue and threshold levels for thermal injury," 1972.
7. M. Stanislawki, J. Meister, T. Mitra, M. Ivanenko, K. Zanger, and P. Hering, "Hard tissue ablation with a free running Er: YAG and a Q-switched CO2 laser: a comparative study," *Applied Physics B*, vol. 72, no. 1, pp. 115–120, 2001.
8. R. R. Anderson and J. A. Parrish, "Selective photothermolysis: precise microsurgery by selective absorption of pulsed radiation," *Science*, vol. 220, no. 4596, pp. 524–527, 1983.
9. S. Afilal, *Ablationsmechanismen von biologischem Hartgewebe bei Bestrahlung mit kurzgepulsten CO2-Lasern*. PhD thesis, 2004.
10. M. Ivanenko, R. Sader, S. Afilal, M. Werner, M. Hartstock, C. von Hänisch, S. Milz, W. Erhardt, H.-F. Zeilhofer, and P. Hering, "In vivo animal trials with a scanning CO2 laser osteotome," *Lasers in Surgery and Medicine: The Official Journal of the American Society for Laser Medicine and Surgery*, vol. 37, no. 2, pp. 144–148, 2005.
11. J. J. Kuttenberger, A. Waibel, S. Stübinger, M. Werner, M. Klasing, M. Ivanenko, P. Hering, B. von Rechenberg, R. Sader, and H.-F. Zeilhofer, "Bone healing of the sheep tibia shaft after carbon dioxide laser osteotomy: histological results," *Lasers in medical science*, vol. 25, no. 2, pp. 239–249, 2010.
12. J. Burgner, M. Müller, J. Raczkowsky, and H. Wörn, "Ex vivo accuracy evaluation for robot assisted laser bone ablation," *The International Journal of Medical Robotics and Computer Assisted Surgery*, vol. 6, no. 4, pp. 489–500, 2010.
13. H. Zahn, V. Jungnickel, T. Ertl, S. Schmid, and G. Müller, "Knochenchirurgie mit dem Er: YAG-laser," *Laser-Medizin: eine interdisziplinäre Zeitschrift; Praxis, Klinik, Forschung*, vol. 13, no. 1-2, pp. 31–36, 1997.
14. W. Deibel, A. Schneider, M. Augello, A. E. Bruno, P. Juergens, and P. Cattin, "A compact, efficient, and lightweight laser head for carlo: integration, performance, and benefits," in *Novel optical systems design and optimization XVIII*, vol. 9579, p. 957905, International Society for Optics and Photonics, 2015.
15. K.-w. Baek, W. Deibel, D. Marinov, M. Griessen, M. Dard, A. Bruno, H.-F. Zeilhofer, P. Cattin, and P. Juergens, "A comparative investigation of bone surface after cutting with mechanical tools and Er: YAG laser," *Lasers in surgery and medicine*, vol. 47, no. 5, pp. 426–432, 2015.
16. H. Kang, I. Rizoiu, and A. Welch, "Hard tissue ablation with a spray-assisted mid-ir laser," *Physics in Medicine & Biology*, vol. 52, no. 24, p. 7243, 2007.
17. M. H. Niemz *et al.*, *Laser-tissue interactions*. Springer, 2007.
18. L. Lamazza, D. Laurito, M. Lollobrigida, O. Brugnoletti, G. Garreffa, and A. De Biase, "Identification of possible factors influencing temperatures elevation during implant site preparation with piezoelectric technique," *Annali di stomatologia*, vol. 5, no. 4, p. 115, 2014.

Chapter 8

Conclusions

In this thesis, a laser head for a computer assisted and robot guided laser osteotome CARLO was developed and investigated for its functionality, safety and applicability. The core development and all basic engineering requirements were shown for such a contact free cutting tool. Reproducible and precise cutting width, smaller than one millimeter were achieved in in-vitro, cadaver and animal studies [58, 74]. In-vitro studies showed a reproducibility for sharp edges with angle variations as low as $\pm 2.59°$ and $\pm 1.70°$ and repositioning accuracies of $\pm 0.02\,\text{mm}$ and $\pm 0.04\,\text{mm}$. Hence, the CARLO demonstrated its superiority to conventional methods, which are usually hand-guided by the surgeon. Furthermore, the compact and lightweight design complies with the requirements for all other devices within the CARLO, such as the robotic arm, and makes the transition into an operating room visible. The developed laser osteotome enables new possibilities in terms of cutting geometries and the overall transfer of preoperative planned osteotomy patterns to the surgical site. Such patterns can be planned according to the bio-mechanics of the treated area, resulting in a higher stability for reconstructive osteotomies and reduce bone abrasion compared to interventions performed with conventional tools. This could lead to less rigid and less stable plates for osteosynthesis and a general rethinking of bone surgery such as fracture treatments and bone tumor removal.

But all the achieved benefits that such a laser osteotome offers could not be utilized in a real-life case, if it would not be safe for the operator and the patient. The central safety feature within the laser head is the tissue conditioning

through the nozzle system that prevents any thermal damage to the treated and surrounding tissue and determines strongly the overall outcome of the osteotomy. The nozzle system is based on secondary gas assisted atomization nozzles with external mixture which was invented, developed and patented to prevent any heat accumulation during the intervention and to keep the operating field clean from all liquids and debris. Furthermore, it can be adapted for different applications and bone structures, through its versatility in spray parameters. In general, the droplets are able to penetrate the achieved cuts, regardless of their depth, relatively small width or alignment to the nozzle system. The cooling system was optimized through considerations and experiments in regards of droplet size, droplet speed and spray density. Other non-physical based requirements were also taken into account during the development, such as a compact design to achieve a long working distance for the laser osteotome or the prevention of pollution of the out-coupling laser head window.

The laser head has undergone intensive testing and optimization. During these tests, the induced heat and its propagation within hard tissue was evaluated. It was shown that the temperature distribution is symmetrical for the heat motion perpendicular to the laser beam propagation direction. Furthermore, an evaluation of the spatial and temporal heat penetration, and its distribution in that region, showed the heat propagating and relaxing uniformly. These results enable a far more advanced pre-operative planning by taking sensitive tissue underneath the treated area into account and to further optimize laser ablation parameters, e.g. cutting speed or energy density to enhance or reduce the ablation depth per pulse.

It was further shown, that under the right setup a laser osteotome is far superior to conventional tools like drills, saws or state-of-the-art piezo electrical devices. Such a laser osteotome was enabled with the development of the here presented laser head. Furthermore, the conducted experiments proved that safe, efficient, precise and reproducible laser osteotomies are not a thing of the future. The CARLO device has the potential to revolutionize bone surgery by enhancing known interventions and create new ones.

Chapter 9

Outlook

The development of the laser head and the research on laser-tissue-interactions were the first steps in the development of a commercial medical device for contact free bone surgery. The whole CARLO must be developed and optimized further, in the following only the outlook for the laser head (including the nozzle system) is discussed.

AOT AG is a privately certified medical device company, that develops according to the *Medical Device Directive 93/42/EEC (MDD)* and operates according to the *ISO 13485 Standard* (quality management system for the design and manufacture of medical devices) to get the *CE-Mark* for CARLO (certification mark that indicates conformity with health, safety, and environmental protection standards).

To reach this goal, the laser head has to undergo further engineering steps and adaptations for production, e.g. the use of medical certified materials where necessary. There is still room for improvement regarding the overall compactness and weight of the laser head such as the development of optical alignment blocks and the miniaturization of the housing itself. The optimization of the navigation system marker could further increase the overall positioning precision. Also, the integration of safety features according to the MDD like a real-time power output measurement, a visual status display of the CARLO or the integration of a real-time depth control system are necessary. All these and more developments are already in progress.

The nozzle system fulfills all technical requirements, but can be optimized

and further developed by incorporating more of the patent claims. Furthermore, the MDD dictates that parts with *external* flowing liquids cannot be reused for different patients, i.e. the tubing and the nozzle system itself. Hence, it must be developed towards a sterile class 1s single use medical product.

Despite all the performed tests and studies, there is the need of further animal studies, human cadaver studies and lastly clinical trials. These are necessary to achieve the CE Mark, and to analyze and confirm each development iteration, e.g. different cutting techniques and their influence on heat induction and propagation. A successful development of the CARLO device could influence all kinds of surgical procedures where functional cuts of hard tissue are requested.

Name:	**Waldemar Deibel**
Born:	04.07.1983, Kant, KGZ
Nationality:	German
Contact:	waldemardeibel@gmx.net

Curriculum Vitae

10/2019 – present	**Development Engineer** Helbling Technik Bern AG (Bern, CH)
02/2013 – present	**Doctoral Studies in Medical Science (Dr. sc. med)** University of Basel (Basel, CH) Thesis: '*The Physics and Engineering of Laser Ablation of Hard Tissue for Osteotomy Purposes*'
01/2018 – 12/2018	**Customer Service Representative** Teleperformace Greece (Athens, GR)
05/2012 – 03/2017	**(Senior) Development Engineer** Advanced Osteotomy Tools AG (Basel, CH) ▪ Hardware development ▪ Quality management ▪ Project management
10/2011 – 04/2012	**Working Student** Advanced Osteotomy Tools AG (Basel, CH)
02/2004 – 02/2012	**Diploma Study (Dipl.-Ing. (FH) of Photonics)** University of Applied Science Emden (Emden, DE) Focus: Medical laser technologies and measurement systems
04/2009 – 03/2010	Visiting Researcher and Graduation Work IESL-FORTH (Creete, GRC) Bose-Einstein Condensation and Matter-Wave Group
10/2008 – 02/2009	Guest Student IESL-FORTH (Creete, GRC) Photonic Materials and Devices Laboratory
10/2007 – 12/2007	Exchange Student with Erasmus Heriot Watt University (Edinburgh, UK)
2001 – 2004	**Gymnasium for Engeneering (Abitur)** BBS II Kerschensteiner Schule (Delmenhorst, DE) Focus: Electrical Engineering

Advanced Training

27.11.2014	**Regulatory Requirements for Medical Devices**	
	DIN-Akademie (Kassel, DE)	
05.11.2014	**Revision of Medical Device Directives**	
	SNV (Kloten, CH)	
02-06.06.2014	**Short Advanced course on MedTech Enterpreneurship**	
	Universita della Svizzera italiana (Lugano, CH)	
04.11.2013	**Medical Device Legislation**	
	TÜV SÜD Akademie (Munich, DE)	
06-08.08.2013	**Projectmanagement Methods**	
	TÜV SÜD Akademie (Hamburg, DE)	
11.04.2013	**Development Management for Medical Devices**	
	TÜV SÜD Akademie (Munich, DE)	

Publications and Patents

[1] Deibel, Waldemar, et al. "A compact, efficient, and lightweight laser head for CARLO: integration, performance, and benefits." *SPIE optical engineering and applications* 9579 (2015): 957905-957905.1

[2] Deibel, Waldemar, et al. “Heat Induction during Laser Bone Ablation: Thermal Imaging Measurements.” – In revision.

[3] Deibel, Waldemar, et al. “Heat Induction during Laser- and Piezo Electrical Saw Osteotomies; A Comparative Study with Thermal Imaging Measurements.” – In revision.

[4] Deibel W., Richter T., Bruno A. E. (2017). *European Patent No. EP3127501 A1*. Basel, Switzerland. European Patent Office.

[5] Bruno A. E., Cattin P., Deibel W. (2015). *European Patent No. EP2938274 A1.* Basel, Switzerland. European Patent Office.

Other authorships, poster and conference contributions are available on request.

Further Skills

Languages:	German – native speaker
	English – fluent (TOEFL)
	Russian – fluent in spoken
Software:	MS Powerpoint, MS Word – very good
	MS Project, MS Excel, Latex – good
	Inventor, Katia, Solid Works – basic

References

[1] T. H. Maiman *et al.*, "Stimulated optical radiation in ruby," 1960. 1

[2] M. M. Zaret, G. M. Breinin, H. Schmidt, H. Ripps, I. M. Siegel, and L. R. Solon, "Ocular lesions produced by an optical maser (laser)," *Science*, vol. 134, no. 3489, pp. 1525–1526, 1961. 1

[3] C. J. Campbell, "The optical master as a retinal coagulator: an evaluation.," *Trans. Am. Acad. Ophthalmol. Otolaryngol.*, vol. 67, p. 58, 1963. 1

[4] H. Zweng, M. Flocks, N. Kapany, N. Silbertrust, and N. Peppers, "Experimental laser photocoagulation," *American journal of ophthalmology*, vol. 58, no. 3, pp. 353–362, 1964. 1

[5] L. Goldman, P. Hornby, R. Meyer, and B. Goldman, "Impact of the laser on dental caries," *Nature*, vol. 203, no. 4943, p. 417, 1964. 1, 2

[6] A. Stafl, E. J. Wilkinson, and R. F. Mattingly, "Laser treatment of cervical and vaginal neoplasia," *American Journal of Obstetrics and Gynecology*, vol. 128, no. 2, pp. 128–136, 1977. 1

[7] G. Nath, W. Gorisch, and P. Kiefhaber, "First laser endoscopy via a fiberoptic transmission system," *Endoscopy*, vol. 5, no. 04, pp. 208–213, 1973. 1

[8] G. Staehler, A. Hofstetter, W. Gorisch, E. Keiditsch, and M. Müssiggang, "Endoscopy in experimental urology using an argon-laser beam," *Endoscopy*, vol. 8, no. 01, pp. 1–4, 1976. 1

[9] P. Ascher, "Newest ultrastructural findings after the use of a co2-laser on cns tissue.," *Acta neurochirurgica. Supplementum*, vol. 28, no. 2, pp. 572–581, 1979. 2

[10] C. T. Dotter and M. P. Judkins, "Transluminal treatment of arteriosclerotic obstruction: description of a new technic and a preliminary report of its application," *Circulation*, vol. 30, no. 5, pp. 654–670, 1964. 2

[11] R. Graaff, A. Dassel, M. Koelink, F. De Mul, J. Aarnoudse, and W. Zijlstra, "Optical properties of human dermis in vitro and in vivo," *Applied optics*, vol. 32, no. 4, pp. 435–447, 1993. 2

[12] G. J. Jako, "Laser surgery of the vocal cords an experimental study with carbon dioxide lasers on dogs," *The Laryngoscope*, vol. 82, no. 12, pp. 2204–2216, 1972. 2

[13] P. Kiefhaber, G. Nath, and K. Moritz, "Endoscopical control of massive gastrointestinal hemorrhage by irradiation with a high-power neodymium-yag laser1," in *Progress in Surgery*, vol. 15, pp. 140–155, Karger Publishers, 1977. 2

[14] J. Moore, "Laser energy in orthopedic surgery," *Orthoped. Surg. Traumat. Excerpta Medica, Amsterdam*, 1973. 2

[15] G. J. P. L. De Oliveira, C. N. C. Rodrigues, L. R. Perussi, A. N. de Souza Rastelli, R. A. C. Marcantonio, and F. L. C. V. Berbert, "Effects on bone tissue after osteotomy with different high-energy lasers: An ex vivo study," *Photomedicine and laser surgery*, vol. 34, no. 7, pp. 291–296, 2016. 2

[16] J. F. Bille, A. W. Dreher, and G. Zinser, "Scanning laser tomography of the living human eye," in *Noninvasive diagnostic techniques in ophthalmology*, pp. 528–547, Springer, 1990. 2

[17] J. Kotowski, G. Wollstein, L. S. Folio, H. Ishikawa, and J. S. Schuman, "Clinical use of oct in assessing glaucoma progression," *Ophthalmic Surgery, Lasers and Imaging Retina*, vol. 42, no. 4, pp. S6–S14, 2011. 2

[18] S. Walia and G. A. Fishman, "Retinal nerve fiber layer analysis in rp patients using fourier-domain oct," *Investigative ophthalmology & visual science*, vol. 49, no. 8, pp. 3525–3528, 2008. 2

[19] V. Semenyuk, "Prediction of temperature and damage in an irradiated human eye during retinal photocoagulation," *International Journal of Heat and Mass Transfer*, vol. 126, pp. 306–316, 2018. 2

[20] M. Messina, A. R. Ross, G. Pocobelli, D. G. Said, and H. S. Dua, "Cataract surgery with intraocular lens implantation in 3 brothers with megalocornea: Long-term follow-up," *Journal of Cataract & Refractive Surgery*, vol. 44, no. 3, pp. 399–402, 2018. 2

[21] N. Kahuam-López, A. Navas, C. Castillo-Salgado, E. O. Graue-Hernandez, A. Jimenez-Corona, and A. Ibarra, "Femtosecond laser versus mechanical microkeratome use for laser-assisted in-situ keratomileusis (lasik)," *Cochrane Database of Systematic Reviews*, no. 2, 2018. 2

[22] R. H. Stern, J. Vahl, and R. F. Sognnaes, "Lased enamel: ultrastructural observations of pulsed carbon dioxide laser effects," *Journal of Dental Research*, vol. 51, no. 2, pp. 455–460, 1972. 2

[23] R. H. Stern, "Dentistry and the laser," in *Laser applications in medicine and biology*, pp. 361–388, Springer, 1974. 2

[24] L. Clayman, T. Fuller, and H. Beckman, "Healing of continuous-wave and rapid superpulsed, carbon dioxide, laser-induced bone defects.," *Journal of oral surgery (American Dental Association: 1965)*, vol. 36, no. 12, pp. 932–937, 1978. 2

[25] S. Gertzbein, D. Dedemeter, B. Cruickshank, and A. Kapasouri, "The effect of laser osteotomy on bone healing," *Lasers in surgery and medicine*, vol. 1, no. 4, pp. 361–373, 1981. 2

[26] M. Pao-Chang, X. Xiou-qi, Z. Hui, L. Zheng, and Z. R. Peng, "Preliminary report on the application of the co2 laser scalpel for operations on the

maxillo-facial bones," *Lasers in surgery and medicine*, vol. 1, no. 4, pp. 375–384, 1981. 2

[27] R. C. Nuss, R. L. Fabian, R. Sarkar, and C. A. Puliafito, "Infrared laser bone ablation," *Lasers in Surgery and Medicine*, vol. 8, no. 4, pp. 381–391, 1988. 3

[28] R. Hibst and U. Keller, "Experimental studies of the application of the er: Yag laser on dental hard substances: I. measurement of the ablation rate," *Lasers in Surgery and Medicine*, vol. 9, no. 4, pp. 338–344, 1989. 3

[29] M. Frentzen, "Bearbeitung der schmelzoberflachen mit gepulster laserstrahlung," *Dtsch Zahnarztl Z*, vol. 49, pp. 166–168, 1994. 3

[30] L. R. Friesen, C. M. Cobb, J. W. Rapley, L. Forgas-Brockman, and P. Spencer, "Laser irradiation of bone: Ii. healing response following treatment by co2 and nd: Yag lasers," *Journal of periodontology*, vol. 70, no. 1, pp. 75–83, 1999. 3

[31] K. M. Sasaki, A. Aoki, S. Ichinose, T. Yoshino, S. Yamada, and I. Ishikawa, "Scanning electron microscopy and fourier transformed infrared spectroscopy analysis of bone removal using er: Yag and co2 lasers," *Journal of periodontology*, vol. 73, no. 6, pp. 643–652, 2002. 3

[32] H. Kang, J. Oh, and A. Welch, "Investigations on laser hard tissue ablation under various environments," *Physics in medicine and biology*, vol. 53, no. 12, p. 3381, 2008. 3, 34, 52

[33] U. K. Akyol, M. Güngörmüs, C. Gündogdu, and H. Erdem, "Histologic evaluation of the effects of er: Yag laser on bone ablation.," *The journal of contemporary dental practice*, vol. 10, no. 5, pp. E065–72, 2009. 3

[34] S. Stübinger, K. Nuss, M. Pongratz, J. Price, R. Sader, H.-F. Zeilhofer, and B. von Rechenberg, "Comparison of er: Yag laser and piezoelectric osteotomy: an animal study in sheep," *Lasers in surgery and medicine*, vol. 42, no. 8, pp. 743–751, 2010. 3

[35] G. L. Martins, E. Puricelli, C. E. Baraldi, and D. Ponzoni, "Bone healing after bur and er: Yag laser ostectomies," *Journal of Oral and Maxillofacial Surgery*, vol. 69, no. 4, pp. 1214–1220, 2011. 4

[36] C. M. Barone, D. F. Jimenez, G. J. Yule, and B. Strauch, "Analysis of bone formation after cranial osteotomies with a high-speed drill.," *The Journal of craniofacial surgery*, vol. 8, no. 6, pp. 466–470, 1997. 4

[37] S. Kondo, Y. Okada, H. Iseki, T. Hori, K. Takakura, A. Kobayashi, and H. Nagata, "Thermological study of drilling bone tissue with a high-speed drill," *Neurosurgery*, vol. 46, no. 5, pp. 1162–1168, 2000. 4

[38] S. Stübinger, "Advances in bone surgery: the er: Yag laser in oral surgery and im-plant dentistry," *Clinical, Cosmetic and Investigational Dentistry*, vol. 2, p. 47, 2010. 4

[39] M. Schlee, "Piezosurgery—a precise and safe new oral surgery technique," *Aust Dent Pract*, vol. 2009, pp. 144–8, 2009. 4

[40] G. Eggers, J. Klein, J. Blank, and S. Hassfeld, "Piezosurgery®: an ultrasound device for cutting bone and its use and limitations in maxillofacial surgery," *British Journal of oral and maxillofacial surgery*, vol. 42, no. 5, pp. 451–453, 2004. 4

[41] D. D. Lo, M. A. Mackanos, M. T. Chung, J. S. Hyun, D. T. Montoro, M. Grova, C. Liu, J. Wang, D. Palanker, A. J. Connolly, *et al.*, "Femtosecond plasma mediated laser ablation has advantages over mechanical osteotomy of cranial bone," *Lasers in surgery and medicine*, vol. 44, no. 10, pp. 805–814, 2012. 4

[42] I. Anic, I. Miletic, S. J. Krmek, J. Borcic, and S. Pezelj-Ribaric, "Vibrations produced during erbium: yttrium–aluminum–garnet laser irradiation," *Lasers in medical science*, vol. 24, no. 5, pp. 697–701, 2009. 4

[43] C. Cozean, C. J. ARCORIA, J. PELAGALLI, and G. L. POW-ELL, "Dentistry for the 21st century? erbium: Yag laser for teeth," *The Journal of the American Dental Association*, vol. 128, no. 8, pp. 1080–1087, 1997. 4

[44] B. Y. Leung, P. J. Webster, J. M. Fraser, and V. X. Yang, "Real-time guidance of thermal and ultrashort pulsed laser ablation in hard tissue using inline coherent imaging," *Lasers in surgery and medicine*, vol. 44, no. 3, pp. 249–256, 2012. 4

[45] F. Pedrotti, L. Pedrotti, W. Bausch, and H. Schmidt, "Optik für ingenieure," 7

[46] H. J. Eichler and J. Eichler, *Laser: Bauformen, Strahlführung, Anwendungen*. Springer-Verlag, 2015. 7

[47] M. H. Niemz, *Laser-tissue interactions: fundamentals and applications*. Springer Science & Business Media, 2013. 16, 19, 20, 21

[48] H. Kang, I. Rizoiu, and A. Welch, "Hard tissue ablation with a spray-assisted mid-ir laser," *Physics in medicine and biology*, vol. 52, no. 24, p. 7243, 2007. 34, 49, 51, 52

[49] E. A. Silk, E. L. Golliher, and R. P. Selvam, "Spray cooling heat transfer: technology overview and assessment of future challenges for micro-gravity application," *Energy Conversion and Management*, vol. 49, no. 3, pp. 453–468, 2008. 34, 39, 42, 48, 52

[50] B. Glassman, "Spray cooling for land, sea, air and space based applications, a fluid managment system for multiple nozzle spray cooling and a guide to high heat flux heater design," 2005. 34, 35

[51] Z. Yan, R. Zhao, F. Duan, T. N. Wong, K. C. Toh, K. F. Choo, P. K. Chan, and Y. S. Chua, "Spray cooling," in *Two Phase Flow, Phase Change and Numerical Modeling*, InTech, 2011. 35, 38

[52] R. P. Selvam, L. Lin, and R. Ponnappan, "Direct simulation of spray cooling: effect of vapor bubble growth and liquid droplet impact on heat transfer," *International Journal of Heat and Mass Transfer*, vol. 49, no. 23, pp. 4265–4278, 2006. 35

[53] G. Wozniak, *Zerstäubungstechnik: Prinzipien, Verfahren, Geräte*. Springer-Verlag, 2013. 35

[54] S. H. Song and S. Y. Lee, "Study of atomization mechanism of gas/liquid mixtures flowing through y-jet atomizers," *Atomization and sprays*, vol. 6, no. 2, 1996. 37

[55] S. Nukiyama, "Experiments on the atomization of liquids in an air stream, report 3, on the droplet-size distribution in an atomized jet," *Trans. Soc. Mech. Eng. Jpn.*, vol. 5, no. 18, pp. 62–67, 1939. 37

[56] T. Bergman and R. Mesler, "Bubble nucleation studies. part i: Formation of bubble nuclei in superheated water by bursting bubbles," *AIChE Journal*, vol. 27, no. 5, pp. 851–853, 1981. 41

[57] M. S. Sehmbey, L. C. Chow, M. R. Pais, and T. Mahefkey, "High heat flux spray cooling of electronics," in *AIP Conference Proceedings*, vol. 324, pp. 903–909, AIP, 1995. 42, 43, 44, 45, 46

[58] K.-w. Baek, W. Deibel, D. Marinov, M. Griessen, M. Dard, A. Bruno, H.-F. Zeilhofer, P. Cattin, and P. Juergens, "A comparative investigation of bone surface after cutting with mechanical tools and er: Yag laser," *Lasers in surgery and medicine*, vol. 47, no. 5, pp. 426–432, 2015. 43, 44, 58, 105

[59] J. Lee, "Role of surface roughness in water spray cooling heat transfer of hot steel plate," *ISIJ international*, vol. 49, no. 12, pp. 1920–1925, 2009. 44

[60] D. E. Tilton, "Spray cooling," tech. rep., Kentucky Univ., Lexington, KY (USA), 1989. 45

[61] M. Visaria and I. Mudawar, "Effects of high subcooling on two-phase spray cooling and critical heat flux," *International journal of heat and mass transfer*, vol. 51, no. 21, pp. 5269–5278, 2008. 45

[62] L. Lin and R. Ponnappan, "Heat transfer characteristics of spray cooling in a closed loop," *International Journal of Heat and Mass Transfer*, vol. 46, no. 20, pp. 3737–3746, 2003. 45

[63] R.-H. Chen, L. C. Chow, and J. E. Navedo, "Effects of spray characteristics on critical heat flux in subcooled water spray cooling," *International Journal of Heat and Mass Transfer*, vol. 45, no. 19, pp. 4033–4043, 2002. 46

[64] M. Visaria and I. Mudawar, "Theoretical and experimental study of the effects of spray inclination on two-phase spray cooling and critical heat flux," *International journal of heat and mass transfer*, vol. 51, no. 9, pp. 2398–2410, 2008. 46, 47

[65] M. Visaria and I. Mudawar, "Application of two-phase spray cooling for thermal management of electronic devices," *IEEE Transactions on Components and Packaging Technologies*, vol. 32, no. 4, pp. 784–793, 2009. 47

[66] B. Horacek, J. Kim, and K. T. Kiger, "Spray cooling using multiple nozzles: visualization and wall heat transfer measurements," *IEEE Transactions on Device and Materials Reliability*, vol. 4, no. 4, pp. 614–625, 2004. 47, 48

[67] L. Lin, R. Ponnappan, K. Yerkes, and B. Hager, "Large area spray cooling," in *Proc. 42nd AIAA Aerospace Sciences Meeting and Exhibit*, pp. 2004–1340, 2004. 48

[68] A. G. Pautsch and T. A. Shedd, "Spray impingement cooling with single-and multiple-nozzle arrays. part i: Heat transfer data using fc-72," *International Journal of Heat and Mass Transfer*, vol. 48, no. 15, pp. 3167–3175, 2005. 48, 52

[69] E. A. Silk, J. Kim, and K. Kiger, "Spray cooling of enhanced surfaces: impact of structured surface geometry and spray axis inclination," *International Journal of Heat and Mass Transfer*, vol. 49, no. 25, pp. 4910–4920, 2006. 48

[70] S. Afilal, *Ablationsmechanismen von biologischem Hartgewebe bei Bestrahlung mit kurzgepulsten CO2-Lasern*. PhD thesis, 2004. 50

[71] G. Altshuler, A. Belikov, and A. Erofeev, "Comparative study of contact and noncontact operation mode of hard tooth tissues er-laser processing," in *The 5th International Congress of the International Society of Laser Dentistry*, pp. 21–25, 1996. 51

[72] D. Fried, N. Ashouri, T. Breunig, and R. Shori, "Mechanism of water augmentation during ir laser ablation of dental enamel," *Lasers in Surgery and Medicine*, vol. 31, no. 3, pp. 186–193, 2002. 51

[73] R.-H. Chen, L. C. Chow, and J. E. Navedo, "Optimal spray characteristics in water spray cooling," *International Journal of Heat and Mass Transfer*, vol. 47, no. 23, pp. 5095–5099, 2004. 52

[74] M. Augello, W. Deibel, K. Nuss, P. Cattin, and P. Jürgens, "Comparative microstructural analysis of bone osteotomies after cutting by computer-assisted robot-guided laser osteotome and piezoelectric osteotome: an in vivo animal study," *Lasers in medical science*, vol. 33, no. 7, pp. 1471–1478, 2018. 105